INSTITUTO SUPERIOR TÉCNICO
Universidade Técnica de Lisboa

Evaluation of aerodynamic criteria in the design of a small wind turbine with the lifting line model

Nicolas BRUMIOUL

A thesis submitted in partial fulfillment of the requirements for the Degree of Master of Science in

Aerospace Engineering

Jury

Chair:	Prof. Fernando José Parracho Lau
Supervisor:	Prof. José Alberto Caiado Falcão de Campos
Examiners:	Prof. Luís Manuel de Carvalho Gato

January 2010

Acknowledgements

I would like first of all to express my gratitude to my supervisor Prof. Falcão de Campos and to Mr. Pôtra for their continuous support, listening, constructive ideas, patience and advice. I also want to thank Mr. Pôtra for joining our meetings every week after his work at the Instituto Superior Técnico.

Thanks are also given to all my friends and colleagues at the Instituto Superior Técnico and in my apartment in Lisbon. With the atmosphere created, their support and sympathy I was able to surmount the ordeals and to carry through my thesis.

Many thanks go to Mr. Barsics, Mrs. Gerlach and Mr. Fourneau for making this Erasmus experience possible. I also thank Mrs. Gerlach for her help and advice, and Mr. Schiffer for the spelling correction.

Thanks to my girlfriend and my friends in Belgium for their boost every day. I am very thankful to all that were able to visit me and bring me their support.

Finally, the deepest gratitude of all goes to my family members for their unconditional encouragement, financial support and without whom this experience would not have been possible.

Abstract

This thesis deals with the optimization of the aerodynamic design of a small wind turbine to maximize energy production.

It is well known that energy production depends on the type of turbine and on the wind characteristics on a given site. In this work we try to maximize the energy production for a given site by optimizing the most important aerodynamic design parameters.

The optimization is carried out with computer codes for the design and analysis of a horizontal axis wind turbine based on lifting line theory. The starting point is a 3-bladed, 2.5 meter diameter variable speed turbine design. The main parameters to be optimized are the type airfoil of blade sections together with its design lift coefficient. The selection of the airfoil is based on the lift and drag data as function of angle of attack at different Reynolds numbers. In particular, the curves of C_L/C_D are used to select the design parameters lift coefficient. Other parameters concern the design wind speed and the tip speed ratio (TSR). The diameter and the number of blades are kept constant in the optimization. A structural constraint for maximum stress on the blades is used to define the rated power.

The variant designs are evaluated by determining their annual energy production (AEP) for two representative sites.

Keywords: Small wind turbine, lifting line theory, design criteria, power coefficient, energy power, annual energy production.

Table of contents

List of tables

List of figures

List of symbols

A	rotor swept area
AEP	annual energy production
c	chord
c	Weibull scale parameter
C_D	drag coefficient
C_L	lift coefficient
C_P	power coefficient
C_T	thrust coefficient
dD	elementary drag force
dL	elementary lift force
dQ	elementary torque
dT	elementary thrust
d_{max}	maximum thickness
D	diameter
HAWT	horizontal axis wind turbine
k	Weibull shape parameter
P	power
Q	axial force
r_h	hub radius
R_e	elastic limit
Re	Reynolds number
R	rotor radius
SWT	small wind turbine
T	torque
TSR, λ	tip speed ratio
U	wind speed
v_a	axial induced velocity
v_r	radial induced velocity
v_t	tangential induced velocity
V	incident velocity at a blade section
VAWT	vertical axis wind turbine
Z	number of blades

α	angle of attack
β	aerodynamic pitch angle
β_i	aerodynamic induced pitch angle
γ	twist angle
Γ	circulation
ε	C_D/C_L ratio
ν	air kinematic viscosity
ρ	air density
σ	nominal stress
σ_{lim}	limit stress
ψ	pitch angle
ω	rotational velocity

Chapter 1
Introduction

Wind energy has always played an important role in our society. 3000 years ago already, humans employed this energy for grinding grain or pumping water. In the Middle Ages, it was used as a means of transport for sailing and discovering continents. Nowadays, for environmental reasons, we are using wind to produce “green energy” which may contribute to slow down the greenhouse effect and replace nuclear energy.

1.1 Background

1.1.1 Wind energy

A large interest in wind energy appeared after the oil crises of the 1970s. Several countries began to invest money for improving wind turbine technology. The first significant market was in California in the 1980s. The financial situation in Europe allowed Germany and Denmark to develop their wind turbines’ industries. From 1997 to 2008, the annual power capacity has grown from 1.5 GW to 27 GW at an average annual growth rate of about 29%, as shown in Fig. 1.1 [1]. The total power capacity by wind energy in the world was 120.8 GW in 2008.

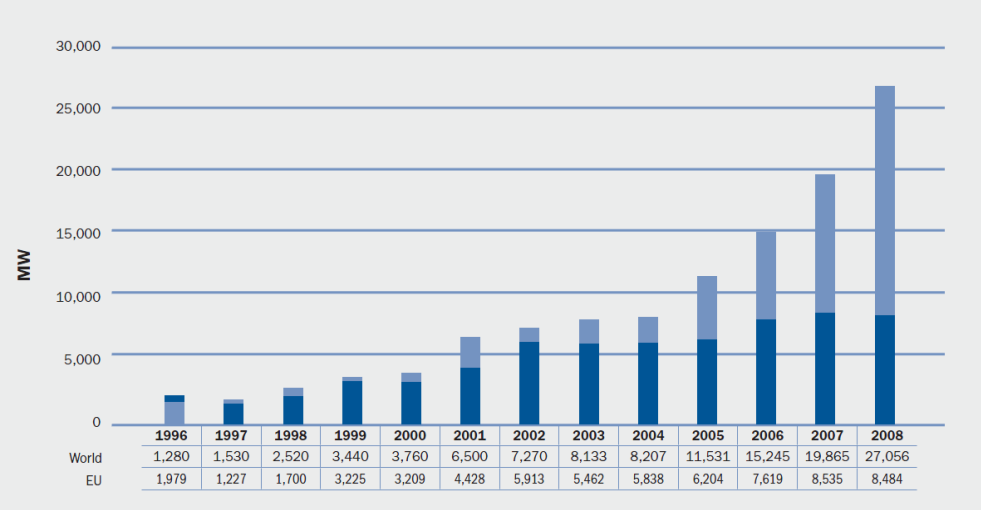

	1996	1997	1998	1999	2000	2001	2002	2003	2004	2005	2006	2007	2008
World	1,280	1,530	2,520	3,440	3,760	6,500	7,270	8,133	8,207	11,531	15,245	19,865	27,056
EU	1,979	1,227	1,700	3,225	3,209	4,428	5,913	5,462	5,838	6,204	7,619	8,535	8,484

Fig. 1.1: Global annual wind power capacity 1996-2008 [1].

Unfortunately, wind energy production is not sufficient to meet the world demand. The wind turbines' energy represents only 0.1% of the world energy production [2].

The wind energy presents some undeniable advantages which respect to the following aspects:

- *Environmental*

  Some energy sources used by mankind cause the planet pollution such as climate change and acid rains. The world concentration of CO_2 has increased by 35% between 1750 and 2005 [2]. Scientists estimate that this concentration will have doubled by 2050. The increase in temperature is already 0.74° since 1906 and will reach 3.5° in 2100 [3]. As a consequence, it is estimated that the ocean levels will increase from 15 to 95 centimetres. Wind energy allows planet pollution to slow down. For example, the European wind energy production already avoids the production of 24 billion tons of CO_2 per year [2].

  Moreover, this energy is clean and does not product waste, unlike nuclear industry.

- *Renewable energy source*

  Renewable energy is energy renewed or regenerated from natural sources [4]. So, in opposition to fossil energy, wind energy is renewable and future generations will be able to use it.

  Wind energy represents only 3.5% of renewable energy market but reaches the third place behind hydroelectricity with 89% and biomass with 5.7% [2].

  However, the European Commission estimates that the part of renewable energy in the world energy consumption will decrease by 13% or 8% between 2000 and 2030; this signifies that the world energy consumption will increase faster than renewable energy production [2].

- *Investment cost*

  The investment cost is lower than for other renewable energies. For example, prices of small wind turbines gravitate around $3-6/Watt in U.S. while solar systems cost $7.6/Watt in 2007 [5]. This difference comes from the prices of materials used to build them. Wind turbines contain 90% steel and incorporate copper in their generators. In consequence, SWTs have a lower price than solar photovoltaic systems, which are composed of copper, aluminium and silicon [5].

- *Local energy*

  Wind energy may be used locally in poor countries where other sources of energy are not yet easily accessible.

  Moreover, its local utilization in Europe reduces line losses due to energy transport.

However, wind energy also brings about some disadvantages:

- *Visual impact*
  The most controversial problem with wind energy is its impact on landscape. However, it is impossible to evaluate this impact because it is a subjective theme. A study shows that people's perception does not only depend on the physical parameters of the landscape but also on their behaviour in relation to pollution problems [6].
  The choice of the location, the colour and the shape may cause a reduction of the visual impact.

- *Noise*
  Wind turbines produce two kinds of noise: aerodynamic and mechanical noise. Aerodynamic noise is caused by the wind flow through the blades, while mechanical noise is caused by the rotation of mechanical elements. The latter has practically disappeared with technical progress.
  These noises may be minimized by the location choice in relation with topography and the surrounding houses. Some norms concerning noise have already been approved by several countries.

- Birds
  Wind turbines may have two effects on birds: collision and habitation decrease. To reduce the collision risk, some studies advise not to build wind turbines on migratory routes.
  Concerning the habitation problem, it does not only affect birds but also wildlife [6].

- *Electrical power quality*
  The electrical power produced by wind turbines is not constant and therefore the power quality is not always good. When the produced power is smaller than the electrical network power, it needs another electrical source. On the other hand, when the output power is larger than the electrical network, it needs a regulation system to keep the frequency and the voltage constant.

Even if the wind energy represents only 0.1% of the world energy production, on a large scale it may play a more important role in our society.

This dissertation is based on the study of a small wind turbine (SWT) and so we concentrate on this specific market.

1.1.2 Small wind turbines

1.1.2.1 Description

The function of small wind turbines is identical to the large wind turbines; they use wind energy to produce electricity economically and durably. The difference is that the term “small wind turbines” regroups wind turbines from 100 Watts up to 100 000 Watts. These are used to produce electricity and to power electrical devices.

1.1.2.2 Purpose and uses

The purpose is that homes, farms, small businesses, schools, and other institutions throughout the country use small wind turbines to lower or eliminate their electricity bills [7]. In fact, SWTs are more accessible to everyone by their small sizes and reasonable costs while the largest turbines are massive and expensive. Uses are diverse but could be associated with photovoltaic panels. In fact, as wind is stronger in winter and sun stronger in summer, both technologies are natural complements and often used together.
SWTs can be used On-grid to be connected to the electric grid for reducing the dependency on the local electrical utility, or Off-grid to provide electricity to remote locations.

1.1.2.3 Market

Concerning the SWT world market, it grew 53% in 2008 [5]. This market is dominated by On-grid connected units, as shown in Table 1.1 and will continue in this trend. In fact, On-grid installations produce 77% of the electricity and represent only 26% of the total units of small wind turbines.

Table 1.1: Results of 2008 world market by market segment [5].

World Total 2008	Units	kW
Off-Grid	13 902	7 536
On-Grid	4 992	26 065
Total	18 894	33 601

As an illustration, we refer to the U.S. market to define the projections for SWTs.
Manufacturers predict a 30-fold increase in the U.S. market in 5 years as shown in Fig. 1.2. The projection is made referring to different factors [5]:

- *Rising electricity prices*
  Electricity prices will increase at annual rates of about 1.8% in 2010 and will contribute to boost small wind turbine sales. The SWTs are more competitive than conventional electricity sources.

- *Federal incentives*
  More and more countries offer people the possibility for investment tax credit or incentive pay. In U.S. the government helps consumers purchase qualified small wind systems with rated capacities of 100 kW and less by 30% federal-level investment tax credit during 8 years.

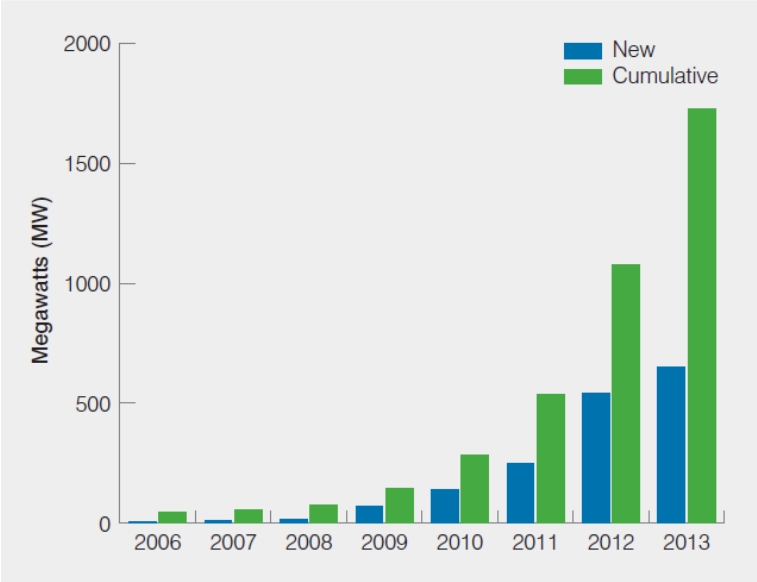

Fig. 1.2: U.S. market growth projections [5].

1.2 Project objectives

This thesis investigates aerodynamic criteria in the design of a small wind turbine.
The main objectives are to improve the power and to show the influence of design parameters choice by the calculation of Annual Energy Production on different sites.
Wind energy market being in full expansion, this study could be interesting in the choice of design criteria for SWTs.

The adoption of better design criteria might improve the output power and so the profitability of the small wind turbine might be increased and the payback period decreased.

1.3 Previous project

This thesis is the continuation of the previous project of Pôtra [8]. The title of his project was “Project and aerodynamic analysis of a rotor of small wind turbines”.
In this project we assume some modifications in the aerodynamic criteria to try to improve the mechanical power found in [8].
The programs which will be used to compute aerodynamic results are based on those employed by Pôtra [8]. Some modifications will have to be made to adapt them to the new criteria.

The final step of this thesis will be to determine the Annual Energy Production for different sites and conclusions will be drawn.

1.4 Literature review

This thesis is based on the evaluation of aerodynamic criteria for the design of a small wind turbine.
The design method of a wind turbine rotor is given by Lysen [9] and comprises two steps:

- The choice of basic parameters, as airfoil type and Tip Speed Ratio
- The calculations of setting angles and chord length at different positions along the blade.

Maalawi and Badr [10] have shown that the airfoil type plays an important role in the design. In fact their results have indicated that rotor blades with thinner airfoils and higher camber are recommended for increasing the power output, and lowering the level of thrust loading [10]. Moreover, for known airfoil type, blade number and hub size, the design Tip Speed Ratio, at which the maximum power occurs, can be directly determined, and hence, the optimum blade geometry [10]. Fuglsang and Madsen [11] have discussed the large number of design methods for wind turbines. The aerodynamic and structural design of rotors is a multi-disciplinary task, involving conflicting requirements on, for example, maximum performance, minimum loads and minimum noise [11]. But optimum design should not be restricted only to aerodynamic performance but also to the minimum cost of energy. This leads to the development of second generation design tools, where the optimization objective is the minimization of the cost of energy [11]. Cost Energy is by definition the ratio of the total costs from manufacture and erection of the wind turbine to the annual energy production [12].
Concerning the cut-in wind speed, Wright and Wood [13] have measured the starting performance of a three bladed, 2m diameter horizontal axis wind turbine in field tests. Their findings suggest that small wind turbines normally start rotating at about 4.6 m/s [13]. Unfortunately, this value is higher than the average wind speed in most built environments.

1.5 Project methodologies

The purpose of this thesis will be attained by adopting the following methodology:

- *Choice of airfoil for blade section design*: the aerodynamic characteristics of several airfoils will be compared with respect to optimum C_L/C_D to determine the best choice for blade section design.

- *Modification of the lifting line code for designing with variable angle of attack at small Reynolds numbers*: the previous study of Pôtra was performed for a constant angle of attack on the design of small wind turbines. In this project, the angle of attack varies along the blade in order to obtain a maximum C_L/C_D in each radial section. Extrapolation of the airfoil data for small Reynolds number needs to be incorporated.

- *Results of design and analysis*: firstly, the performance data with two different design options will be compared. These designs concern *Constant angle of attack* and the *Optimum* C_L/C_D (variation of angle of attack). Secondly, the performance data with the previous and the new airfoil, calculated with the best design found before, will be analyzed.

- *Stress analysis*: the calculation of mechanical stresses on blade sections airfoils will be performed and then analyzed to determine at which wind speed the limit stress occurs. This step allows the determination of the final power curve.

- *Results analysis of Annual Energy Production*: the data of energy production for two airfoils from selected sites will be compared and analyzed. In function of the results, conclusions will be drawn.

1.6 Thesis outline

This thesis comprises 10 chapters which are organized as below:

Chapter 1 presents the background, objectives, previous project and literature review.

Chapter 2 characterizes in general the wind resource and the different kinds of wind turbines and their power. The two types of wind turbines are compared through their advantages and disadvantages. Basic principles of the wind and characteristics of small wind turbines are presented. Basic results concerning the power that may be extracted from wind are reviewed including Betz' law.

In Chapter 3, the lifting line theory is described step by step.

Chapter 4 explains the computational method and the modification introduced in this thesis to accommodate with the new requirements.

Chapter 5 presents the design criteria selected. The variants concern the type of airfoil and the design method of angle of attack. The profile, characteristics and optimum conditions of the airfoil are compared.

Chapter 6 presents the results for the design variants chosen before.

Chapter 7 explains the stress analysis and the determination of the power curve.

In Chapter 8, the annual energy production is calculated with the help of Weibull distribution and analyzed for two different sites in Portugal with respectively relatively high and low wind resources.

Chapter 9 draws the major conclusion for this thesis.

Chapter 2
Wind and Wind turbine requirements

2.1 Wind

Wind is an endless, clean and free resource of energy. These three words may reflect the purpose of wind energy. This section outlines the origin and the influence of various obstacles on the wind characteristics.

As the wind direction at a given site is determined by the concurrence of global and local winds, we will briefly examine these two kinds of winds.

2.1.1 Global winds

The origin of the wind or air circulation in the atmosphere is caused by temperature differences created by the sun. In fact the regions near the equator are warmer than the rest of the world because radiation from the sun is highest as a consequence of the earth inclination. As hot air has a lower density than cold air, the hot air from Equator rises into the atmosphere until about 10km and spreads to the North and the South. Fig. 2.1 schematically illustrates the air circulation on the earth's surface.

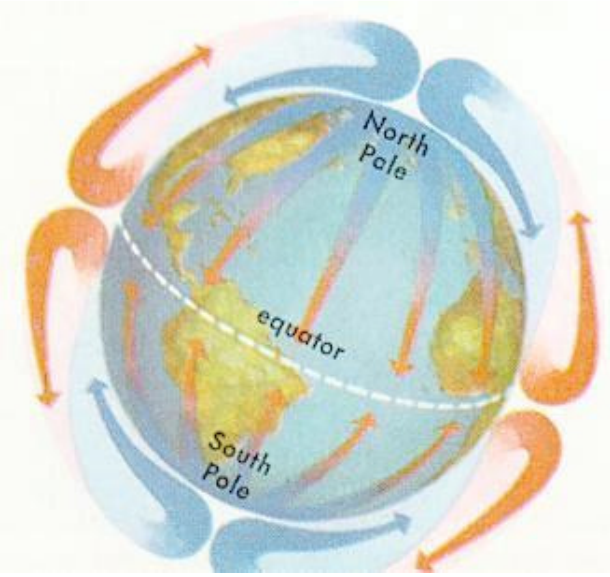

Fig. 2.1: Air circulation on the earth surface.

Around 30° latitude, the air from Equator cannot go farther due to the Coriolis force. This creates a high pressure area at these latitudes. The air which rises from Equator creates a low pressure at ground. This low pressure attracts winds from the North and South.
From this simple model, prevailing wind directions, also called geostrophic wind, may be indicated.

2.1.2 Local winds

Local winds are surface winds which are influenced by the effect of the sun on the earth. There are different types of local winds:

- *Sea breezes*

With sunbeams, the land gets warm more quickly than the sea during the day. Therefore, there is a rising of hot air above the land. This rising creates a low pressure area which attracts cold air of the sea. This natural phenomenon is called sea breezes.

During the night, the situation is reversed; the wind blows to the sea. But the wind speed is lower because the difference of temperature is not so high.
Fig. 2.2 illustrates the origin of sea breezes.

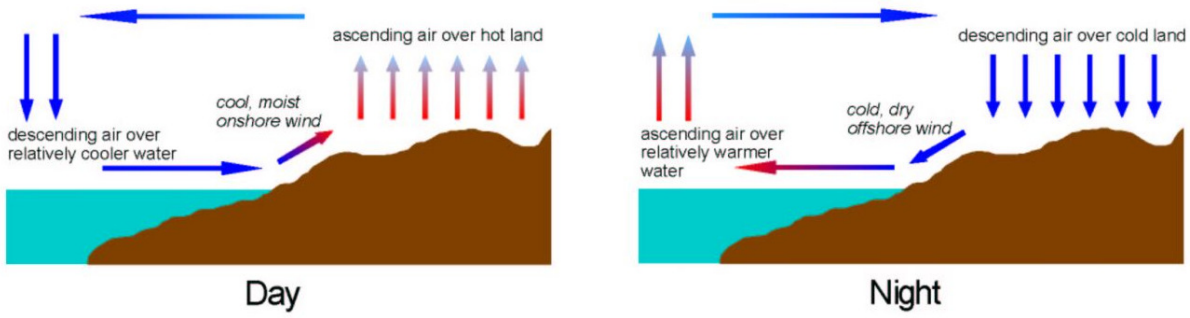

Fig. 2.2: Sea breezes.

- *Mountain winds*

In the mountain regions where the sun warms the air on the slopes, there is a decrease of air density. Thereof the air rises to the top by following the slope's surface. During the night, the direction of the wind is reversed.

2.1.3 Roughness and wind shear

The surface wind speeds are very influenced by the earth's surface roughness and obstacles.

There are two parameters which allow categorizing the wind potential:

- *Roughness class*: represent the ruggedness of the landscape. The surface of sea is the reference and its value is zero. The terrains with buildings, trees, etc… have a high class of roughness [14].

- *Roughness length*: is a parameter which is a measure of terrain roughness. It is formally the height at which the mean wind speed is zero. Although it is not a physical length, it can be considered as a length-scale, a representation of the roughness of the surface [4].

The wind shear is the variation of the wind speed as a function of the distance above the ground. For example, Fig. 2.3 shows the wind shear for a roughness class of two and roughness length of 1m.
For a wind turbine with a high diameter, the wind speeds will not be the same at the top and at the bottom. In consequence the blades will be subject to variation of strength and so to fatigue.

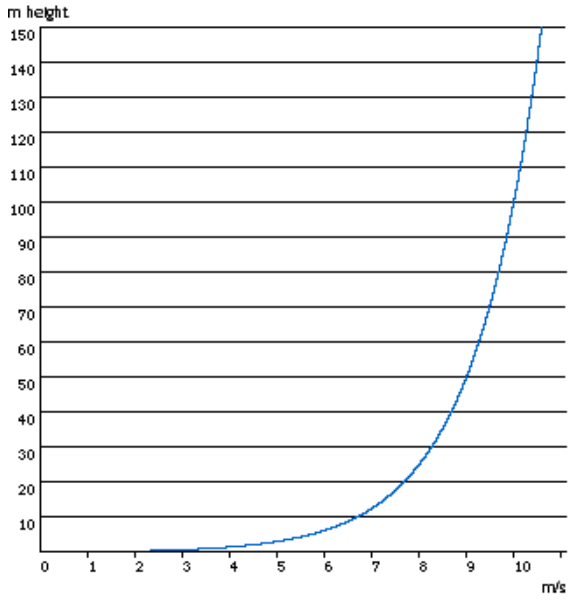

Fig. 2.3: The wind shear for a roughness class of two [14].

2.1.4 Winds in Europe

Fig. 2.4 shows the European wind atlas [15] for onshore winds at 50 metres above ground level.
In comparison with northern countries, Portugal does not possess favourable wind characteristics. However, the landscapes being very hilly, this allows obtaining mountain winds and to benefit from wind acceleration. In fact Portugal has a lot of wind turbines placed at the top of hills.
As a consequence, this country gets better winds than countries which have theoretically better wind characteristics in the European wind atlas.

Note also that in Belgium, despite good theoretical features, there were only 287 wind turbines in 2007 against 2150 in Portugal [15].

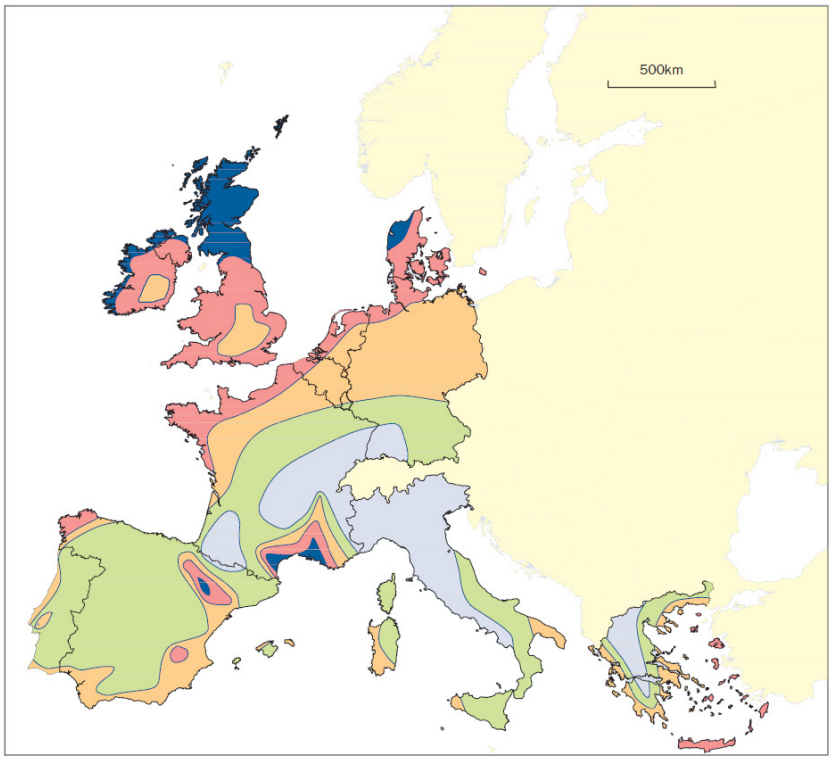

Wind resources at 50 metres above ground level for five different topographic conditions

	Sheltered terrain		Open terrain		At a sea coast		Open sea		Hills and ridges	
	ms^{-1}	Wm^{-2}	ms^{-1}	Wm^{-2}	ms^{-1}	Wm^{-2}	ms^{-1}	Wm^{-2}	ms^{-1}	Wm^{-2}
	>6.0	>250	>7.5	>500	>8.5	>700	>9.0	>800	>11.5	>1800
	5.0–6.0	150–250	6.5–7.5	300–500	7.0–8.5	400–700	8.0–9.0	600–800	10.0–11.5	1200–1800
	4.5–5.0	100–150	5.5–6.5	200–300	6.0–7.0	250–400	7.0–8.0	400–600	8.5–10.0	700–1200
	3.5–4.5	50–100	4.5–5.5	100–200	5.0–6.0	150–250	5.5–7.0	200–400	7.0–8.5	400–700
	<3.5	<50	<4.5	<100	<5.0	<150	<5.5	<200	<7.0	<400

Fig. 2.4: European wind atlas [15].

2.2 Wind turbines

Wind turbines convert kinetic energy of the wind into mechanical energy. They are composed of blades rotating around an axis by the action of the wind.

2.2.1 Types of Turbines

There are two main categories of wind turbines: Horizontal Axis Wind Turbine (HAWT) and Vertical Axis Wind Turbine (VAWT) as shown in Fig. 2.5.

HAWT VAWT

Fig. 2.5: Horizontal and vertical axis wind turbines.

2.2.1.1 HAWT

The axis of these wind turbines is horizontal, approximately parallel to the ground. They have evolved from the traditional “Dutch” windmill used for grain grinding.
Several kinds of HAWTs are commercialised.

- *Among the advantages, we mention:*

  - They may have a variable pitch to give the optimum angle of attack and thus to collect the maximum of wind energy.
  - The high towers allow getting advantage of the strong wind on sites with wind shear. The electricity production may be increased by placing the wind turbine a few meters higher.
  - HAWTs have a high efficiency.

- *Among the disadvantages, we point out:*

  - The long blades and towers are difficult to transport.
  - The mounting is hard and needs high and expensive cranes.
  - High HAWTs may disturb radar installations.
  - They need a mechanism to turn the rotor into the wind.
  - The large wind turbines disrupt the landscapes because of their massiveness.

2.2.1.2 VAWT

These kinds of wind turbines, invented by Georges Darrieus in 1931, possess a vertical axis. The VAWTs are not very much used in the world because they present serious disadvantages.

- *Some of the advantages are:*

  - As the structure is not so massive, the mounting of VAWTs is easier.
  - They start generating electricity from a wind of 4 m/s.
  - VAWTs have a lower noise signature.
  - They do not need a mechanism to turn the rotor into the wind.

- *Some of the disadvantages are:*
  - Having the rotor located close to the ground, VAWTs do not profit from high fast winds.
  - Their power coefficient is about 50% lower than Horizontal Axis Wind Turbines,
  - Guy-wires are used to keep the VAWTs in place, which may make the surrounding fields impractical to cultivate.
  - They do not start automatically, so they need a starting torque.

2.2.2 Small Wind Turbines

Some of the SWT characteristics are as follows:

- *Power and rotor diameter*
  The rotor diameter of the small wind turbines varies from 1 meter until 20 meters to generate power from 100 to 100 000 Watts.

- *Yaw mechanism*
  The axis of wind turbines needs to be aligned against the wind to turn and produce electricity. This is realized by the addition of a yaw mechanism. Generally, there are two kinds of

positioning system but for small wind turbines the most used is the rudder for its simplicity, reliability and low cost. The other kind of wind turbines employs the other type to control the position, namely electric motors and gearboxes.

- *Blade characteristics*

  Usually, small wind turbines are composed of two or three blades. The materials employed for the manufacture of the blades vary and have known a great progress. Previously, wood was used due to its low price, easy manufacturing and availability [4]. However, this material needs frequent maintenance during its lifetime. At present, most of SWT blades are manufactured with polymer materials, individual or reinforced by composite materials [4].

- *Rotational speed control*

  The variation of the rotational speed allows to keep a constant Tip Speed Ratio.

  However to operate at an optimum power coefficient, the Tip Speed Ratio has to be changed functions of wind speed.

- *Power control*

  There are different methods to control the power.

  Generally, stall regulation is used for small wind turbines due to its low cost. In this case, the blades are bolted onto the hub at a fixed angle. However, the geometry of the blades has been designed to cause flow separation from the side of the blade which is not facing the wind when the wind speed becomes too high. In consequence, the blade is slightly twisted to ensure that the blades stall gradually when the wind speed reaches its critical value.

  The largest wind turbines employ pitch regulation which consists in the modification of the pitch angle to regulate the power. If the output power becomes too high, the blades are turned out of the wind and conversely when the wind drops.

2.3 Power

2.3.1 Most influential factor

The power of a wind turbine may be characterized by the power coefficient C_P:

$$C_P = \frac{2\ P}{\rho\ A\ U^3} \tag{2-1}$$

where ρ is the air density , A is the rotor swept area (πR^2) and U is the wind speed. The power coefficient is a function of the turbine rotor geometry and the various non-dimensional operating parameters.

For a given power coefficient, the most influential factor is the wind speed; therefore the location of the wind turbine will be very important.

However, the value of the power coefficient is also important because its value cannot be increased beyond limits and may be well below the value of 1. In fact, Albert Betz discovered that a wind turbine is not able to capture all of the energy in the wind.

2.3.2 Betz' law

Albert Betz published between 1922 and 1925 that, by applying elementary physical laws, the mechanical energy extractable from an air stream passing through from a given cross-sectional area is restricted to a certain fixed proportion of the energy or power contained in the air stream [16].

This fixed proportion is represented by a value of the power coefficient C_P, the ratio of the extractable mechanical power to the power contained in the air stream.

Fig. 2.6. shows the stream tube where U_1 is the undelayed free-stream velocity, the wind speed, before it reaches the converter, whereas U_2 is the flow velocity far behind the converter.

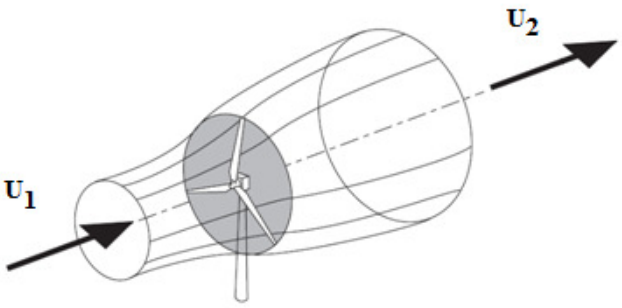

Fig 2.6: Stream tube.

When U_2/U_1 = 1/3, the maximum ideal power coefficient becomes:

$$C_P = \frac{16}{27} = 0.593 \tag{2-2}$$

Betz was the first to derive this important value; it is frequently called the “Betz factor”.

For the complete demonstration of the Betz’ law, we refer to [16].

Fig. 2.7 shows the ideal power coefficient versus the flow speed ratio of the flow before and after the energy converter [16]. This graphic allows to note that the maximum power coefficient occurs at a velocity ratio U_2/U_1 = 0.333.

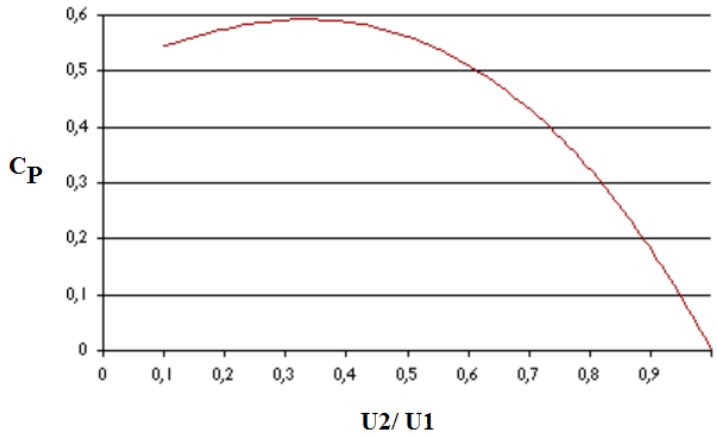

Fig. 2.7: Ideal power coefficient versus the flow speed ratio U_2/U_1.

2.4 Weibull distribution

Even if the variation in annual mean wind speeds remains difficult to predict year-to-year, the wind speed variations during the year can be well characterized in terms of probability distribution [17]. To do this, the probability density equation of Weibull is used according to:

$$f(x,k,c) = \frac{k}{c^k}\, x^{k-1}\, e^{-(x/c)^k} \tag{2-3}$$

where *c* is the scale parameter, *k* is the shape parameter and *x* is the variable (in this case, the wind speed).

The Weibull distribution has been found to give a good representation of the variation wind speed over a year on a given site [17]. In the wind turbine industry, the wind variation is very important to know. This information is used to optimize the design criteria according to the site or to calculate the energy production.

Chapter 3
Lifting line theory

The aerodynamics of the rotor blades is described by lifting line theory. The calculations of this thesis are based on this theory. A brief description of the theory is given below. For a more detailed account, we refer to [18].

3.1 Lifting line model

The theory, previously applied to wings of airplanes, is applied likewise to wind turbines and marine turbines. This model is based on the classical helical vortex model of constant pitch to determine the optimum blade circulation distribution for maximum power extraction.
Consider a rotor of a horizontal axis turbine with radius R (diameter D), with Z blades, placed in a fluid stream and rotating around its axis with the angular speed ω. The blades are symmetrically placed around a cylindrical hub of radius r_h. We assume that the fluid stream at great distances upstream of the rotor is uniform with velocity U in the direction of the rotor axis. The fluid is assumed to be inviscid and incompressible with density ρ.

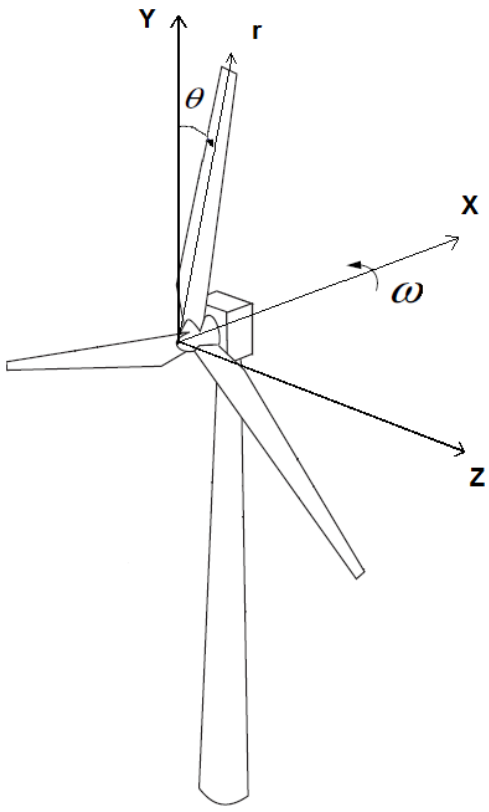

Fig. 3.1: Cartesian coordinate system

In Fig. 3.1 we introduce a Cartesian coordinate system (x, y, z) with the x axis coinciding with the turbine axis. The y axis coincides with the reference line of one of the blades and the right-hand is completed by the system z axis.

According to the lifting line theory, each turbine blade is represented by a radial line vortex of varying circulation strength $\Gamma(r)$, extending from the hub to the tip.
We assume that the circulation vanishes at the hub and the tip radii:

$$\Gamma(r_h) = \Gamma(R) = 0 \tag{3-1}$$

By definition, the circulation is produced by the vortex and represents the vortex strength, as shown in Fig. 3.2.

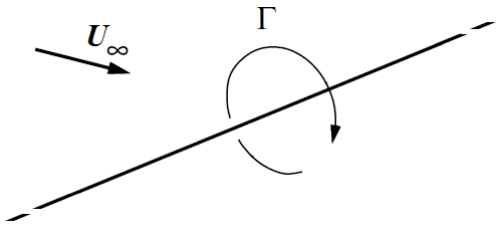

Fig. 3.2: Circulation

At present, we define $v_a(r), v_r(r), v_t(r)$ as respectively, the axial, radial and tangential components of the induced velocity at the lifting line $k = 1$. From symmetry the induced velocity on any other lifting line is identical.

The law of Kutta-Joukowski may compute the forces on the lifting line. The axial force and the torque on the rotor are obtained by integration along the radius and summing on the number of blades:

$$T = \rho\, Z \int_{r_h}^{R} (\omega r + v_t)\, \Gamma(r)\, dr \tag{3-2}$$

$$Q = \rho\, Z \int_{r_h}^{R} (U - v_a)\, \Gamma(r)\, r\, dr \tag{3-3}$$

Fig. 3.3 shows the velocities triangle, induced velocities, angle of attack α and twist angle γ and pitch angle ψ. Note that ψ is $\frac{\pi}{2} - \gamma$.

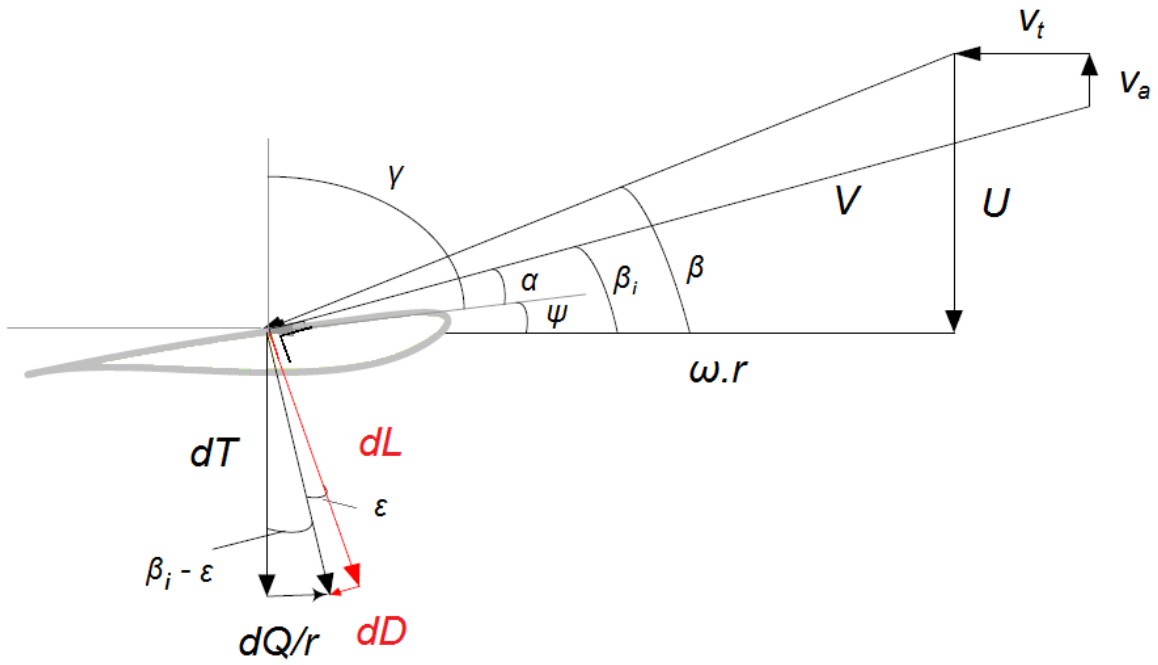

Fig. 3.3: Velocities triangle and forces on a blade section

We introduce dimensionless quantities by using the rotor radius R as reference length and the uniform stream speed U as reference velocity. The axial force and power coefficients are defined by

$$C_T = \frac{T}{\frac{1}{2}\rho U^2 \pi R^2}; \qquad C_P = \frac{P}{\frac{1}{2}\rho U^3 \pi R^2} = \frac{\omega Q}{\frac{1}{2}\rho U^3 \pi R^2} \tag{3-4}$$

From equations (3-2) and (3-3):

$$C_T = \frac{2Z}{\pi}\int_{r_h}^{1}(r\lambda + v_t)\,\Gamma(r)\,dr, \qquad C_P = \frac{2Z\lambda}{\pi}\int_{r_h}^{1}(l - v_a)\,\Gamma(r)\,r\,dr \tag{3-5}$$

where $\lambda = \frac{\omega R}{U}$ is the tip speed ratio.

Taking into account viscous effects by introducing the drag to lift ratio $\frac{C_D}{C_L}$ of the blade section from Fig. 3.3, the equations become:

$$C_T = \frac{2Z}{\pi}\int_{r_h}^{1}(r\lambda + v_t)\,\Gamma(r)\,(1 + \frac{C_D}{C_L}tan\,\beta_i)\,dr$$

$$C_P = \frac{2Z\lambda}{\pi}\int_{r_h}^{1}(l - v_a)\,\Gamma(r)\,(1 - \frac{C_D}{C_L}cot\ \beta_i)\,r\,dr \tag{3-6}$$

where the blade section drag and lift coefficients are defined by:

$$C_L = \frac{dL/dr}{\frac{1}{2}\rho V^2 c} \qquad C_D = \frac{dD/dr}{\frac{1}{2}\rho V^2 c} \tag{3-7}$$

where V is the effective inflow velocity and c the section chord, as shown in Fig. 3.4 [19].

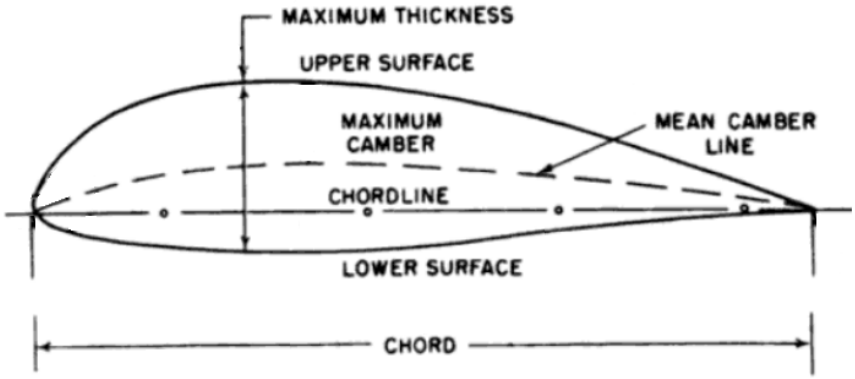

Fig. 3.4: Base airfoil description [19].

From the Kutta-Joukowski law the dimensionless circulation is related to the section lift coefficient by

$$C_L = \frac{2\,\Gamma}{V\,c} \tag{3-8}$$

And the section pitch angle is

$$\psi = \beta_i - \alpha \tag{3-9}$$

where α is the section angle of attack at the corresponding lift coefficient and β_i the aerodynamic induced pitch angle.

3.2 The vortex lattice model

A more numerical approach will be used by discretizing the lifting lines and their shed vortex sheets by a lattice of concentrated vortices [20].
According to this numerical model, the lifting line is discretized into M elements along the radius. A cosine distribution for the element corner points is used, as it gives good numerical convergence for the classical wing and rotor problems:

$$r_i = \frac{1}{2}(1 + r_h) - \frac{1}{2}(1 - r_h)\cos\frac{(i-1)\pi}{M} \quad for\ i = 1,2, \dots M + 1 \tag{3-10}$$

The induced velocity is calculated at control points given by:

$$\overline{r_i} = \frac{1}{2}(1 + r_h) - \frac{1}{2}(1 - r_h)\cos\frac{(i-\frac{1}{2})\pi}{M} \quad for\ i = 1,2, \dots M \tag{3-11}$$

and is

$$v_{a,t_i}(I) = \sum_{j=1}^{M} v_{a,t_{ij}}\ \Gamma_j \tag{3-12}$$

The axial force coefficient is given by

$$C_T = \frac{2Z}{\pi}\sum_{i=1}^{M}\left(\overline{r_i}\,\lambda + v_{t_i}\right)\ \Gamma_i\ \left(1 + \left(\frac{C_D}{C_L}\right)_i * tan\,\beta_i\right)(r_{i+1} - r_i) \tag{3-13}$$

And the power coefficient by

$$C_P = \frac{2Z\lambda}{\pi}\sum_{i=1}^{M}(1 - v_{a_i})\,\overline{r_i}\ \Gamma_i\ \left(1 - \left(\frac{C_D}{C_L}\right)_i * cot\,\beta_i\right)(r_{i+1} - r_i) \tag{3-14}$$

Chapter 4
Computational procedures

This chapter explains the computational procedure and the programs used to design and analyze the turbine rotor. Some modifications have been made to adapt the software to the additional requirements.

4.1 Computational Method

The calculation method for design and analysis is based on a loop using three programs written in FORTRAN. The names of these are: "Windturll", "Calcorda" and "Analise" and all of them are based on the lifting line model described in Chapter 3.

Fig. 4.1 shows the flow chart of the computational method.
Before running the computational loop, we determine our design criteria which are the nominal tip speed ratio TSR, the wind speed U, the airfoil and the nominal C_L/C_D.
These choices imply indirectly the choice of some design parameters such as angle of attack α. Moreover we also chose other design parameters such as the turbine diameter D, air density ρ and air kinematic viscosity ν. After, we introduce these values in different input files. The computational loop can start.

Firstly, we run the program "Windturll" which makes the aerodynamic design by employing the values of the nominal TSR, the nominal C_L/C_D and thrust coefficient C_T. With "Windturll" we obtain the circulation and the induced velocities. The following remarks should be made:
- The thrust coefficient C_T is determined to get the maximum value of power coefficient. We find it thanks to several successive calculations.
- For the first iteration, the nominal C_L/C_D is taken constant along the blade and specified by an arbitrary Reynolds number. However, it is advised to choose a good approximation of Reynolds number to limit the number of iterations.

Secondly, the program "Calcorda" is run. To compute the chord and the twist angles, it uses the circulation and the induced velocities calculated with "Windturll", but also the angle of attack and the value of C_L introduced before.

Thirdly, we run "Analise", which computes aerodynamic results. The program uses the chord and twist angles computed by "Calcorda". Moreover, it also needs the TSR, wind speed, turbine diameter, air density and air kinematic viscosity introduced before.

Then, if the design method is the variation of angle of attack, we perform an interpolation of the optimum conditions with the Reynolds numbers obtained in the previous iteration with “Analise”. This interpolation allows us to get, for each radius, the optimum C_L/C_D, angle of attack and C_L.
For the other method design, constant angle of attack, we just replace in the input files the C_L/C_D, C_L and angle of attack by the value found with “Analise”.

Finally, the previous operations are carried out anew. At present, “Windturll” and “Calcorda” will use the new optimum data for the Reynolds number found by “Analise”, respectively the optimum C_L/C_D for “Windturll”, and the optimum angle of attack and C_L for “Calcorda”.

This loop will be completed when the results of “Analise” converge to the same value as “Windturll” at design conditions.

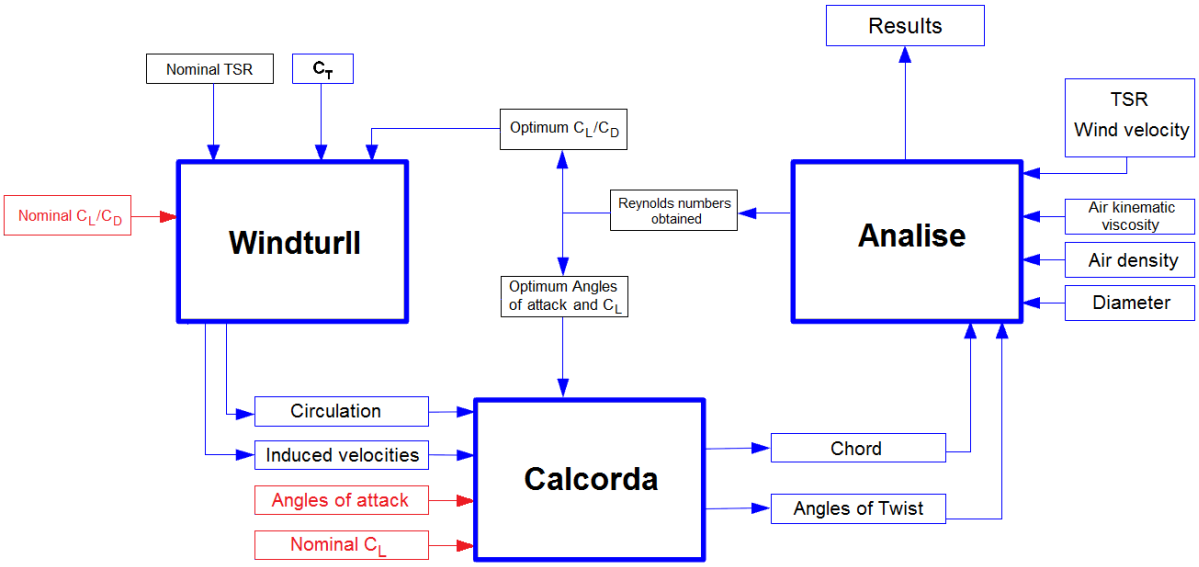

Fig. 4.1: Flow chart of the computational method.

4.2 Programs

4.2.1 Windturll

The calculations realized by this program are explained step by step in Appendix A.
To work, the program needs two input files:

- “Clcd.dat”, which comprises the data of C_L/C_D for different sections of the blade.
- “LL1data.dat”, which contains several data that allow Windturll to select the computational method. But it also comprises other data about the wind turbine like for example: the number of blades, rotor radius and hub radius in percent, tip speed ratio and thrust coefficient.

With these data, “Windturll” computes the following variables:

- Circulation distribution
- Pitch distribution
- Tangent distribution (β_i)
- Axial induced velocities
- Tangential induced velocities
- The number of iterations performed and the value of the power coefficient

All of the results above are calculated for inviscid conditions. C_L/C_D is used to obtain final values of C_T and C_P according to eq. (3-13) and (3-14).

4.2.2 Calcorda

The calculations performed by “Calcorda”, are explained step by step in Appendix B.
This program requires five input files:

- “LL1_data.dat”, which is the same file as before.
- “Perfil.dat”, which comprises the data of C_L and angles of attack for different sections of the blade.
- Values of the circulation computed by “Windturll”.
- Values of the axial induced velocities.
- Values of the tangential induced velocities.

“Calcorda” calculates the non-dimensional chord and the twist angles.

4.2.3 Analise

The calculations realized by this program, are explained step by step in Appendix C.
The input files for “Analise” are:

- “LL1data.dat”, which is the same as before.
- “Input_Analise.dat”, which contains the data of air density, air kinematic viscosity, tip speed ratio interval and wind speed interval.
- “C_L_C_D table.dat”, which comprises the values of C_L and C_D in function of the angles of attack. A part of this table will be shown in Appendix D.
- Values of the non-dimensional chord.
- Value of the twist angles.

In this case, the calculations are realized for viscous flow conditions.

4.2.4 Viscous and inviscid conditions

The loop, shown in Fig. 4.1, is completed when the data computed by “Analise” converge to the same value as “Windturll”. But why could the results converge to the same values if calculations are not realized in the same conditions?

The reason is that the circulation Γ, which has a lot of influence, is practically equal between the programs. The formula is:

$$\Gamma = \frac{C_L * V * c}{2} \tag{4-1}$$

As the chord c and V are the same, the circulation Γ depends on the lift coefficient C_L.

Fig 4.2 shows an example for the theoretical curves of C_L in function of angle of attack for the inviscid and viscous conditions. As shown in the graphic, the programs get a different angle of attack but finally the same lift coefficient value.
As a consequence, as the circulation is the same, the output results of “Windturll” are equal to “Analise”. Only the angle of attack is different.

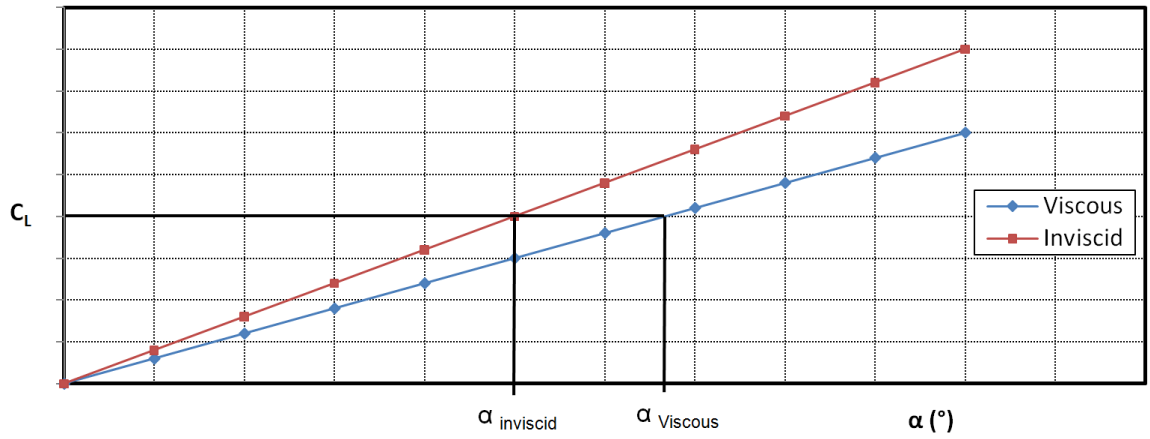

Fig. 4.2: Theoretical curves of C_L in function of angle of attack for the inviscid and viscous flow conditions.

4.3 Modifications

4.3.1 Programs modifications

The programs described previously are practically the same that were used in the previous project [8]. The only difference is the method to introduce the data of C_L and C_D for each Reynolds number in "Analise":

Previously the equations of two curves for each Reynolds number were employed:

- C_L in function of angles of attack.
- C_D in function of C_L.

At present, we introduce the file "C_L_C_D table.dat"; it consists of a table comprising the value of C_D and C_L in function of angles of attack, as shown in Appendix D.

Moreover, with the new design criteria of this thesis, the values of C_L are higher near the hub and the tip of the blades than before. In fact, this increase is caused by the variation of angles of attack to get the optimum conditions. This is going to pose problems.

The solution to this problem is explained in Appendix D.

Chapter 5
Design Criteria

This chapter describes the design criteria used to base the design for maximizing the power coefficient.

5.1 Aerodynamic Design Criteria

The Table 5.1 presents the aerodynamic design parameters used in this thesis. Some parameters are kept fixed and have been determined based on the previous project of Pôtra [8]. The following parameters were varied according to different criteria:

- *The choice of airfoil*: Airfoil will be different to try to improve the power.

- *The angle of attack*: In this thesis, it varies along the blade to give the optimum conditions. In the previous project, the angle of attack was kept constant.

Table 5.1: Aerodynamic Design Parameters.

Number of blades	3
Rotor diameter	2.5 m
Hub diameter	0.375 m
Tip speed ratio	7
Wind speed	10 m/s
Angle of attack (α)	Optimum C_L/C_D
Airfoil	?

The wind speed U of 10m/s and the Tip Speed Ratio TSR of 7, chosen for the designs, determine the velocity triangle geometry. In consequence, the aerodynamic pitch angle β will be fixed for each radius on the blade.
The velocity triangle is represented in Fig. 3.3 and is composed by ωr and U.

Moreover, as the power of SWTs is generally controlled by stall regulation, the geometry is fixed. By this way, the pitch angle ψ will be constant for each radius along the blade. So the angle of attack will depend only on the aerodynamic induced pitch angle β_i.

Fig. 5.1 shows the main dimensions of the present wind turbine designs.

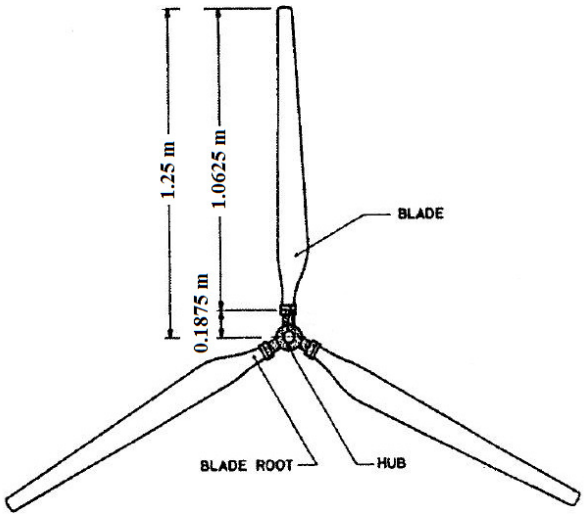

Fig. 5.1: Main dimensions of the present wind turbine designs.

5.2 Candidate airfoils

One of the important design criteria is the choice of the airfoil. Several airfoils found on internet have been compared with their aerodynamic characteristics for different Reynolds numbers (Re). Finally, two airfoils have been selected [21]:

- *Eppler E387*
- *Wortmann FX 63-137*

The Eppler *E387* airfoil was the previous one used by Pôtra in his project [8]. This airfoil will be used to compare the new method (variation of angle of attack for Optimum C_L/C_D) and the previous one (constant angle of attack).

The base airfoils of *E387* and *FX 63-137* are depicted in the Fig. 5.2. Note that the maximum thickness of *FX 63-137* represents 13.63 % of the chord while *E387* has a maximum thickness of 9.06 % chord. Inspection of the airfoil shapes shows that the airfoil *FX 63-137* has more camber than *E387*, and this difference gives a higher lift coefficient at the same angle of attack.

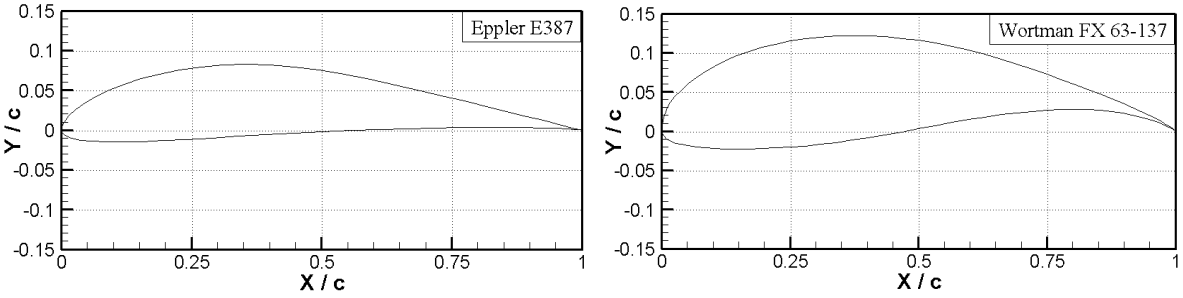

Fig. 5.2: E387 and FX 63-137 base airfoils.

The characteristics of these airfoils are shown in Appendix E.1 and E.2 [21].
These characteristics have been calculated using the XFOIL code with free transition [21]. XFOIL is an interactive program which allows the design and analysis of airfoils. Free transition means that the transition point on the airfoil was let free during the calculation. So the transition point in the boundary layer which separates the laminar and the turbulent flow could move along the airfoil and was not fixed.

Fig. 5.3 shows aerodynamic curves for different Reynolds numbers for *E387*.
Note that the C_L curves are almost identical until the angle of attack of 8°.
When the data of C_L/C_D calculated by XFOIL are plotted, we remark that the curves are not very smooth. The curves for Reynolds numbers of 100 000 and 500 000 differ from the others.

Fig. 5.4 shows aerodynamic curves for different Reynolds numbers for *FX 63-137*.
In this case, the C_L curves differ and the difference is clearly visible. Note that when the Reynolds number increase, the lift coefficient increases for the same angle of attack. This is not seen in the case of Eppler.
Always concerning *FX 63-137*, the forms of C_L/C_D curves are similar. Moreover, they are also smoother.

Table 5.2 shows the maximum C_L/C_D values from data for both airfoils. Note that the C_L/C_D characteristics of Wortmann are better for each Reynolds number.

Table 5.2: Maximum values of C_L/C_D for E387 and FX 63-137.

	Re = 100 000		Re = 200 000		Re = 350 000		Re = 500 000	
Name	C_L/C_D max	α (°)	C_L/C_D max	α (°)	C_L/C_D max	α (°)	C_L/C_D max	α (°)
E387	56.79	7	81.94	6	103.04	6	115.08	5
FX 63-137	59.14	8	90.64	6	112.66	5	126.68	5

When the curves for both airfoils are compared, we see that the values of C_L/C_D for *FX 63-137* are higher for every Reynolds number.

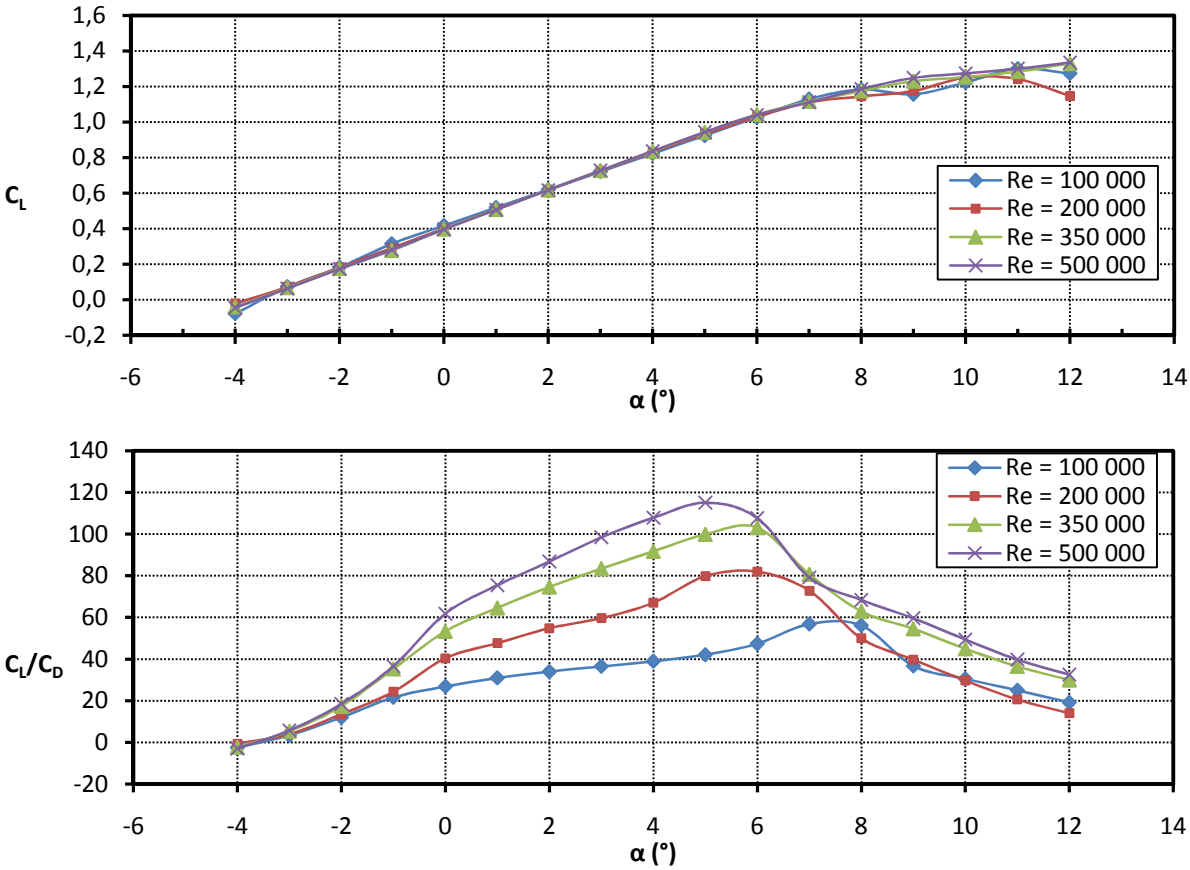

Fig. 5.3: Aerodynamic curves for E387.

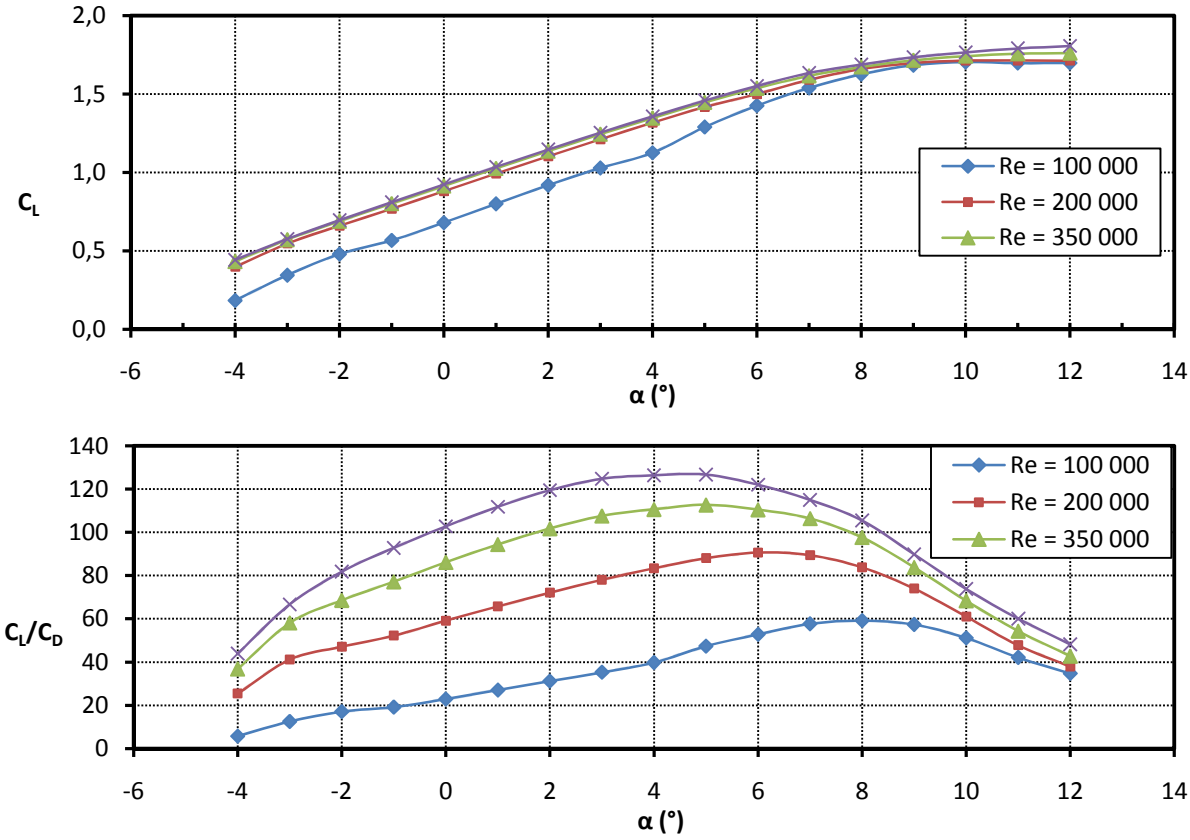

Fig. 5.4: Aerodynamic curves for FX 63-137.

5.3 Optimum conditions

5.3.1 Description

According to the new aerodynamic design criteria, the angle of attack varies along the blade to give maximum C_L/C_D in each radius. These conditions are called “Optimum conditions”.

But now the question is: How to find the optimum conditions for each radius?

At the beginning, with the help of the data for both airfoils, the maximum C_L/C_D is determined by quadratic interpolation for each Reynolds number. After that, the corresponding angle of attack, optimum C_L and C_D may be found. So now we have the optimum data giving the maximum C_L/C_D. Table 5.3 presents these optimum characteristics for both airfoils.

The Reynolds number varies with radius because the chord and the incident velocity vary. We perform the interpolation with the Reynolds number at each radius in the table with the optimum condition and we may find the optimum characteristics at that radius. So, we obtain the optimum angle of attack giving the maximum C_L/C_D by knowing the Reynolds number.

Table 5.3: Interpolated optimum characteristics for E387 and FX 63-137.

E387

Re	C_L/C_D max	α opt (°)	C_L	C_D
100 000	57.738	7.431	1.152	0.02028
200 000	82.487	5.689	1.000	0.01220
350 000	104.84	5.626	1.005	0.00975
500 000	115.086	4.995	0.943	0.00820

FX 63-137

Re	C_L/C_D max	α opt (°)	C_L	C_D
100 000	59.146	7.946	1.620	0.02740
200 000	90.703	6.180	1.516	0.01671
350 000	112.664	4.981	1.445	0.01282
500 000	127.162	4.566	1.414	0.01112

Fig. 5.5 represents the optimum curves for the E387 airfoil. Note that the C_L and angle of attack curves show some oscillations. This leads to a high gradient between Reynolds number of 100 000 and 200 000. This large gradient may be a source of errors in the extrapolation to low Reynolds numbers.

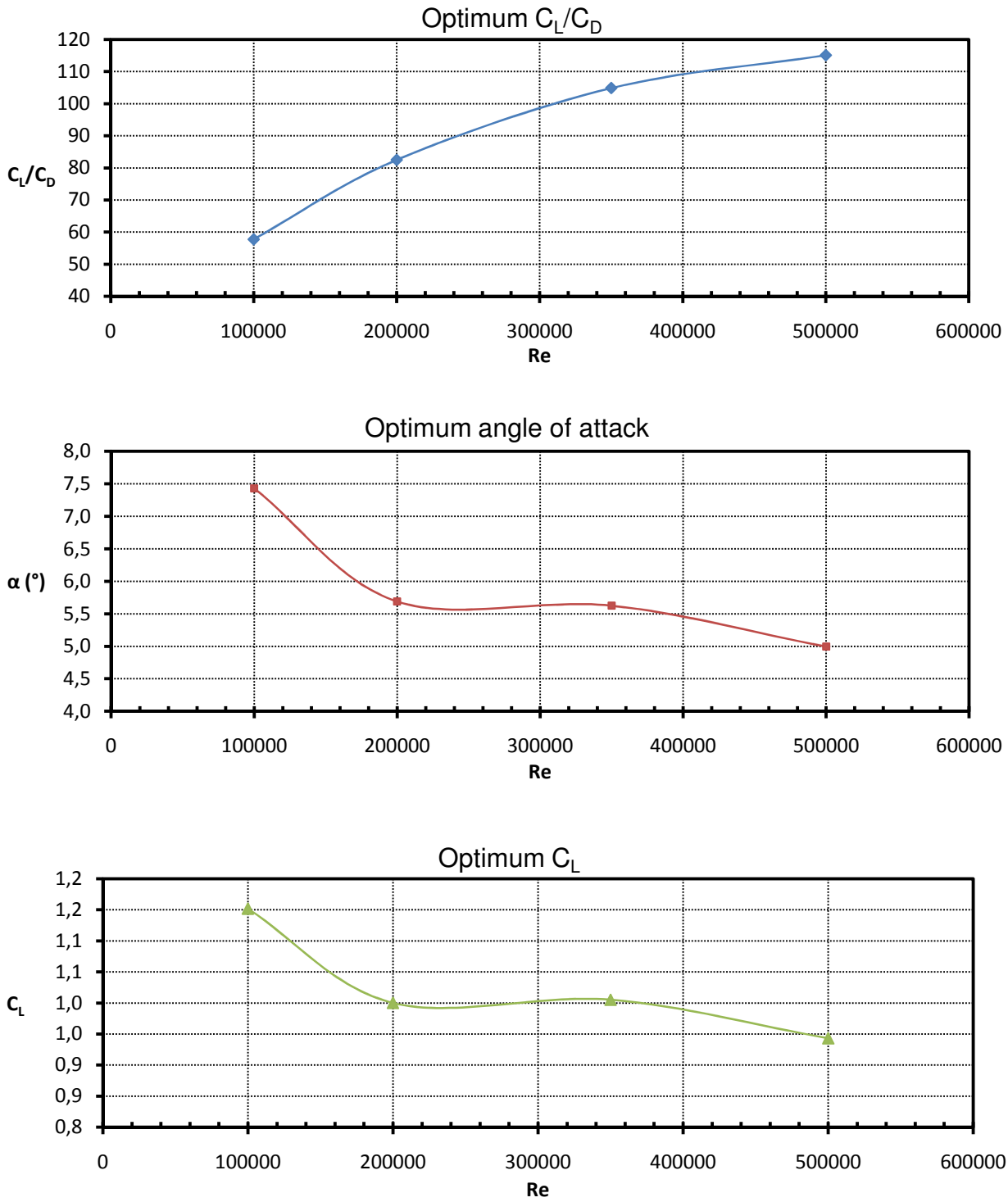

Fig. 5.5: Optimum curves for airfoil E387.

Fig. 5.6 shows optimum curves for airfoil *FX 63-137*. Remark that these curves oscillate less than the curves for *E387*.

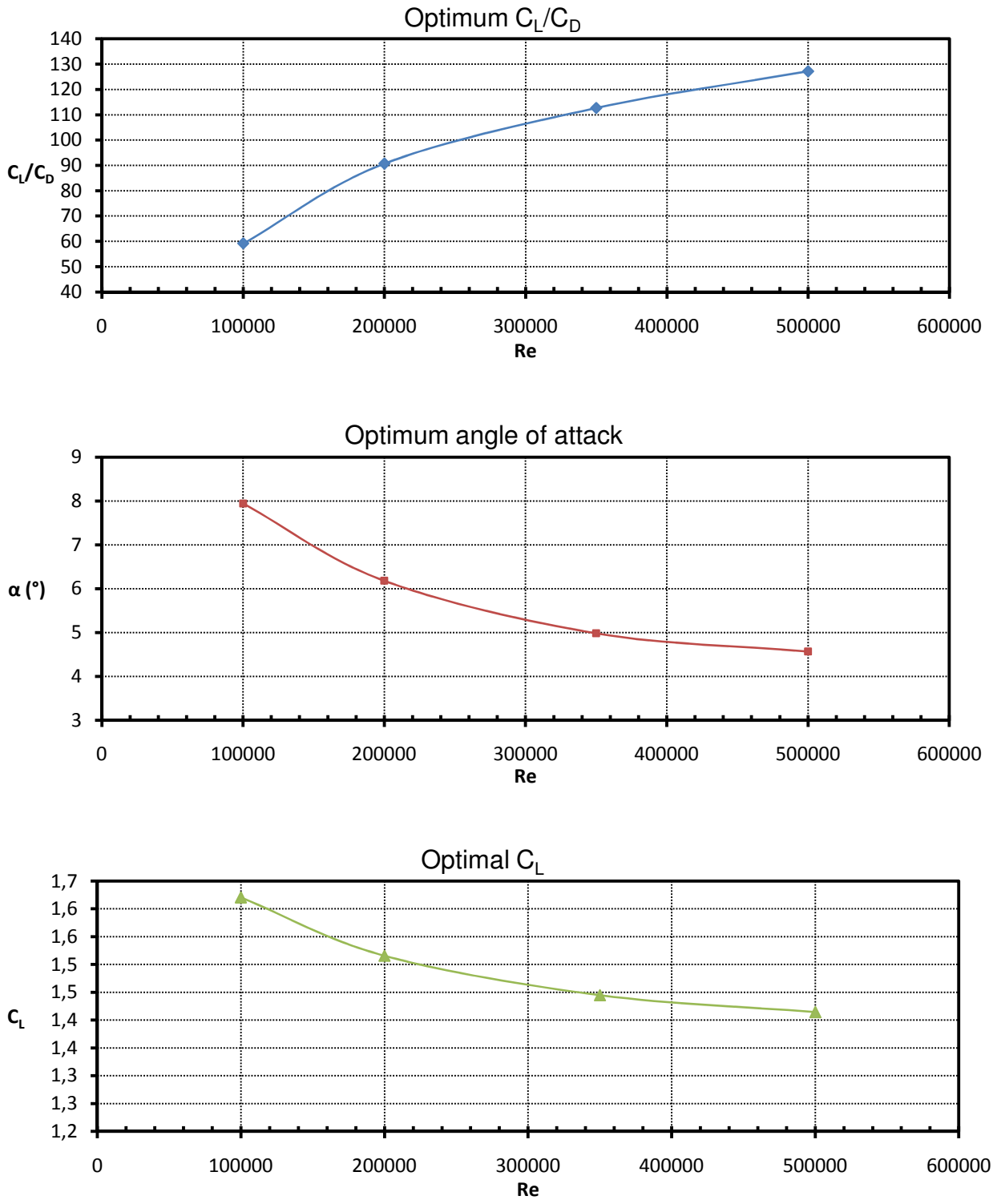

Fig. 5.6 Optimum curves for airfoil FX 63-137.

5.3.2 Modification for low Reynolds numbers

We know that small values of the Reynolds number are obtained near the hub and the tip of the blades. These small values of Reynolds number on the tip and hub of the blades are caused by the calculated small chord values at the tip and hub. Unfortunately, this poses a problem.

The problem occurs because the program realizes a rough extrapolation for the low Reynolds numbers. In fact, the aerodynamic characteristics for both airfoils are only available for a minimum value of Reynolds number of 100 000 [Appendix E.1 and E.2]. Moreover, as the optimum curves of C_L and α plotted in the Fig. 5.5 have a high gradient between Reynolds numbers of 100 000 and 200 000, the program will find by linear extrapolation unreal values, too high, for these characteristics.

For this reason, a new curve for a Reynolds number of 10 000 has been added. Fig. 5.7 shows the new curves for the small Reynolds number for airfoils *E387* and *FX 63-137*. These curves have been plotted from a quadratic equation and then modified by moving the maximum point to give almost the same form than the other curves.
At present, the program performs an interpolation between 10 000 and 100 000. By this way, the value of C_L is reduced. It is expected that this procedure gives more reliable results than the previous linear extrapolation.

The comparison between the extrapolation and the interpolation to obtain C_L values is shown in Table 5.4 for the airfoil *E387*. This table clearly shows that the values near the tip and hub have decreased but elsewhere they have stayed almost unchanged.

Table 5.4: Comparison between extrapolation and interpolation for E387.

		Value of C_L	
r/R	Re/1000	Extrapolation	Interpolation
0.151	23.79	1.266	1.165
0.162	69.62	1.203	1.158
0.182	111.15	1.138	1.136
0.213	150.16	1.079	1.077
0.252	180.96	1.032	1.030
0.299	201.91	1.002	1.000
0.353	211.39	1.002	1.001
0.412	217.09	1.002	1.001
0.476	220.60	1.002	1.001
0.542	222.80	1.002	1.001

		Value of C_L	
r/R	Re/1000	Extrapolation	Interpolation
0.608	224.12	1.002	1.001
0.674	224.61	1.002	1.001
0.738	223.87	1.002	1.001
0.797	220.77	1.002	1.001
0.851	213.14	1.002	1.001
0.898	196.95	1.006	1.005
0.937	162.55	1.059	1.059
0.968	119.07	1.127	1.127
0.988	73.50	1.197	1.157
0.999	25.05	1.260	1.165

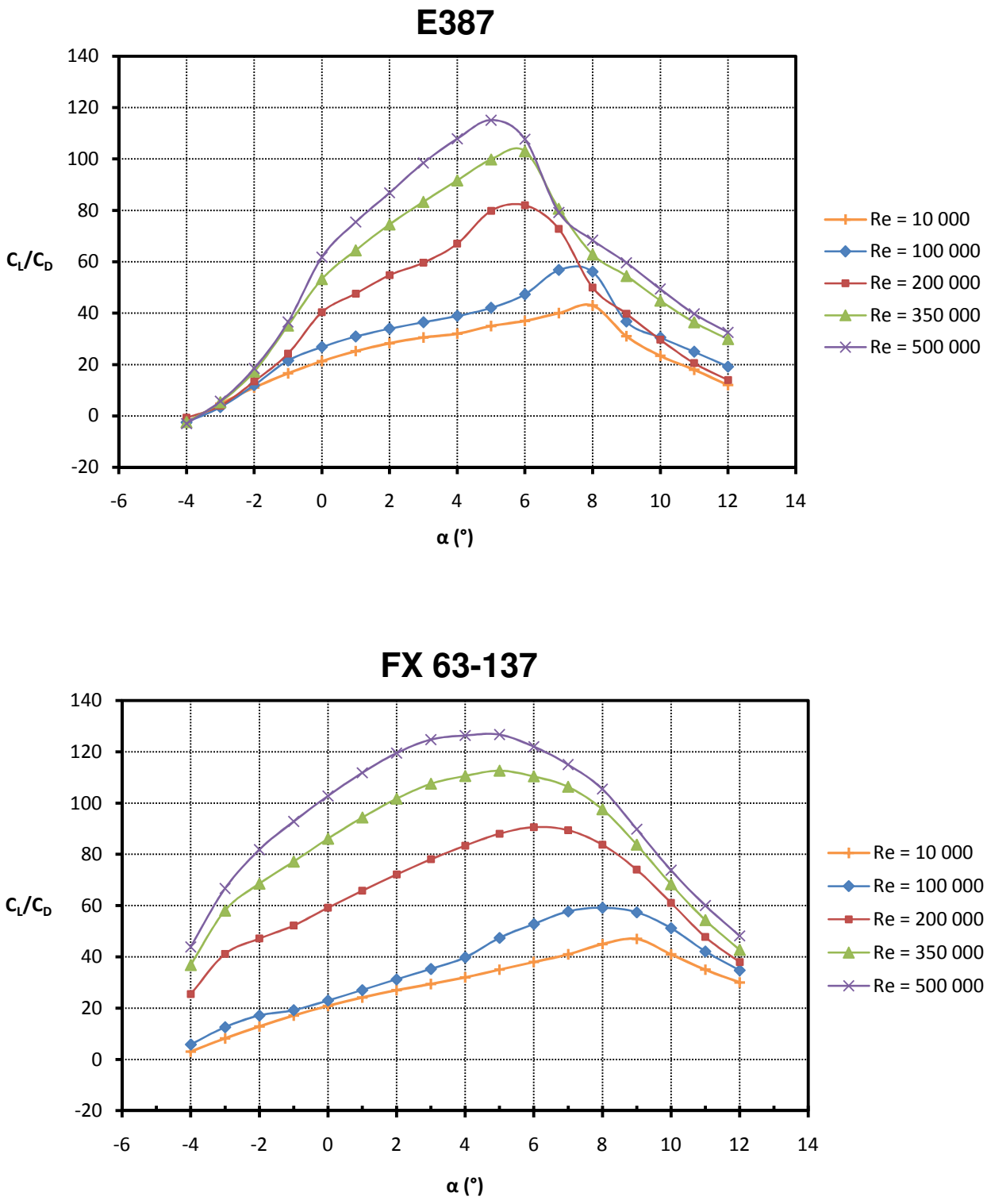

Fig. 5.7: Airfoil C_L/C_D data with the new curves for a Reynolds number of 10 000.

Chapter 6
Aerodynamic Designs and Analysis

This chapter presents and compares the designs of a small wind turbine using different aerodynamic design criteria. Two different comparisons are shown. The first compares the designs for *Constant angle of attack* and for varying angle of attack, giving optimum C_L/C_D, for the *E387* airfoil. The second compares the *E387* and *FX 63-137* airfoil for the design at *Optimum* C_L/C_D.

6.1 Assumption

In the calculations, the air is assumed to have a kinematic viscosity equal to $1.4607*10^{-5}$ m^2/s at a temperature of 15°C and a density of 1.225 kg/m^2.

The calculations are made with the design parameters defined in chapter 5, except for the other method in the first comparison. In this case, the angle of attack will be kept constant.

6.2 Comparison between designs at constant angle of attack and Optimum C_L/C_D

The first comparison concerns two different design options:

- *Constant angle of attack*: the angle of attack is kept constant along the blades. This method has been used in [8].
- *Optimum* C_L/C_D: the angle of attack varies along the blades to give the optimum conditions.

To compare both designs, the Eppler *E387* airfoil will be used. The complete detailed aerodynamic results are shown in Appendix F.

6.2.1 Aerodynamic point of view

Fig. 6.1 shows the comparison between both designs. The distribution of the non-dimensional chord is shown in Fig. 6.1.a. Note that the chord with *Optimum* C_L/C_D is larger than *Constant angle of attack*.

The circulation shown on Fig. 6.1.b is the same for *Constant angle of attack* and *Optimum* C_L/C_D.

Fig. 6.1.c concerns the angle of attack and it is different between both design methods. The angles in the middle of the blades for the red circle curve, which represents the *Optimum* C_L/C_D, are almost constant and smaller than *Constant angle of attack*. Near the hub and tip of the blades, the situation is reversed; the angles are higher for *Optimum* C_L/C_D.

In Fig. 6.1.e, the values of drag coefficient C_D for *Optimum* C_L/C_D are smaller.

The lift coefficient C_L was constant with *Constant angle of attack* as shown in Fig. 6.1.f. At present, *Optimum* C_L/C_D leads to a variation in the value of C_L which is the same graphic form than for Fig. 6.1.c. Clearly, we note that the angle of attack influences C_L.

In Fig. 6.1.g showing Reynolds number, we remark that the Reynolds number for *Optimum* C_L/C_D is also larger. In fact, this is explained by this formula:

$$Re = \frac{V\,c}{\nu} \tag{6-1}$$

For a constant incident velocity V and viscosity ν, as the chord c is larger, the Reynolds number is also larger.

And finally the last Fig. 6.1.h shows an increase of C_L/C_D with *Optimum* C_L/C_D. This increase is mainly due to the increase of Reynolds number.

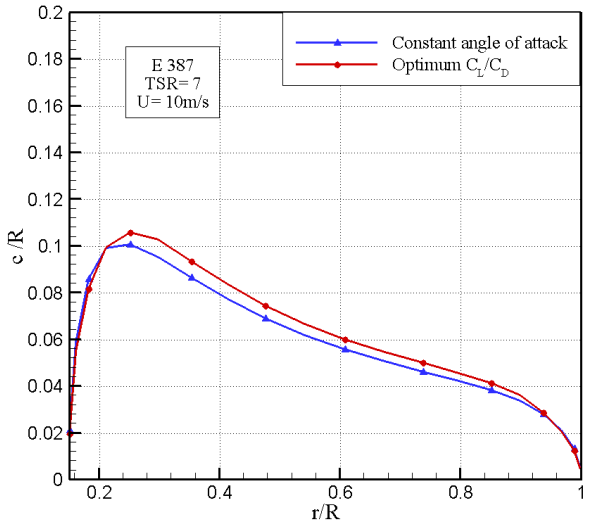

a) Chord/R

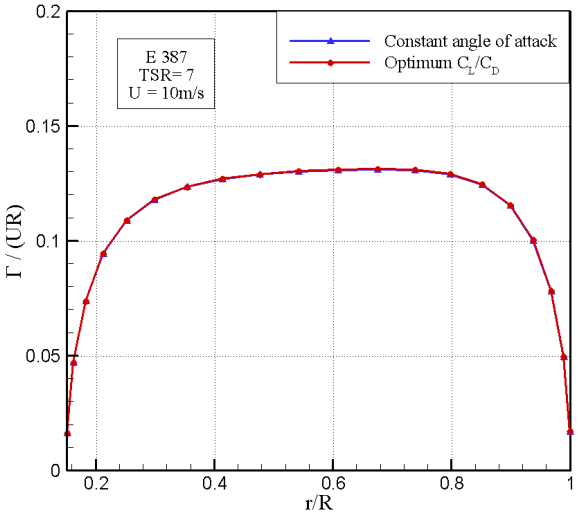

b) Circulation

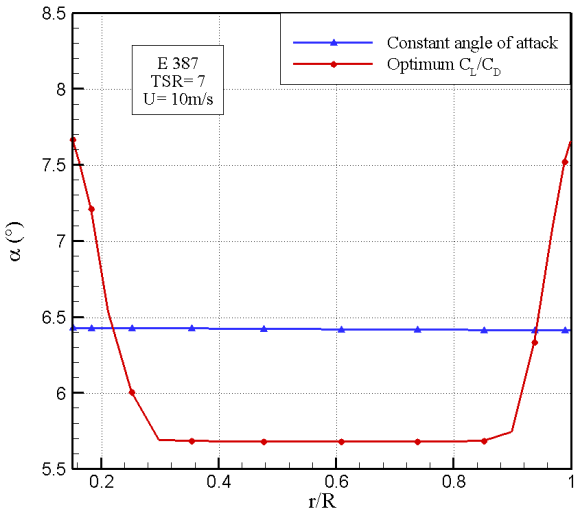

c) Angle of attack

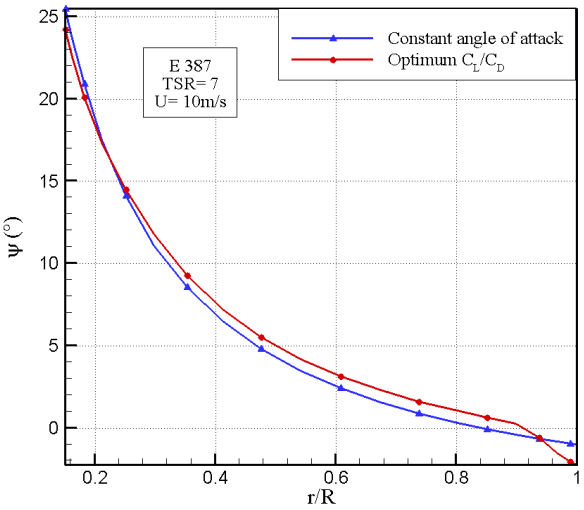

d) Pitch angle

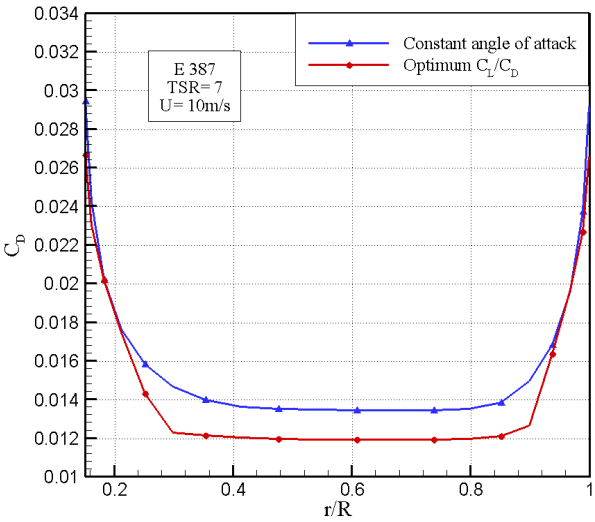

e) C_D

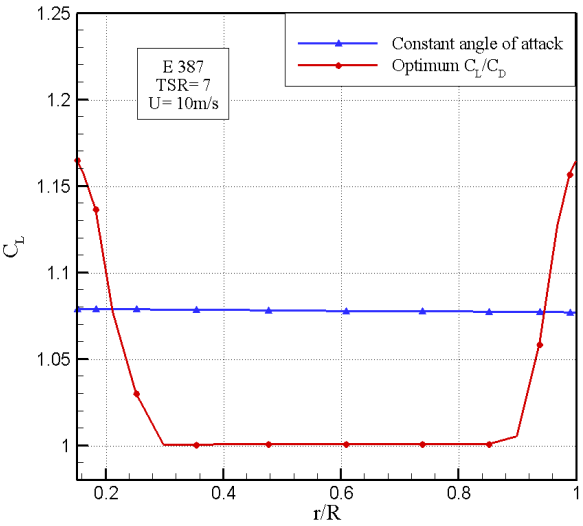

f) C_L

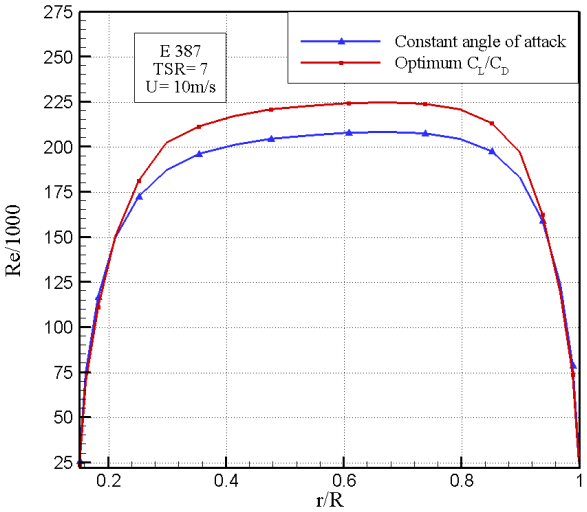

g) Reynolds number

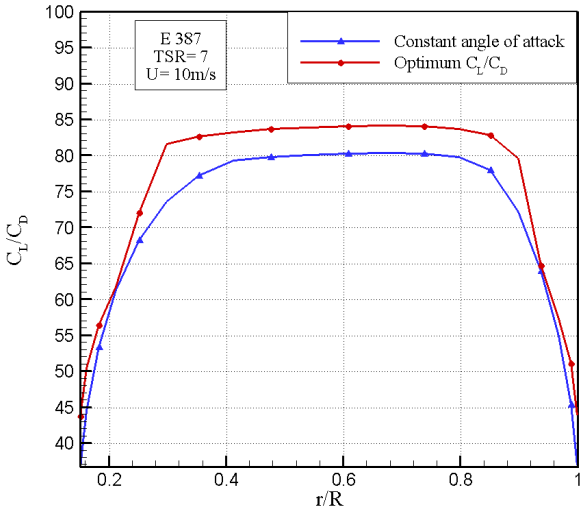

h) C_L/C_D

Fig. 6.1: Comparison between Constant angle of attack and Optimum C_L/C_D for E387.

6.2.2 Power and Thrust coefficient

Table 6.1 shows the values of the power coefficient C_P and thrust coefficient C_T for both designs.

The comparison of the results indicates a slight increase of C_P and C_T with the design of *Optimum* C_L/C_D. This is caused by the higher values of C_L/C_D as seen in the formula (3-37) and (3-38).
However, by analysing Fig. 6.4.f, we note that, generally along the blade, the increase of C_L/C_D is about 4.7% compared with *Constant angle of attack*. This causes only a C_P increase of 0.6%. We come to the conclusion that for this design condition the value of C_L/C_D has a relatively small influence in the C_P.

Table 6.1: Power and Thrust coefficient for both design methods.

	C_T	C_P
Constant angle of attack	0.777	0.463
Optimum C_L/C_D	0.779	0.467

6.3 Comparison of airfoils for design method at optimum C_L/C_D

The second comparison concerns the design at *Optimum* C_L/C_D applied to:

- *The airfoil Eppler E387*
- *The airfoil Wortmann FX 63-137*

Both airfoils have already been compared in chapter 5. The complete detailed aerodynamic results are shown in Appendix F.

6.3.1 Aerodynamic point of view

Fig. 6.2 shows the comparison between *E387* and *FX 63-137*. Fig. 6.2.a concerns the non-dimensional chord. The blade chord of *FX 63-137* is smaller than *E387*. This is due to the larger design lift coefficient of *FX 63-137*, as shown in Fig. 6.2.f according to:

$$c = \frac{2\,\Gamma}{C_L * V} \tag{6-2}$$

The circulation is identical for both airfoils, as shown in Fig. 6.2.b.

In Fig. 6.2.c, the angle of attack of *FX 63-137* is a lot higher than the angle of attack of *E387*.

For each radius, the pitch angle of *E387* is larger than *FX 63-137*, as shown in Fig. 6.2.d.

Fig. 6.2.e shows that *FX 63-137* has a larger drag coefficient C_D.

The larger angle of attack of *FX 63-137* leads to a larger lift coefficient C_L than *E387,* as shown in Fig. 6.2.f.

In Fig. 6.2.g, the Reynolds number of the *FX 63-137* is smaller as consequence of the chord, as explained before with eq. (6-1).

Finally, Fig. 6.2.h shows a decrease of C_L/C_D for *FX 63-137* compared with *E387*. This result seems strange because it does not accord with the initial aerodynamic characteristics. Indeed, the chapter 5 showed that C_L/C_D was better for *FX 63-137*.
This explanation arises from the Reynolds number. Let us remember that “Analise” performs the interpolation of C_L/C_D in function of the Reynolds number found. So, as the blades of *FX 63-137* have a smaller chord than *E387*, the Reynolds number is smaller and the C_L/C_D also.

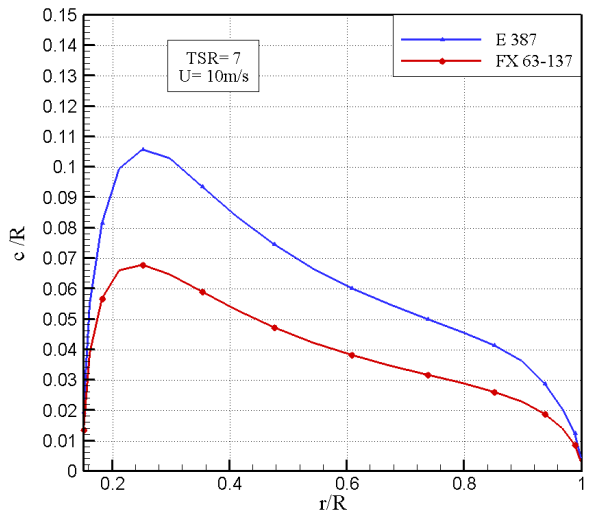

a) Chord/R

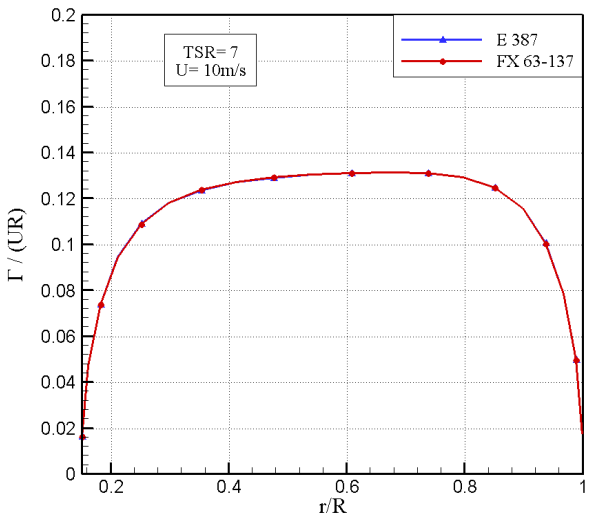

b) Circulation

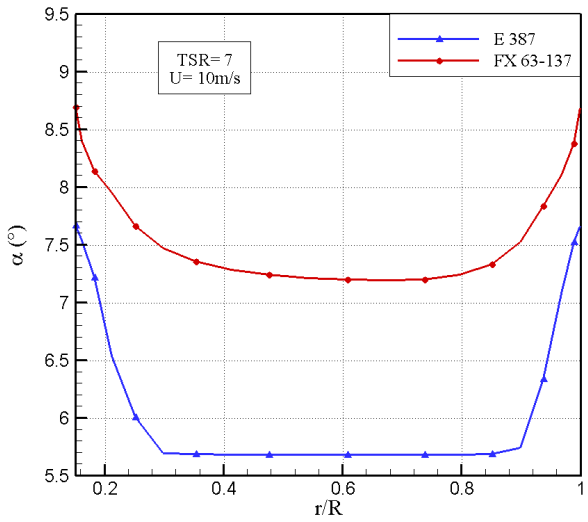

c) Angle of attack

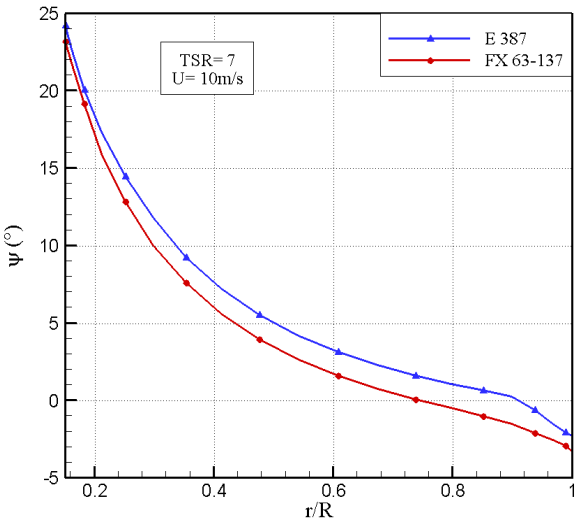

d) Pitch angle

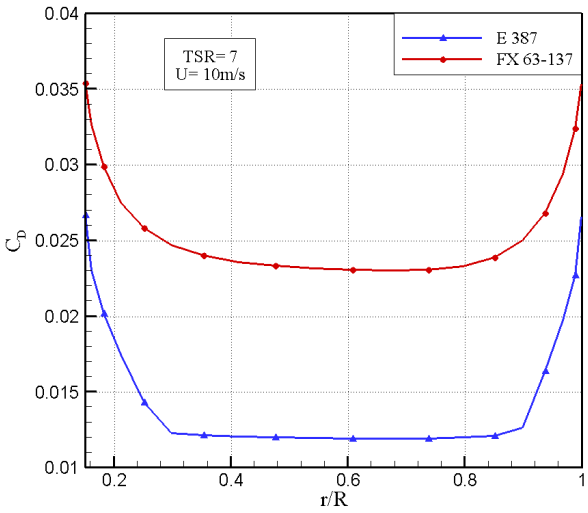

e) C_D

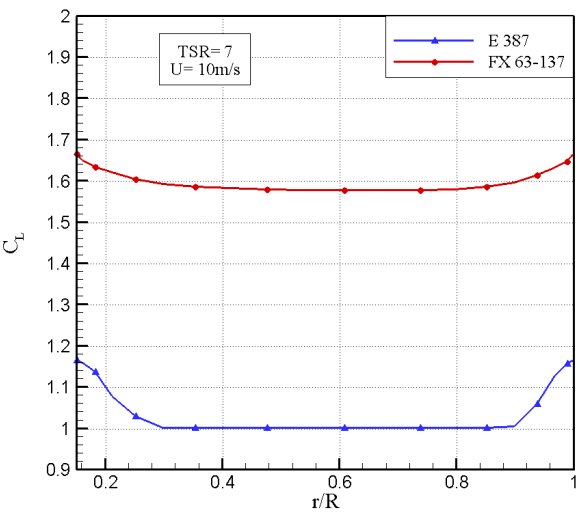

f) C_L

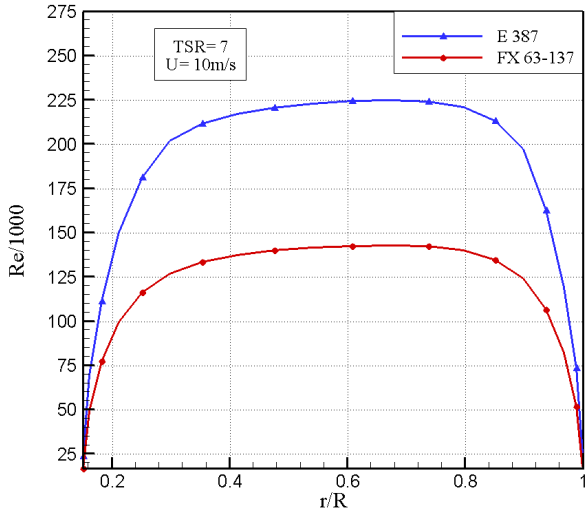

g) Reynolds number

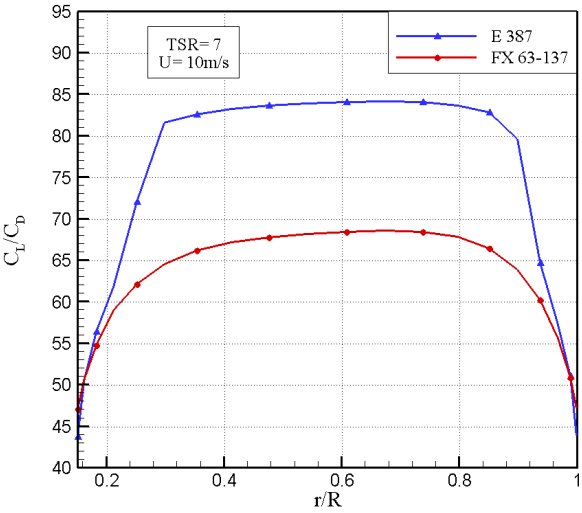

h) C_L/C_D

Fig. 6.2: Comparison between E387 and FX 63-137 for design at Optimum C_L/C_D.

6.3.2 Power and Thrust coefficient

Table 6.2 shows the values of the power coefficient C_P and thrust coefficient C_T of *E387* and *FX 63-137* for design at Optimum C_L/C_D.

The comparison of the results indicates a decrease of C_P for airfoil *FX 63-137*. Indeed, if the curves in Fig. 6.2.h are compared, the C_L/C_D of *FX 63-137* decreases by 18.51% compared with *E387*, which causes a decrease of 2.14% in C_P.

Table 6.2: Power and Thrust coefficient for both airfoils.

	C_T	C_P
E387	0.779	0.467
FX 63-137	0.78	0.457

6.4 Remark

At the end of this chapter, we have shown that the best design is achieved with *E387* with *Optimum* C_L/C_D. At present, we can determine the power curve for this design in order to calculate the Annual Energy Production (AEP). However, it is interesting to compare the AEP for both airfoils at *Optimum* C_L/C_D to draw conclusions. Therefore, the AEP calculations will be realized for *E387 and FX 63-137*

Chapter 7
The Power curve

This chapter explains the analysis, modifications and choices made to determine the turbine power curve. This is required to evaluate the Annual Energy Production of a wind turbine on a specific site.

7.1 Chord modifications

The previous chord distributions, found in chapter 6 for both airfoils, are theoretical and are a result of the lifting line calculation which assumes zero circulation, so zero chords, at the tip and hub. Although this is not real at the hub, the calculations remain valuable because this assumption does not influence much the results.
In reality, the chord and the circulation are larger near the hub. So, to get acceptable results of the stress, the chord near the hub needs to be larger. To that end, we assume a chord near the hub equal to the maximum chord. So, the chord at the hub for *E387* is $0.106 * 1.25m = 13.25\ cm$ and for *FX 63-137*, the chord at the hub is $0.068 * 1.25m = 8.5\ cm$.

Fig. 7.1.a and Fig. 7.1.b show respectively the modification of the chord for *E387* and *FX 63-137*. This modification avoids too large stresses and it does not have much influence on the power coefficient C_P.

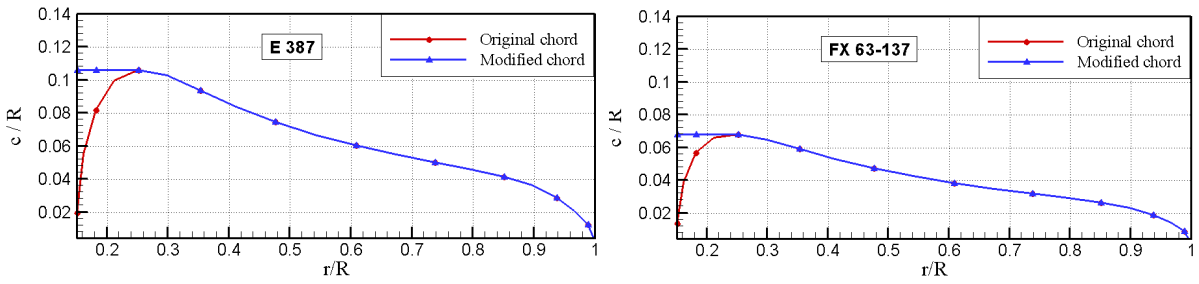

a) Chord of E387

b) Chord of FX 63-137

Fig. 7.1: Chord modification for the designs with E387 and FX 63-137.

7.2 Analysis at varying Tip Speed Ratio

7.2.1 Power curves

To calculate the energy production of wind turbines, the power as function of wind speed, namely the power curve, is necessary. This curve may be plotted with the help of the program “Analise”, which computes the power for different TSRs and wind speeds.

For each TSR, we obtain different powers at each wind speed, so each TSR represents a different power curve. The purpose of this step is to determine the value of TSR that maximizes the power.

Fig 7.2.a and Fig 7.2.b show respectively the power curves of *E387* and *FX 63-137* for different TSRs. Note that the power begins to increase from 4 m/s. This value is the cut-in wind speed which defines the starting point of wind turbine operating curve. In addition, when both graphs are compared for a TSR of 7, we can see that the power curves are the same for *E387* and *FX 63-137*. In reality, the power values are slightly different because of power coefficient divergence, but it is impossible to notice it on these graphs. The reason of this arises from the large influence of the wind speed in the power formula. Moreover, as scheduled in design criteria, the optimum TSR giving the largest power is 7 for *E387* and *FX 63-137*. However, this value may be refined. To do this, as the power curve does not allow differentiating very close values, we have to plot the power coefficient versus wind speed.

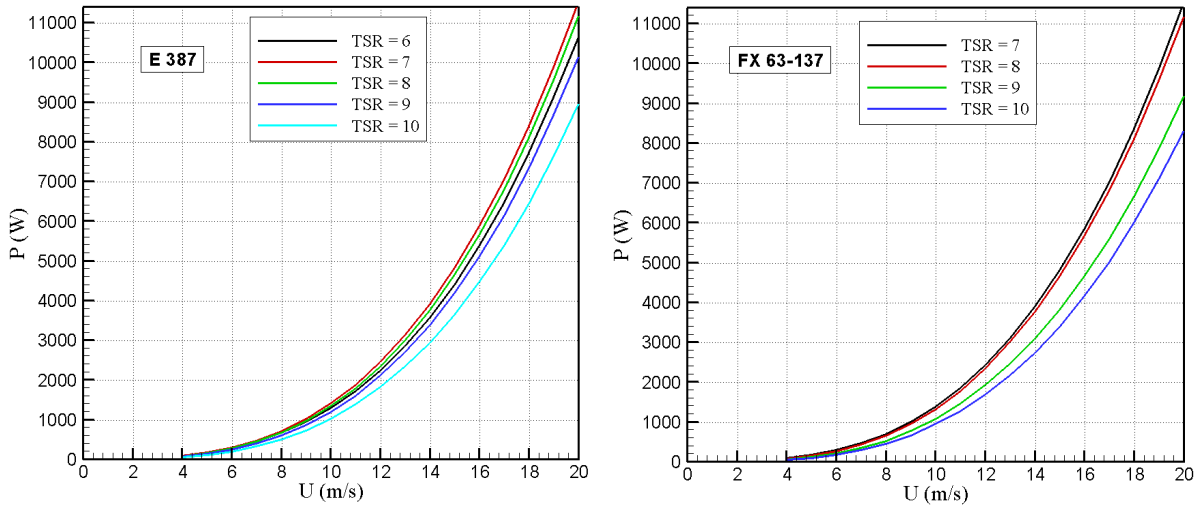

a) E387 b) FX 63-137

Fig. 7.2: First Power curves for the designs with E387 and FX 63-137.

7.2.2 Power coefficient curves

Fig. 7.3 shows power coefficient graphs as function of wind speed. This allows getting curves with better precision and simplifying the choice of optimum TSR to give maximum power.

As the best TSR for *E387* was 7 in the previous power curve, we have plotted, in the Fig. 7.3.a as function of wind speed, the TSRs around 7 to refine our choice. At present, note that there are different TSRs, 6.5, 6.75 and 7, giving the best power coefficient as function of wind speed. We can generate a more precise curve which shows the optimum TSR versus wind speed, as presented in Fig. 7.4.a.

Concerning *FX 63-137* in Fig. 7.3.b, note that there are also different TSRs, 6.75, 7 and 7.25, giving the best power coefficient in function of wind speed. A more precise curve which shows the optimum TSR versus wind speed is presented in Fig. 7.4.b.

As the power depends on the cube of the wind speed, large wind speeds are more important than small ones. Therefore, for the calculations, we consider only TSRs giving the best C_P from a wind speed of 7 m/s. In fact, the best TSRs before this wind speed are not interesting to study because they have a small influence on the power due to the small wind speed. Moreover, Fig. 7.4 being too precise, the choice of TSR values is made in Fig. 7.3.

So, four cases will be considered:

- *Airfoil Eppler E387 with TSR = 6.75,* renamed "*Ep-6.75*".
- *Airfoil Eppler E387 with TSR = 7,* renamed "*Ep-7*".
- *Airfoil Wortmann FX 63-137 with TSR = 7* renamed "*Wo-7*".
- *Airfoil Wortmann FX 63-137 with TSR = 7.25*, renamed "*Wo-7.25*".

The power and power coefficient of selected TSRs are shown in Appendix G.

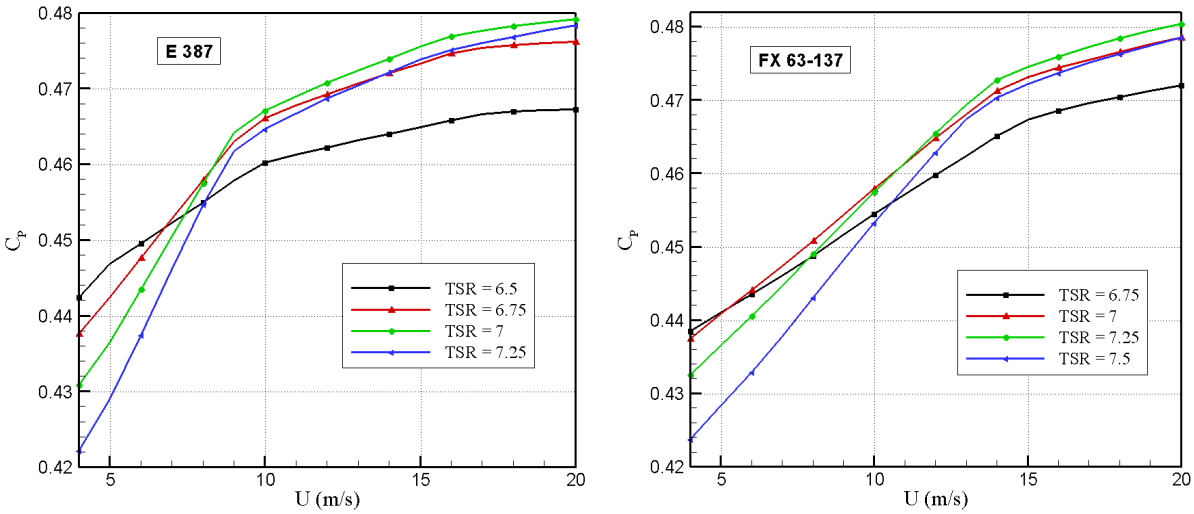

a) E 387 b) FX 63-137

Fig. 7.3: Power coefficient curves for E387 and FX 63-137.

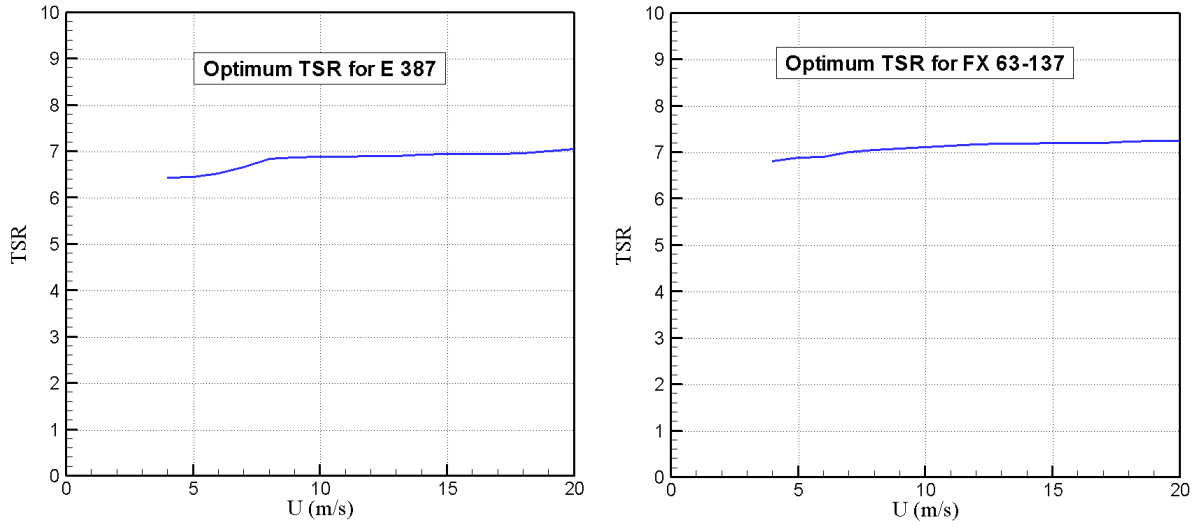

a) E387 b) FX 63-137

Fig. 7.4: Optimum TSR for the designs with E387 and FX 63-137.

7.3 Stresses on the blades

The power curves shown before in Fig. 7.2 were theoretical. In fact, it is obvious that a wind turbine will have its limit stress and is not able to increase the power for all wind speeds without exceeding this limit. As a consequence, the stresses have to be calculated on the blades to define the rated wind speed.

7.3.1 Program description

The stress and different other parameters on the blades are calculated by the program “Blade force”. This program was used by Pôtra and is described in [8]. However, a brief description of this software is presented hereafter.

7.3.1.1 Input files

The input files for the program “Blade force” are:

- “LL1data.dat”, which comprises the hub radius and the number of lifting line elements.
- “Blade_Force_Input.dat”, which is explained hereunder.
- “Input_Analise.dat”, which contains the data of air density, air kinematic viscosity, tip speed ratio slot and wind speed slot.
- Results of “Analise” for different wind speeds and TSRs.
- Values of the non-dimensional chord.
- Values of twist angle.

7.3.1.2 New input explanation

The input “Blade_Force_Input.dat” comprises data which have to be calculated beforehand. The first value is the blade density and depends on the material of the blade. As in the thesis of Pôtra [8], we consider a massive blade made in Polycarbonate Plastic reinforced with carbon fibers and whose density is 1400 kg/m^3. This material has been chosen for its cheap price and its possibility of manufacturing process by injection. However, this plastic has a low tensile strength value but a good mechanical resistance. The addition of carbon fibers allows improving the resistance.

Secondly, the equation of the thickness distribution has to be introduced. To get this thickness curve, we use the program Microsoft Excel and we calculate the difference between the upper and the lower surface values. With these data, the polynomial curve is plotted to obtain the approximate equation of the thickness distribution. Fig. 7.5 shows all of these curves for *E387* and *FX 63-137*.

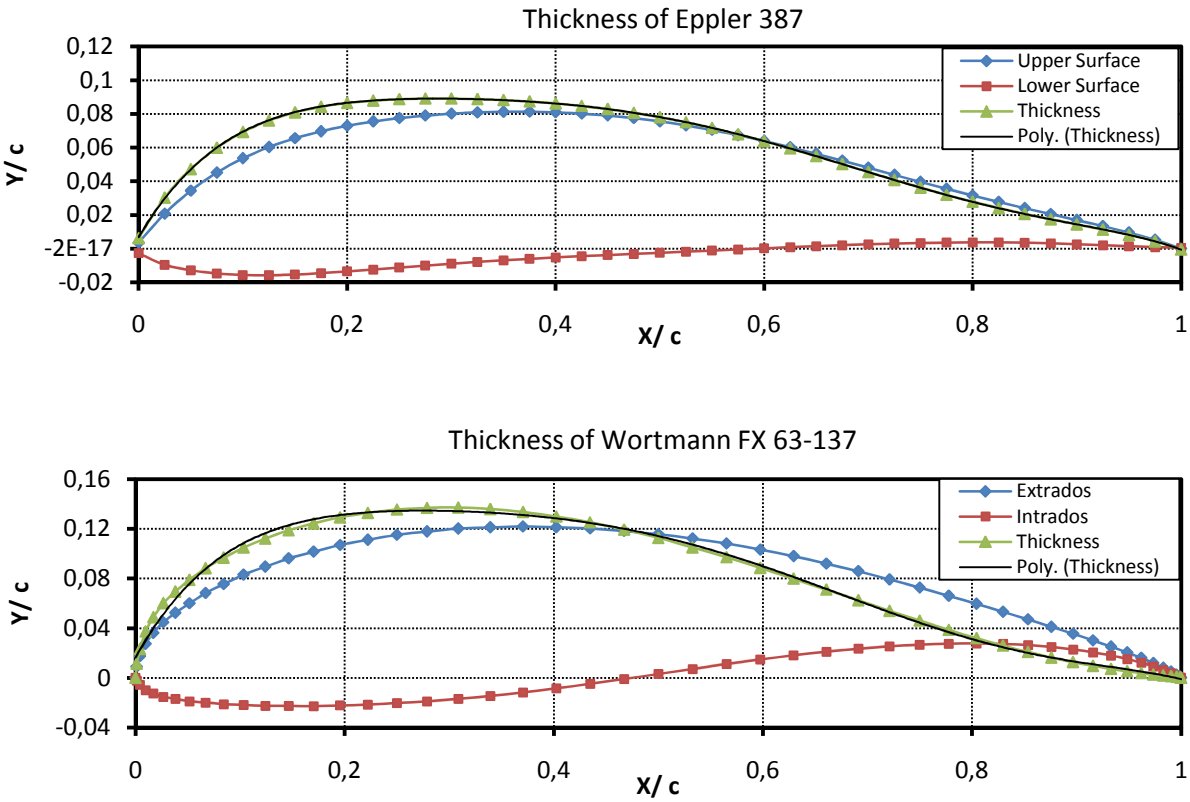

Fig. 7.5: Thickness curves for E387 and FX 63-137.

Finally, the last values introduced are the maximum thickness and the form factor whose formula is:

$$FF = \frac{A}{c * d_{max}} \tag{7-1}$$

where A is the area section, c is the chord and d_{max} is the maximum thickness. The data of these parameters for both airfoils are shown in Table 7.1.

Table 7.1: Maximum thickness and form factor for E387 and FX 63-137.

	Eppler 387	Wortmann FX 63-137
Maximum thickness	0.088	0.134
Form factor	0.64	0.61

7.3.1.3 Output file

The only output file of the program “Blade Force” is “Blade_Force_Output.dat”. For each TSR at each wind speed, the program computes different results for several radii along the blades. Here are the data calculated:

- Bending moment caused by the axial forces.
- Normal stress due to the bending moment.
- Normal force generated by centrifugal speed.
- Normal stress caused by the centrifugal speed.
- Sum of both stresses.

For a more detailed account about these forces and stresses, we refer to [8].

7.3.2 Stress analysis

As the material chosen for the blades is Polycarbonate reinforced by carbon fibers, the limit stress value assumed, including a safety factor [17], is:

$$\sigma_{lim} = \frac{R_e}{s} = \frac{200}{1.35} \approx 150\ MPa$$

where R_e is the elastic limit and s is the safety factor.

The stresses along the blades calculated by the program “Blade Force” will have to be lower than this limit. So, for selected TSRs chosen before, the rated wind speed will be determined and the stress will not exceed the limit stress value. Note that the total stress is composed by the sum of both normal stresses. The normal stress due to the bending moment is the most important and represents almost all of the total stress.

Fig. 7.6 presents the total stress curves for *E387* with selected TSRs. In this graph, the maximum wind speed admitted (rated wind speed) is 18 m/s for both selected TSRs. In fact, at this rated wind speed, the blades are exposed to a maximum stress of 142 MPa for *Ep-6.75* and 148 MPa for *Ep-7*. In consequence, to stay under the limit of 150 MPa, the maximum rotational velocities are:

$$\omega_{Ep-6.75} = \frac{TSR * U}{R} = \frac{6.75 * 18}{1.25} = 97.2\ rad/s = 928\ RPM$$

$$\omega_{Ep-7} = \frac{TSR * U}{R} = \frac{7 * 18}{1.25} = 100.8\ rad/s = 962\ RPM$$

Fig. 7.7 shows the total stress curves for *FX 63-137* with selected TSRs. In both cases, the maximum admissible stress occurs for a wind speed of 13 m/s. At this rated wind speed, the maximum stress reaches 138 MPa for *Wo-7* and 145 MPa for *Wo-7.25*. Therefore, the maximum rotational velocities are:

$$\omega_{Wo-7} = \frac{TSR * U}{R} = \frac{7 * 13}{1.25} = 72.8\, rad/s = 695\, RPM$$
$$\omega_{Wo-7.25} = \frac{TSR * U}{R} = \frac{7.25 * 13}{1.25} = 75.4\, rad/s = 720\, RPM$$

Rated power (maximum power) for the wind turbine occurs at these rated wind speeds. For larger wind speeds, the limit will be exceeded and serious damage could appear. Therefore, to avoid these consequences and continue to generate energy, the rotational velocity and so the TSR has to decrease from the rated wind speed.
So, in brief, until the rated wind speed, the wind turbine rotor will have to operate at variable rotational velocity to keep a constant TSR. Then the TSR and the rotational velocity decrease to keep a constant power until the cut-out wind speed, the speed at which the turbine is shut.

Fig. 7.8 shows the comparison between the power curves of *Ep-7* and *Wo-7* with the rated wind speeds found before. The cut-out wind speed is assumed equal to 25 m/s. Note that the other selected TSRs, *Ep-6.75* and *Wo-7.25*, will give almost the same plot. On the graph, we can see that the power of generators used by the wind turbines is not the same. In fact, for *Ep-7* it reaches around 8 kW while only 3 kW for *Wo-7*. As a consequence, there is no sense to compare the Annual Energy Production with two different generators. Of course, the largest generator will produce more energy on windy sites.

The rated wind speed of *Ep-6.75* and *Ep-7* (18 m/s) is too large and so, the maximum rotational velocity around 900 RPM is unrealistic. To be more realistic and to get a fair comparison between airfoils, we will set the rated wind speed at 13 m/s. In that case, the same class of generators (about 3 kW) will be obtained for *Ep-6.75, Ep-7, Wo-7* and *Wo-7.25*, and a better comparison will be made.

Therefore, with the new rated wind speed, the blades are exposed to a stress of only 74 MPa for *Ep-6.75* and 76 MPa for *Ep-7*. The new rotational velocities for Eppler are:

$$\omega_{Ep-6.75} = \frac{TSR * U}{R} = \frac{6.75 * 13}{1.25} = 70.2\, rad/s = 670\, RPM$$
$$\omega_{Ep-7} = \frac{TSR * U}{R} = \frac{7 * 13}{1.25} = 72.8\, rad/s = 695\, RPM$$

Finally, at the same rated wind speed of 13 m/s, note that the stress for *FX 63-137* is a lot larger than *E387*. The reason for this arises from the small chord of *FX 63-137* which decreases the solidity.

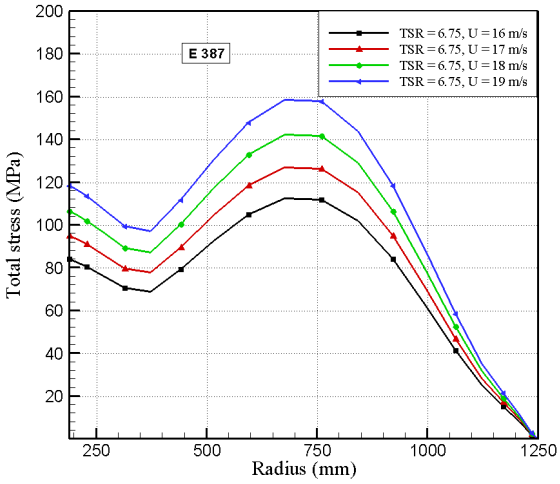

a) Ep-6.75

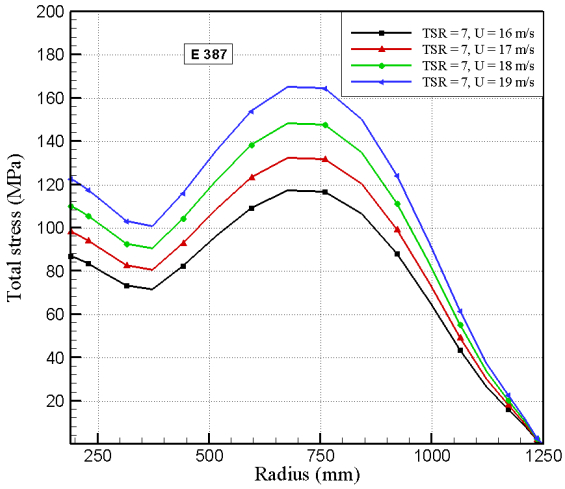

b) Ep-7

Fig. 7.6: Total stress curves for E387 with selected TSRs.

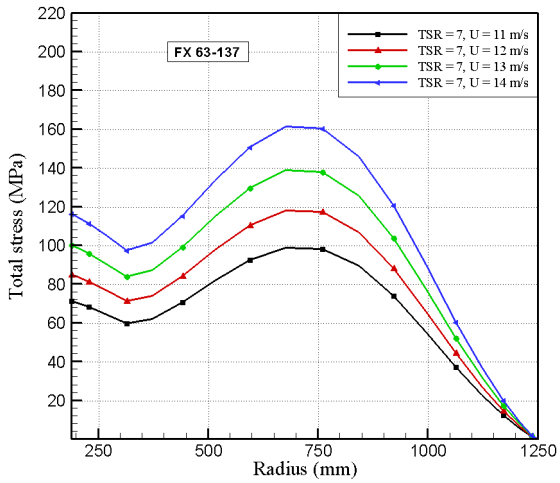

a) Wo-7

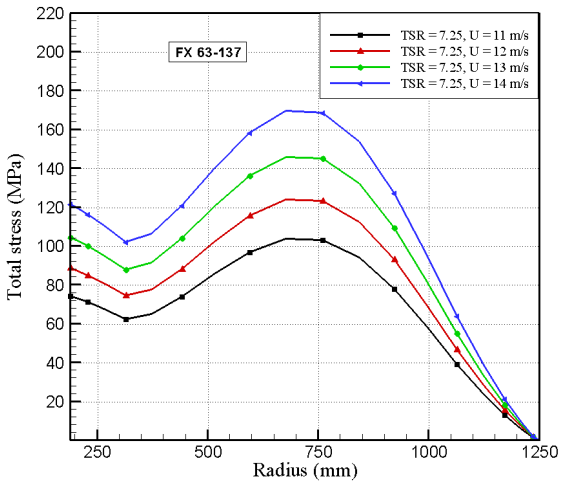

b) Wo-7.25

Fig. 7.7: Total stress curves for FX63-137 with selected TSRs.

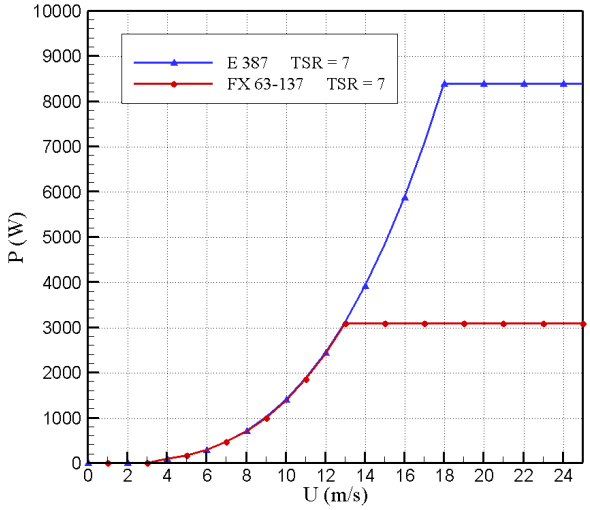

Fig. 7.8: Power curves with unreal rated wind speed.

7.4 Real Power curves

With the choices and modifications described before, the real power curves of wind turbines may be plotted.

Fig. 7.9 shows the real power curves for *E387*. Note that the curves for both selected TSRs are almost the same but the difference cannot be noticed on these graphs. Therefore, the graph of power coefficient versus wind speed has to be plotted. In addition, the maximum power delivered by the wind turbine is 3109.1 W for *Ep-6.75* and 3120.04 W for *Ep-7*, as shown in Appendix G for a wind speed of 13 m/s.

Fig. 7.10 presents the real power curves for *FX 63-137*. The maximum power produced by the wind turbine is 3091.81 W for *Wo-7* and 3100.39 W for *Wo-7.25*. But to differentiate more precisely the curves, power coefficient versus wind speed also has to be plotted.

Fig. 7.11 shows the real power coefficient curves for *E387* and *FX 63-137* with selected TSRs. In Fig 7.11.a, at the beginning, *Ep-6.75* generates more power than the other until a wind speed of 8 m/s. After that, the situation is reversed and *Ep-7* becomes better to produce energy. To understand this change, aerodynamic characteristic curves are plotted in Appendix H. Note that the reason comes from the change of C_L/C_D. Note also that after the rated wind speed, the value of C_P decreases fast not to exceed the maximum power and keep it constant.

Concerning *FX 63-137* in Fig. 7.11.b, *Wo-7* curve is larger until 11 m/s. Then *Wo-7.25* produces more power. Aerodynamic characteristic curves are shown in Appendix I and allow explaining the change of TSR to get maximum C_P. The reason is the same than *E387*. Moreover, after the rated wind speed, the value of C_P also decreases to keep the maximum power constant.

By comparison between both airfoils, we can already say that *E387* will generate more power than FX *63-137*. In fact, *E387* has a better power coefficient C_P and this for all selected TSRs.

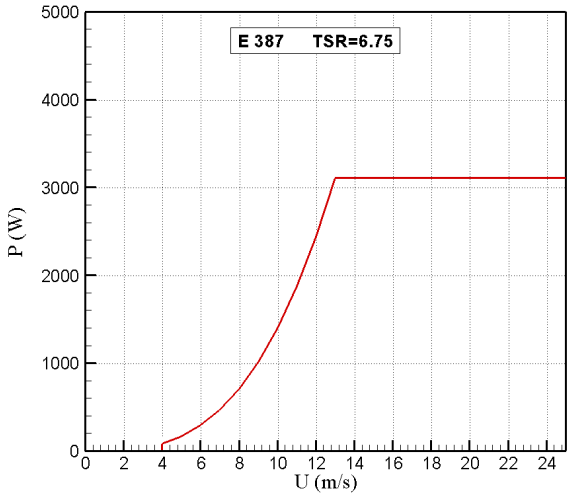

a) Ep-6.75

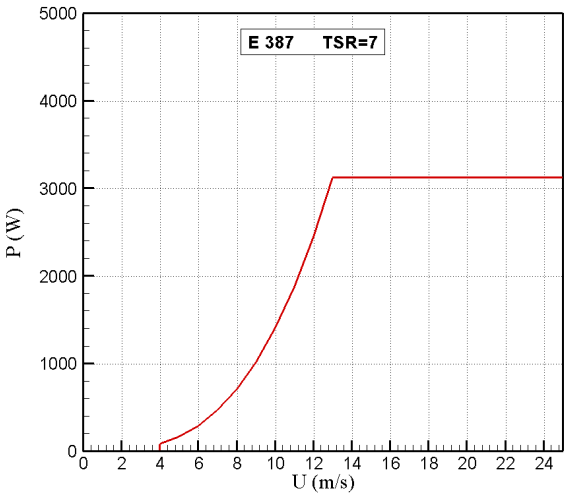

b) Ep-7

Fig. 7.9: Real power curves for E387 with selected TSRs.

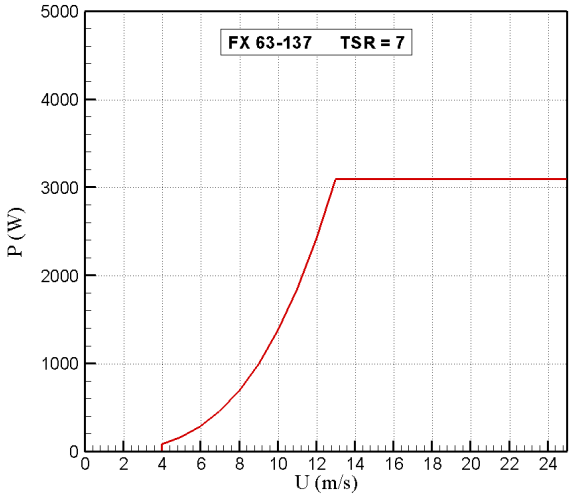

a) Wo-7

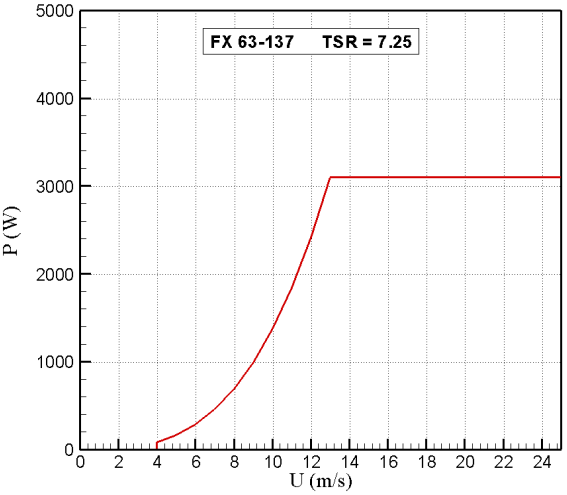

b) Wo-7.25

Fig. 7.10: Real power curves for FX 63-137 with selected TSRs.

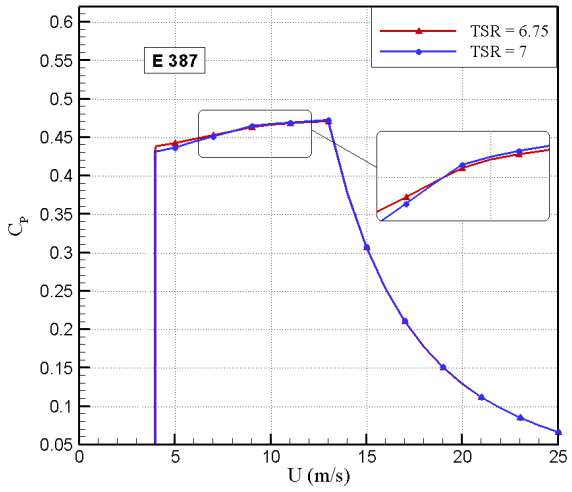

a) E387

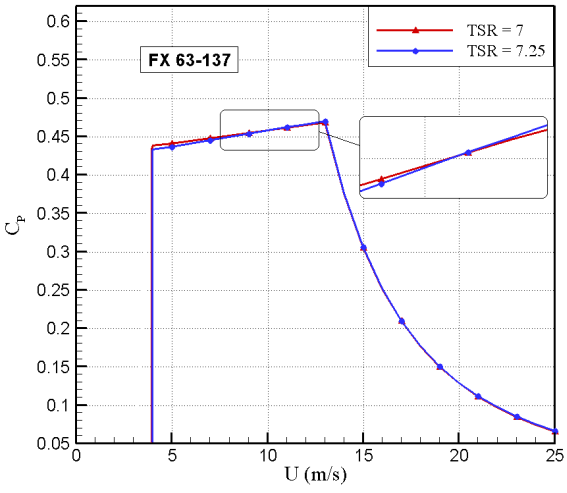

b) FX 63-137

Fig. 7.11: Real power coefficient curves with selected TSRs.

Chapter 8
Results of Annual Energy Production

8.1 Sites description

To calculate the Annual Energy production AEP, two different sites are selected, a weakly windy site and a strongly windy site:

- *Montijo*
  This location is situated in Lisbon, as shown in Fig. 8.1. The mean wind speed reaches only 4.09 m/s. The scale parameter *c* of the Weibull distribution is 4.7 m/s whereas the shape parameter *k* is 2.01. The wind turbine is placed at an altitude of 11m and the tower height is 10m.

- *Picarreira*
  This site is situated in Vila Real in the north of Portugal, as shown in Fig. 8.1. Picarreira is very windy and the mean wind speed is around 6.38 m/s. Concerning the Weibull distribution, the scale parameter *c* is 7.3 m/s and the shape parameter *k* is 1.75. The wind turbine is installed at an altitude of 1056 m and the tower height is 30 m.

Note that the wind shear is ignored due to the small diameter of the wind turbine.

Fig. 8.1: Localization of selected sites.

8.2 Weibull distributions

Fig. 8.2 shows the Weibull distributions of the selected sites. Concerning Montijo, note that frequency percentage is very high at low wind speeds but falls down quickly to reach zero around 12 m/s. In Picarreira, the frequency percentage is not so high at low wind speeds, which allows getting a curve falling down slowly to reach zero around 19 m/s.

As the power depends on the cube of wind speed, a small frequency for high wind speeds is more important than a high frequency for small wind speeds. As a consequence, a wind turbine placed in Picarreira will produce more power than in Montijo.

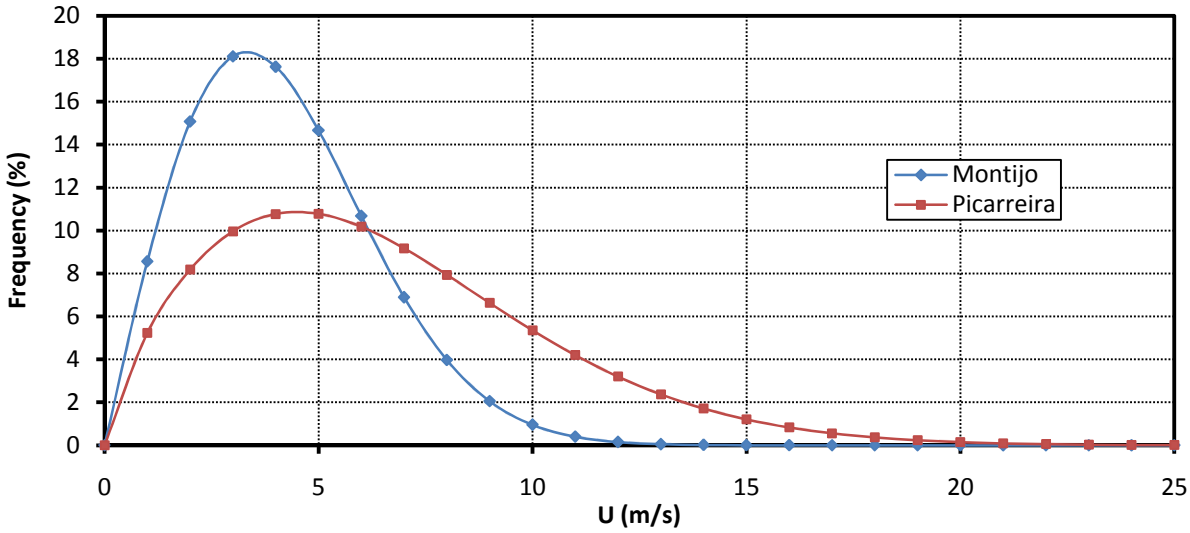

Fig. 8.2: Weibull distribution of selected sites.

8.3 Results

8.3.1 Montijo

The annual energy production of a small wind turbine using *E387* for selected TSRs in Montijo is shown in Appendix J.1. Note that, as previously mentioned, until a wind speed of 8 m/s, *Ep-6.75* produces more energy than *Ep-7*. From 9 m/s, *Ep-7* generates more energy. In consequence, *Ep-6.75*, namely *E387* with TSR of 6.75 will be more effective on a less windy site, like Montijo.
In fact, *Ep-6.75* allows getting an Annual Energy Production of 1562.99 kWh against 1554.92 kWh for *Ep-7*, as shown in Table 8.1. However, the difference represents only 0.5 %.

Fig. 8.3 shows the density of energy production as function of the wind speed in Montijo for the wind turbine using *E387*. The maximum energy produced occurs at a wind speed of 7 m/s and reaches 282.11 kWh per year for *Ep-6.75* and 280.66 kWh per year for *Ep-7*.

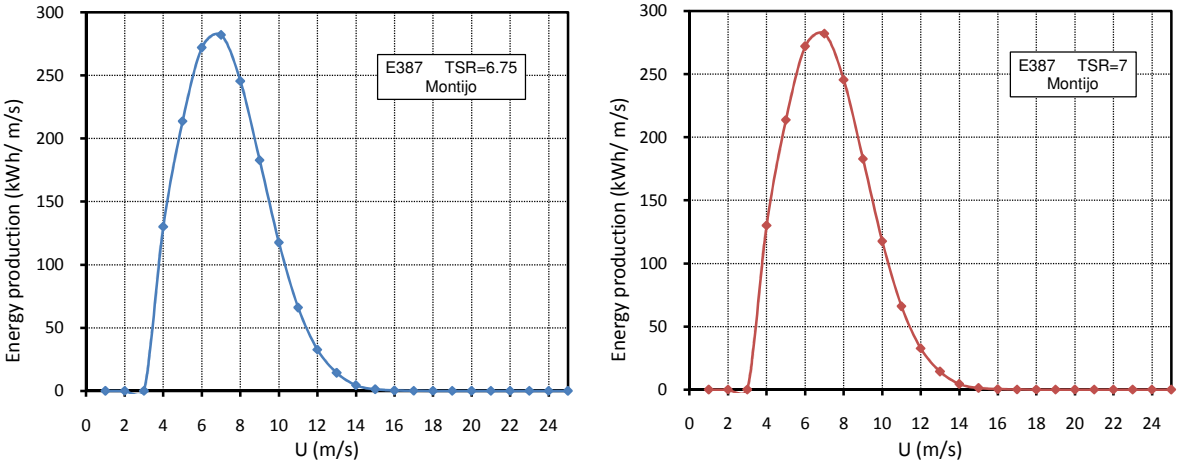

a) Ep-6.75 b) Ep-7

Fig. 8.3: Density of energy production in Montijo as function of wind speed for E387.

Appendix J.2 represents the AEP of a small wind turbine using *FX 63-137* for selected TSRs in Montijo. Until 10 m/s, the AEP is larger with *Wo-7* than *Wo-7.25*. As Montijo has very high frequency at low wind speeds, *Wo-7* will be better. This supposition is confirmed by Table 8.1 where *Wo-7* produces 1546.01 kWh against 1537.15 kWh for *Wo-7.25*. This difference is only 0.6 %.

Fig. 8.4 presents the density of energy production as function of the wind speed in Montijo for the wind turbine using *FX 63-137*. The maximum energy produced also occurs at a wind speed of 7 m/s but reaches 278.72 kWh per year for *Wo-7* and 276.99 kWh per year for *Wo-7.25*.

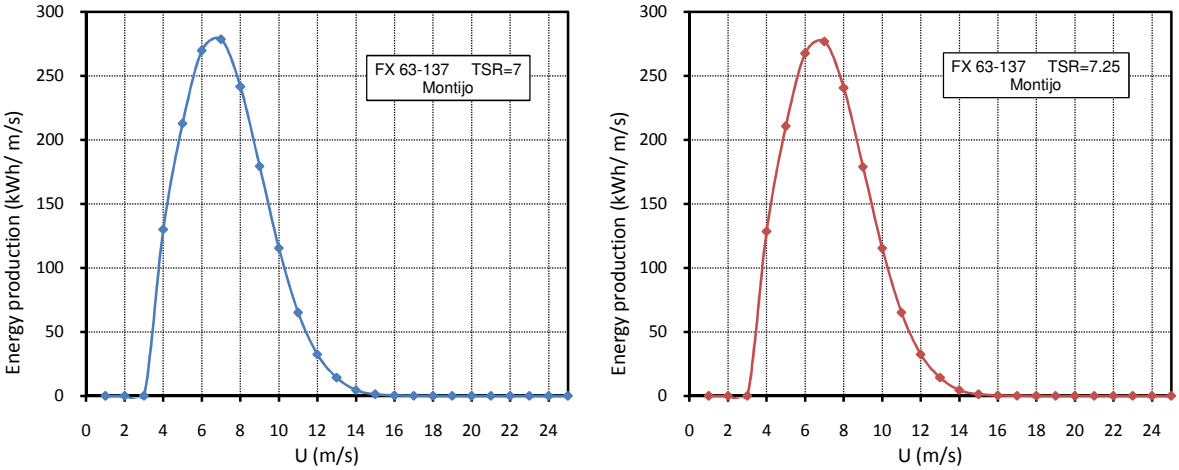

a) Wo-7 b) Wo-7.25

Fig. 8.4: Density of energy production in Montijo as function of wind speed for FX 63-137.

Generally, as expected previously, the comparison of the AEP results indicates that *E387* produces more electricity than *FX 63-137*. However, when the best results for each airfoil are compared, the AEP of *Ep-6.75* is only 1.1 % larger than *Wo-7*.

Table 8.1: Annual Energy Production.

	Annual Energy Production (kWh)	
Airfoil	Montijo	Picarreira
E387 with TSR=6.75	1562.99	6066.01
E387 with TSR=7	1554.92	6071.88
FX63-137 with TSR=7	1546.01	6001.19
FX63-137 with TSR=7.25	1537.15	5997.2

8.3.2 Picarreira

Appendix J.3 shows the AEP of a wind turbine using *E387* in Picarreira. As said previously, until a wind speed of 8 m/s, *Ep-6.75* produces more energy than *Ep-7*. However, Picarreira being windy, most energy is produced after this wind speed. As a consequence, *Ep-7* will produce more energy on this site. In fact, in the Table 8.1, the Annual Energy Production reaches 6071.88 kWh for *Ep-7* against 6066.01 kWh for *Ep-6.75*. The difference represents only 0.1%.

Fig. 8.5 shows the density of energy production as function of the wind speed in Picarreira for the wind turbine using *E387*. On this site, the maximum energy produced occurs at a wind speed of 11 m/s and reaches 688.7 kWh per year for *Ep-6.75* and 690.4 kWh per year for *Ep-7*.

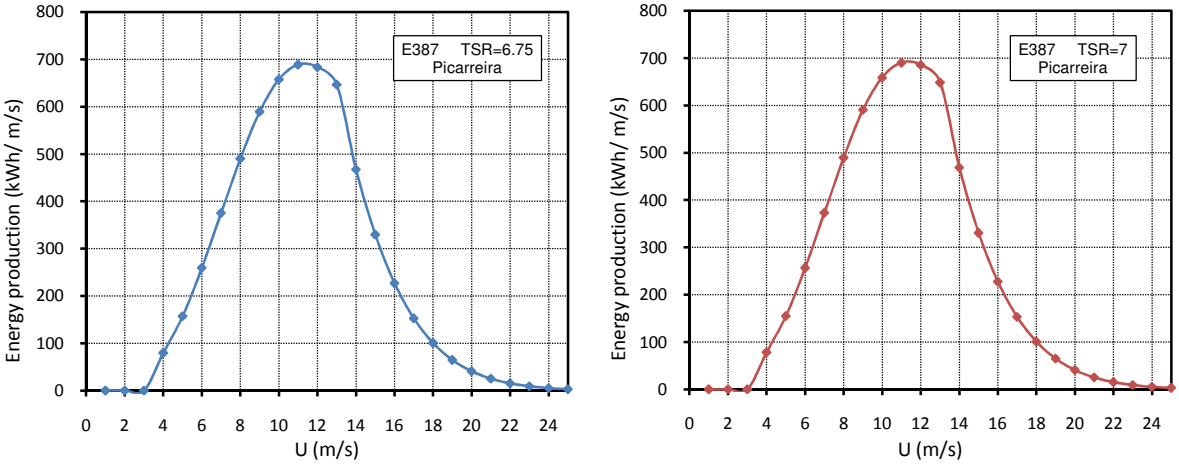

a) Ep-6.75 b) Ep-7

Fig. 8.5: Density of energy production in Picarreira as function of wind speed for E387.

The Annual Energy Production of a wind turbine using *FX 63-137* in Picarreira is represented in Appendix J.4. Although most energy is generated after a wind speed of 10 m/s, *Ep-7* remains the best, as shown in Table 8.1. In fact, the difference between the power coefficients of both selected TSRs is not so high after 10 m/s. So, the energy production for *Wo-7* is 6001.19 kWh per year and 5997.2 kWh for *Wo-7.25*. This difference is 0.1 %.

Fig. 8.6 represents the density of energy production as function of the wind speed in Picarreira by the wind turbine using *FX 63-137*. The maximum energy produced also occurs at a wind speed of 11 m/s but reaches 679.28 kWh per year for *Wo-7* and 679.43kWh per year for *Wo-7.25*.

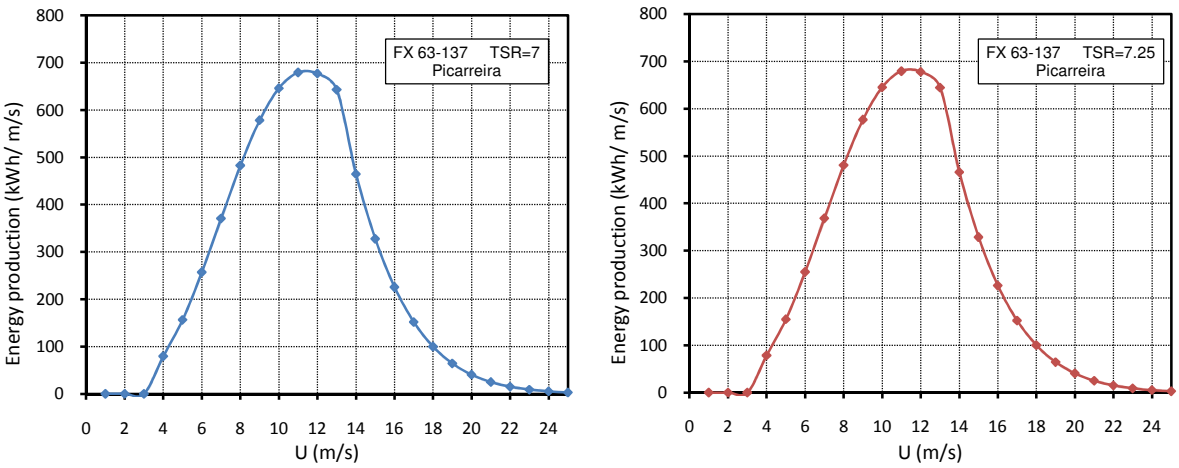

a) Wo-7 b) Wo-7.25

Fig. 8.6: Density of energy production in Picarreira as function of wind speed for FX 63-137.

At present, when the best results of both airfoils are compared in Picarreira, the AEP of *Ep-7* is only 1.2 % larger than *Wo-7*.

8.3.3 Comparison between Montijo and Picarreira

The difference of Annual Energy Production between Montijo and Picarreira is very large. Indeed, for each selected TSRs for both airfoils, the increase reaches around 290%. Note also that the best TSR for *E387* has changed between these two sites. In Montijo, the best design is *Ep-6.75* while in Picarreira it is *Ep-7*.

Chapter 9
Conclusions

This chapter presents the conclusions drawn from the results obtained for the design criteria and the Annual Energy production.

9.1 Conclusions

The aerodynamic designs for this thesis were performed for a certain Tip Speed Ratio, variable-angle of attack with power coefficients as high as possible.
The purpose of the project was the improvement of output energy power for a small wind turbine through the modification of the design parameters, in particular the airfoil and the design angle of attack.

The following conclusions can be drawn:

- As the optimum chord is small near the tip, the study of the blades remains difficult because of the difficulty in studying C_L and C_D data for low Reynolds numbers for most airfoils.
- The choice of an “optimum” angle of attack for the maximization of C_L/C_D allows getting better results.
- An airfoil with a high lift coefficient leads to a smaller chord which deteriorates the power coefficient C_P due to smaller values of C_L/C_D caused by low Reynolds numbers effect.
- The airfoil E387 obtains a better power coefficient than Wortmann FX 63-137.

- The wind turbine using Eppler E387 produces more energy than FX 63-137 for all sites analyzed.
- The optimum TSR for Eppler E387 changes as function of the site.
- The small chord of Wortmann FX 63-137 does not penalize itself concerning the AEP.
- At a given wind speed, the stresses on the blades for Eppler E387 are lower, due to its large chord.
- The AEP may be improved by changing optimum TSR for each wind speed but the improvement will not be significant with this design case.
- The site has a strong influence on the Annual Energy Production.
- Concerning the AEP of a small wind turbine, the modification of the design criteria enables only very small gains.
- The aerodynamic design optimization may be less important for a small wind turbine than for a large turbine.

Bibliography

[1] Morthorst, Poul-Erik, and Awerbuch, Shimon, "*The Economics of Wind Energy"*, European Wind Energy Association, 2009.

[2] Arthus-Bertrand, Yann, "*www.goodplanet.info"*, GoodPlanet Association.

[3] "*Climate Policy*", Assessment of US GHG cap-and-trade proposals, 2008.

[4] "*www.wikipedia.org*", Wikimedia Foundation.

[5] "*Small Wind Turbine: Global Market Study"*, American Wind Energy Association, 2009.

[6] Cloes, Guy, "*Guide des Energies Renouvelables*", Ministère de la Région Wallonne, 1994.

[7] "In the Public Interest: How and Why to Permit for Small Wind Systems", American Wind Energy Association, 2008.

[8] Pôtra, João F. T. ," *Projecto e análise aerodinâmica do rotor de pequenas turbinas eólicas",* MARETEC RT-FJ16-8, 2007.

[9] Lysen, E.H., "*Introduction to wind energy*", Consultancy services Wind energy Developing countries, 1983.

[10] Maalawi K.Y. and Badr M.A, "*A practical approach for selecting optimum wind rotors*", National Research Center in Cairo, 2002

[11] Fuglsang, P. and Madsen, H.A., "*Optimization method for wind turbine rotors*" Riso National Laboratory, 1998.

[12] B. Hendriks, J.G. Schepers, T.G. van Engelen, A.J. Stern, G.K. Boerstra, "*Aeroelastically optimized cost efficient wind turbine - a case study*", European Union Wind Energy Conf, 1996.

[13] Wright, A.K. and Wood, D.H., "*The starting and low wind speed behaviour of a small horizontal axis wind turbine*", Wind Eng. Ind. Aerodyn. , 2004.

[14] *"www.windpower.org"*, Danish Wind Industry Association.

[15] *"Wind energy: the facts"*, European Wind Energy Association, 2009.

[16] Hau, Erich, *"Wind Turbines: Fundamentals, Technologies, Application, Economics*", Springer, 2000.

[17] Burton, Tony, et al, "*Wind Energy Handbook"*, Wiley, 2002.

[18] Falcão de Campos, J. A. C. , "*Hydrodynamic Power Optimization of a Horizontal Axis Marine Current Turbine with Lifting Line Theory"*, Proceedings of the 17th International Offshore and Polar Engineering Conference, Vol.1, ISOPE, PP. 307-313, 2007.

[19] Lewis, James E., and Dole, Charles E., "*Flight theory and aerodynamics: a practical guide for operational safety"*, Wiley-IEEE, 2000.

[20] Kerwin, JE, Coney, WB, Hsin, C-H, "Optimum Circulation Distribution for Single and Multi-component Propulsors", 21st American Towing Tank Conference, 1986.

[21] Somers D.M. and Maughmer M.D., "*Theoretical Aerodynamic Analyses of Six Airfoils for Use on Small Wind Turbines"*, NREL, 2002.

Appendix A
Windturll program explanation

To begin, the program calculates the elements of the lifting line using a Cosine distribution. The lifting line is discretized into M elements along the radius.

$$\overline{r_I} = \frac{1}{2}(1 + r_h) - \frac{1}{2}(1 - r_h)\cos\frac{(I - \frac{1}{2})\pi}{M} \quad for\ I = 1,2, \dots M$$

$$r_J = \frac{1}{2}(1 + r_h) - \frac{1}{2}(1 - r_h)\cos\frac{(J - 1)\pi}{M} \quad for\ J = 1,2, \dots M$$

Then, it realizes the interpolation in the file "clcd.dat" with the new elements of the lifting line $\overline{r_i}$. Now for each section given by $\overline{r_i}$ corresponds a value of C_L/C_D.

After that, "Windturll" enters in a loop: Do while the absolute value of $(\frac{CT}{0.78})$-1 is larger than 0,0005. Note that 0,78 is the value of C_T given in the file "LL1data.dat".

- <u>For the first iteration in the loop:</u>

  With the method of Lerbs it calculates the induced angle β_i:

$$tan\,\beta_i(I) = \frac{1}{\overline{r_I} * \lambda} \quad for\ I = 1,2, \dots M$$

$$FUNCTI(I) = F(I) = 1 \qquad FUNCTJ(I) = F(I) = 1$$

$$K = \frac{1}{\lambda * FUNCTJ(I)}$$

$$Pitch(I) = 2\pi * \tan\beta_i\,(I) * \overline{r_i}$$

  After, calculation of induced velocities and circulation:

  $V_a\_ij = \frac{1}{4\pi}\ \frac{i_a}{\overline{r_I} - r_J}$ $\quad V_t\_ij = \frac{1}{4\pi}\ \frac{i_t}{\overline{r_I} - r_J}$ where i_a and i_t are determined before.

  This equation is not solved for J=1, because at this moment the program does not yet have the values of $\mathrm{prv_{vaij}}$ and $\mathrm{prv_{vtij}}$.

$$V_{aij}\,(I, J-1) = -(V_a\_ij - \mathrm{prv_{vaij}}) \qquad V_{tij}\,(I, J-1) = -(V_t\_ij - \mathrm{prv_{vtij}})$$

$$\mathrm{prv_{vaij}} = V_a\_ij \qquad \mathrm{prv_{vtij}} = V_t\_ij$$

The computation of the circulation is based on the formulas:

$Matrix(I,J-1) = V_{aij}\,(I,J-1) + K * \frac{FUNCTI(I)}{\bar{r}_i} * V_{tij}\,(I,J-1)$ also not solved for J=1

$$RHS(I) = 1 - K * \lambda * FUNCTI(I)$$

Then when the data of the Circulation $\Gamma(I)$ are obtained, the program is able to calculate the induced velocities:

$$V_{a_i}(I) = \sum_{J=1}^{M} V_{aij}(I,J) * \Gamma(J) \qquad V_{t_i}(I) = \sum_{J=1}^{M} V_{tij}(I,J) * \Gamma(J)$$

When the circulation and the induced velocities are calculated, "Windturll" computes C_P and C_T:

$$C_T = \frac{2Z}{\pi} \sum_{I=1}^{M} \left(\bar{r}_I\,\lambda + v_{t_i}(I)\right) * \Gamma(I)\,\left(1 + \left(\frac{C_D}{C_L}\right)_I * \tan\beta_i\,(I)\right)(r_J(I+1) - r_J(I))$$

$$C_P = \frac{2Z\lambda}{\pi} \sum_{I=1}^{M} (1 - v_{a_i}(I))\,\bar{r}_I * \Gamma(I)\,\left(1 - \left(\frac{C_D}{C_L}\right)_I * \cot\beta_i\,(I)\right)(r_J(I+1) - r_J(I))$$

- <u>For the other iterations in the loop:</u>

First, it calculates the induced angle β_i:

$$FUNCTI(I) = F(I) = 1 \qquad FUNCTJ(I) = F(I) = 1$$

$$K = (the\ previous\ K) * (1 + \frac{\frac{C_T}{0.78} - 1}{15})$$

$$\tan\beta_i\,(I) = K * \frac{FUNCTI(I)}{\bar{r}_i}$$

$$Pitch(I) = 2\pi * \tan\beta_i\,(I) * \bar{r}_i$$

Then, calculation of induced velocities and circulation:

$V_a\_ij = \frac{1}{4\pi}\,\frac{i_a}{\bar{r}_I - r_J}$ $V_t\_ij = \frac{1}{4\pi}\,\frac{i_t}{\bar{r}_I - r_J}$ where i_a and i_t are determined before.

This equation is not solved for J=1, because at this moment the program does not yet have the values of $\mathrm{prv_{vaij}}$ and $\mathrm{prv_{vtij}}$.

$$V_{aij}\,(I,J-1) = -(V_a\_ij - \mathrm{prv}_{\mathrm{vaij}}) \qquad V_{tij}\,(I,J-1) = -(V_t\_ij - \mathrm{prv}_{\mathrm{vtij}})$$

$$\mathrm{prv}_{\mathrm{vaij}} = V_a\_ij \qquad \mathrm{prv}_{\mathrm{vtij}} = V_t\_ij$$

The computation of the circulation is based on the formulas:

$Matrix(I,J-1) = V_{aij}\,(I,J-1) + K * \frac{FUNCTI(I)}{\bar{r}_i} * V_{tij}\,(I,J-1)$ also not solved for J=1

$$RHS(I) = 1 - K * \lambda * FUNCTI(I)$$

When the data of the Circulation $\Gamma(I)$ are obtained, the program is able to calculate the induced velocities:

$$V_{a_i}(I) = \sum_{J=1}^{M} V_{aij}(I,J) * \Gamma(J) \qquad V_{t_i}(I) = \sum_{J=1}^{M} V_{tij}(I,J) * \Gamma(J)$$

When the circulation and the induced velocities are calculated, “Windturll” computes C_P and C_T:

$$C_T = \frac{2Z}{\pi} \sum_{I=1}^{M} \left(\bar{r}_I\,\lambda + v_{t_i}(I)\right) * \Gamma(I)\,\left(1 + \left(\frac{C_D}{C_L}\right)_I * \tan\beta_i\,(I)\right)(r_J(I+1) - r_J(I))$$

$$C_P = \frac{2Z\lambda}{\pi} \sum_{I=1}^{M} (1 - v_{a_i}(I))\,\bar{r}_I * \Gamma(I)\,\left(1 - \left(\frac{C_D}{C_L}\right)_I * \cot\beta_i\,(I)\right)(r_J(I+1) - r_J(I))$$

After the loop, it calculates $tan\,\beta(I) = \frac{1}{\bar{r}_I * \lambda}$.

Appendix B
Calcorda program explanation

First, the program reads the values of circulation Γ, induced velocities Va, Vt and the induced angle β_i calculated by "Windturll".

Then, it computes the velocities:

$$V(I) = \sqrt{(1 - Va(I))^2 + ((\frac{r}{R}(I) * \lambda) + Vt(I))^2}$$

After, with C_L in the input file "Perfil.dat", "Calcorda" computes the chord distribution:

$$Chord(I) = \frac{2 * \Gamma(I)}{C_L(I) * V(I)}$$

Finally, with α in "Perfil.dat", the program finds the twist angle:

$$Twist(I) = 90 - \beta_i + \alpha$$

Appendix C
Analise program explanation

To begin, the program computes the elements of the lifting line using a Cosine distribution. The lifting line is discretized into M elements along the radius.

$$\overline{r_I} = \frac{1}{2}(1 + r_h) - \frac{1}{2}(1 - r_h)\cos\frac{(I - \frac{1}{2})\pi}{M} \quad for\ I = 1,2, \dots M$$

$$r_J = \frac{1}{2}(1 + r_h) - \frac{1}{2}(1 - r_h)\cos\frac{(J - 1)\pi}{M} \quad for\ J = 1,2, \dots M$$

After that, "Analise" enters in a loop which says: Do while $\frac{\sum_{I=1}^{M}\left|\frac{tan\beta_i(I) - tan\beta_{i\,new}(I)}{tan\beta_{i\,new}(I)}\right|}{M}$ is larger than 0.00005.

- <u>For the first iteration in the loop:</u>

  First, it computes the value of:

  $$tan\ \beta_i(I) = \frac{0{,}6}{\overline{r_I} * \lambda}$$

  After that, calculation of induced velocities and circulation:

  $V_a\_ij = \frac{1}{4\pi}\ \frac{i_a}{\overline{r_I} - r_J}$ $\quad V_t\_ij = \frac{1}{4\pi}\ \frac{i_t}{\overline{r_I} - r_J}$ where i_a and i_t are determined before.

  This equation below is not solved for J=1, because at this moment the program does not yet have the values of $\mathrm{prv_{vaij}}$ and $\mathrm{prv_{vtij}}$.

  $$V_{aij}\,(I, J-1) = -(V_a\_ij - \mathrm{prv_{vaij}}) \qquad V_{tij}\,(I, J-1) = -(V_t\_ij - \mathrm{prv_{vtij}})$$

  $$\mathrm{prv_{vaij}} = V_a\_ij \qquad \mathrm{prv_{vtij}} = V_t\_ij$$

  The computation of the circulation is based on the formulas:

  $$Matrix(I, J-1) = V_{aij}\,(I, J-1) + \tan\beta_i\,(I)\ * V_{tij}\,(I, J-1)$$ also not solved for J=1

  $$RHS(I) = 1 - \tan\beta_i(I) * \overline{r_I} * \lambda$$

  When the data of the Circulation $\Gamma(I)$ are obtained, the program is able to calculate the induced velocities:

  $$V_{a_i}(I) = \sum_{J=1}^{M} V_{aij}(I,J) * \Gamma(J) \qquad V_{t_i}(I) = \sum_{J=1}^{M} V_{tij}(I,J) * \Gamma(J)$$

With these values calculated above and with the input files, it estimates:

$$V(I) = \sqrt{(1 - V_{ai}(I))^2 + ((\overline{r_I} * \lambda) + V_{ti}(I))^2}$$

$$C_L(I) = \frac{2 * \Gamma(I)}{V(I) * Chord(I)}$$

$$Re(I) = \frac{V(I) * Vwind * Chord(I) * \frac{Diameter}{2}}{Viscosity}$$

Then, "Analise" finds, with C_L and Re, the values of C_D and α by interpolation in the file "C_L_C_D table.dat".

Next,

$$\tan \beta_{i\,new}(I) = \tan(90 - Twist(I) + \alpha(I))$$

With the help of the new values of C_L, it evaluates the new Circulation:

$$\Gamma(I) = \frac{C_L(I) * V(I) * Chord(I)}{2}$$

Thus, C_P and C_T are:

$$C_T = \frac{2Z}{\pi} \sum_{I=1}^{M} \left(\overline{r_I}\,\lambda + v_{t_i}(I)\right) * \Gamma(I) \left(1 + \left(\frac{C_D}{C_L}\right)_I * \tan \beta_i\,(I)\right) (r_J(I+1) - r_J(I))$$

$$C_P = \frac{2Z\lambda}{\pi} \sum_{I=1}^{M} (1 - v_{a_i}(I))\,\overline{r_I} * \Gamma(I) \left(1 - \left(\frac{C_D}{C_L}\right)_I * \cot \beta_i\,(I)\right) (r_J(I+1) - r_J(I))$$

- <u>For the other iterations :</u>

First, it computes another value of $tan\ \beta_i$ from the previous values:

$$tan\ \beta_i(I) = 0.8 * \tan \beta_i(I) + 0.2 * \tan \beta_{i\,new}$$

After that, it calculates the induced velocities and circulation:

$V_a\_ij = \frac{1}{4\pi}\ \frac{i_a}{\overline{r_I} - r_J}$ $\quad V_t\_ij = \frac{1}{4\pi}\ \frac{i_t}{\overline{r_I} - r_J}$ where i_a and i_t are determined before.

This equation below is not solved for J=1, because at this moment the program does not yet know the values of $\mathrm{prv_{vaij}}$ and $\mathrm{prv_{vtij}}$.

$$V_{aij}\,(I, J-1) = -(V_a\_ij - \mathrm{prv_{vaij}}) \qquad V_{tij}\,(I, J-1) = -(V_t\_ij - \mathrm{prv_{vtij}})$$

$$\mathrm{prv_{vaij}} = V_a\_ij \qquad \mathrm{prv_{vtij}} = V_t\_ij$$

The computation of the circulation is based on the formulas:

$Matrix(I,J-1) = V_{aij}\,(I,J-1) + \tan\beta_i\,(I)\ * V_{tij}\,(I,J-1)$ also not solved for J=1

$$RHS(I) = 1 - \tan\beta_i(I) * \overline{r_I} * \lambda$$

When the data of the Circulation $\Gamma(I)$ are obtained, the program is able to calculate the induced velocities:

$$V_{a_i}(I) = \sum_{J=1}^{M} V_{aij}(I,J) * \Gamma(J) \qquad V_{t_i}(I) = \sum_{J=1}^{M} V_{tij}(I,J) * \Gamma(J)$$

With these values calculated above and with the input files it estimates:

$$V(I) = \sqrt{(1 - V_{ai}(I))^2 + ((\overline{r_I} * \lambda) + V_{ti}(I))^2}$$

$$C_L(I) = \frac{2 * \Gamma(I)}{V(I) * Chord(I)}$$

$$Re(I) = \frac{V(I) * Vwind * Chord(I) * \frac{Diameter}{2}}{Viscosity}$$

Then, "Analise" finds, with C_L and Re, the values of C_D and α by interpolation in the file "C_L_C_D table.dat".

Next,

$$\tan\beta_{i\,new}(I) = \tan(90 - Twist(I) + \alpha(I))$$

With the help of the new values of C_L, it evaluates the new Circulation:

$$\Gamma(I) = \frac{C_L(I) * V(I) * Chord(I)}{2}$$

Thus, C_P and C_T are:

$$C_T = \frac{2Z}{\pi} \sum_{I=1}^{M} \left(\overline{r_I}\,\lambda + v_{t_i}(I)\right) * \Gamma(I) \left(1 + \left(\frac{C_D}{C_L}\right)_I * \tan\beta_i\,(I)\right)(r_J(I+1) - r_J(I))$$

$$C_P = \frac{2Z\lambda}{\pi} \sum_{I=1}^{M} (1 - v_{a_i}(I))\,\overline{r_I} * \Gamma(I) \left(1 - \left(\frac{C_D}{C_L}\right)_I * \cot\beta_i\,(I)\right)(r_J(I+1) - r_J(I))$$

At the end of the loop the program calculates:

$$\tan\beta = \frac{1}{\overline{r_I} * \lambda} \qquad Pitch = \tan^{-1}(\tan\beta_i(I) - \alpha)$$

$$C_L/C_D\,(I) = \frac{CL(I)}{CD(I)}$$

Appendix D
Programs Modifications

D.1 Error explanation

The data in the file "C_L_C_D table.dat", used by the program "Analise", are shown in Table D.1

Table D.1: Example with part of the table comprising values of C_L and C_D as function of the angles of attack.

For Reynolds number = 100 000

α (°)	C_L data	α (°)	C_D data
-4	-0.0783	-4	0.03174
-3	0.073	-3	0.02135
-2	0.1826	-2	0.01522
-1	0.3151	-1	0.0146
0	0.4172	0	0.01555
1	0.5187	1	0.01677
2	0.6198	2	0.01824
3	0.721	3	0.01977
4	0.822	4	0.02113
5	0.9233	5	0.02194
6	1.0267	6	0.02169
7	1.1285	7	0.01987
8	1.183	8	0.02109
		9	0.03149
		10	0.04002
		11	0.05206
		12	0.06631
		13	0.08644
		14	0.1163
		15	0.15607

For Reynolds number = 200 000

α (°)	C_L data	α (°)	C_D data
-4	-0.0205	-4	0.03097
-3	0.0735	-3	0.01848
-2	0.1825	-2	0.01354
-1	0.2914	-1	0.012
0	0.4022	0	0.00996
1	0.5099	1	0.01071
2	0.6182	2	0.01128
3	0.7253	3	0.01216
4	0.8324	4	0.01242
5	0.9337	5	0.0117
6	1.03	6	0.01257
7	1.1121	7	0.01528
8	1.1443	8	0.02292
9	1.1754	9	0.02956
10	1.2506	10	0.04214
		11	0.06044
		12	0.0821

We will take an example in this case for the first iteration in the loop in "Analise" for the first radius $\overline{r_1} = 0{,}15131$ of the blades near the hub.

First, "Analise" evaluates C_L and Re with these formulas:

$$C_L(1) = \frac{2*\Gamma(1)}{V(1)*Chord(1)} = 1.395527 \quad \text{(D-2)}$$

$$Re(1) = \frac{V(1)*Vwind*Chord(1)*\frac{Diameter}{2}}{Viscosity} = 22596.44 \quad \text{(D-3)}$$

Knowing the value of the lift coefficient, the program enters in the file "C_L_C_D table.dat" and realizes the interpolation to find the angle of attack corresponding, for Re=100 000 and Re=200 000. However, it is not able to do so because C_L is higher than in the table. Then, it takes the last value in the table:

For Re=100 000 → C_L=1.183 and α = 8°
For Re=200 000 → C_L=1.2506 and α = 10°

After this step, the program knows the corresponding angles of attack (α) and is able to realize the interpolation of C_D. Table D.2 shows the interpolation method of C_D in the file "C_L_C_D table.dat".

Table D.2: Interpolation method of C_D in the file "C_L_C_D table.dat".

	Re = 100 000		Re = 200 000	
C_L_C_D Table →	α (°)	C_D	α (°)	C_D
	8	0.02109	9	0.02956
	9	0.03149	10	0.04214
Interpolation →	α (°) wanted	C_D corresp	α (°) wanted	C_D corresp
	8	0.02109	10	0.04214

Next, with these data, "Analise" extrapolates to find the C_D corresponding to Reynolds number found in (D-3). Table D.3 shows the extrapolation of C_D for a specific Reynolds number.

Table D.3: Extrapolation of C_D for a specific Reynolds number.

Extrapolation	
Re	C_D
100 000	0.02109
200 000	0.04214
Re wanted	C_D corresp
22596.44	0.004796551

The extrapolation of C_D is depicted in Fig. D.1.

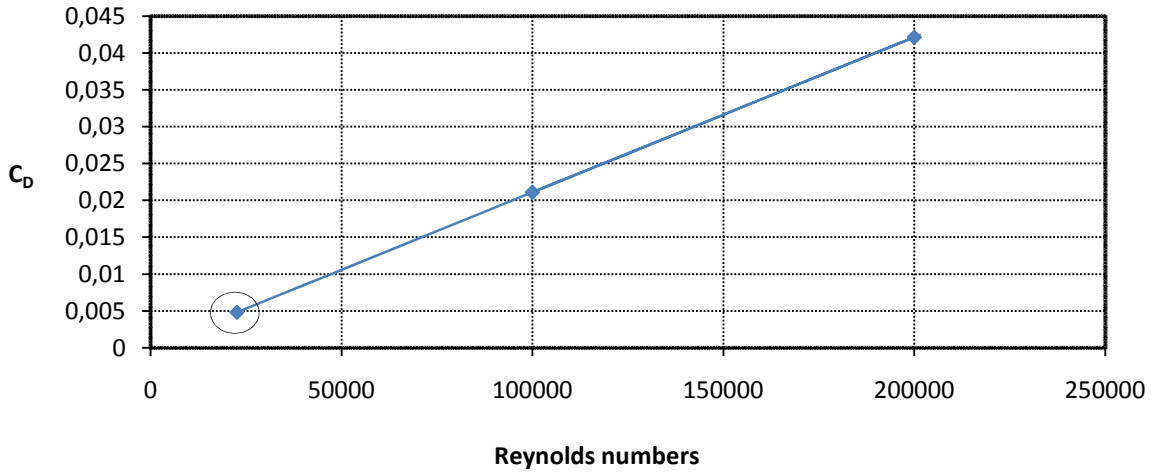

Fig. D.1: Picturing of the extrapolation of C_D.

Finally, the program performs the extrapolation for C_L. Table D.4 shows the extrapolation of C_L for a specific Reynolds number.

Table D.4: Extrapolation of C_L for a specific Reynolds number.

Extrapolation

Re	C_L
100 000	1.183
200 000	1.2506

Re wanted	C_L corresp
22596.44	1.131

The final results for the first iteration of the loop are:

$$\frac{C_L}{C_D}(1) = \frac{1.131}{0.004796551} = 235.79 \quad \text{(D-4)}$$

$$\Gamma(1) = \frac{C_L(1) * V(1) * Chord(1)}{2} = 0.0149 \quad \text{(D-5)}$$

To sum up, the impossibility to perform the first extrapolation for a high C_L causes an error in the extrapolation of C_D and thus a large increase of C_L/C_D is obtained.

Moreover, this impossibility for the first extrapolation causes the decrease of the lift coefficient and consequently a decrease of the circulation Γ.
This case was for a radius near the hub but this problem also occurs near the tip of the blades.

The values of the circulation at the tip are the most important. Indeed the vortices at this place have a great influence on the rest of the blade. As a consequence, if the value of the circulation is wrong at the tip, all of the other values calculated will also be wrong.

D.2 Solution method

The only modification which has been realized concerns the method to find the angle of attack from C_L. The C_L_C_D Table has remained the same as before.

We are going to take the same example as before, but considering the modification of the program.

$$C_L(1) = \frac{2*\Gamma(1)}{V(1)*Chord(1)} = 1.395527 \quad \text{(D-6)}$$

$$Re(1) = \frac{V(1)*Vwind*Chord(1)*\frac{Diameter}{2}}{Viscosity} = 22596.44 \quad \text{(D-7)}$$

Before, at this moment, “Analise” was not able to realize the extrapolation and took the higher value in the table. After the modification for both Reynolds numbers, the program achieves the extrapolation and finds the angles of attack corresponding to the value of C_L calculated in (D-6) even if the value of C_L is higher than in the table. Table D.5 shows the new extrapolation of C_L in the file “C_L_C_D table.dat”.

Table D.5: New extrapolation of C_L in the file “C_L_C_D table.dat”.

	Re = 100 000		Re = 200 000	
C_L_C_D Table →	C_L	Alpha	C_L	Alpha
	1.1285	7	1.1754	9
	1.183	8	1.2506	10
Extrapolation →	C_L wanted	α (°) corresp	C_L wanted	α (°) corresp
	1.395527	11.90	1.395527	11.93

Then, “Analise” determines the C_D corresponding to the angles of attack (α) found in Table D.5. Table D.6 shows the new interpolation of C_D in the file “C_L_C_D table.dat”.

Table D.6: New interpolation of C_D in the file “C_L_C_D table.dat”.

	Re =100 000		Re =200 000	
C_L_C_D Table →	α (°)	C_D	α (°)	C_D
	11	0.05206	11	0.06044
	12	0.06631	12	0.0821
Interpolation →	α (°) wanted	C_D corresp	α (°) wanted	C_D corresp
	11.90	0.06487	11.93	0.0805

Next, with these C_D, the program extrapolates to find the C_D for the Reynolds number found in (D-7). Table D.7 shows the new extrapolation of C_D for a specific Reynolds number.

Table D.7: New extrapolation of C_D for a specific Reynolds number.

Extrapolation

Re	C_D
100000	0.06487
200000	0.0805

Re wanted	C_D corresp
22596.44	0.0527695

Fig. D.2 depicts the graphic showing the new extrapolation of C_D.

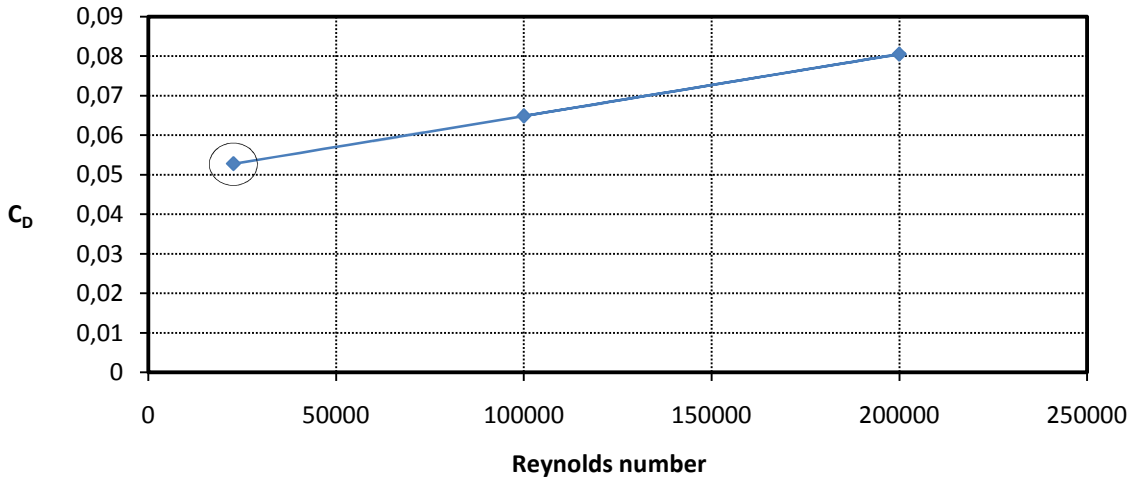

Fig. D.2: Corrected extrapolation of C_D.

Finally, "Analise" achieves the extrapolation for C_L. Table D.8 shows the new extrapolation of C_L for a specific Reynolds number.

Table D.8: New extrapolation of C_L for a specific Reynolds number.

Interpolation	
Re	C_L
100 000	1.395527
200 000	1.395527
Re wanted	C_L corresp
22596.44	1.395527

The final results with the modification are:

$$\frac{C_L}{C_D}(1) = \frac{1.395527}{0.0527695} = 26.44 \quad \text{(D-8)}$$

$$\Gamma(1) = \frac{C_L(1) * V(1) * Chord(1)}{2} = 0.0184 \quad \text{(D-9)}$$

Finally, with the execution of the first extrapolation for a large lift coefficient, the new value of C_L/C_D for the first iteration in (D-8) is smaller than before. Furthermore, as the extrapolation has been performed, C_L is high and so the circulation is higher.

Appendix E

Aerodynamic Characteristics

E.1 Eppler E387 airfoil

	Re = 100 000			Re = 200 000			Re = 350 000			Re = 500 000		
Alpha	C_L	C_D	C_L/C_D	C_L	C_D	C_L/C_D	C_L	C_D	C_L/C_D	C_L	C_D	C_L/C_D
-4	-0.078	0.03174	-2.467	-0.021	0.03097	-0.662	-0.041	0.01679	-2.412	-0.044	0.01492	-2.969
-3	0.073	0.02135	3.419	0.074	0.01848	3.977	0.067	0.01254	5.343	0.064	0.01106	5.750
-2	0.183	0.01522	11.997	0.183	0.01354	13.479	0.176	0.01017	17.296	0.174	0.0094	18.489
-1	0.315	0.0146	21.582	0.291	0.012	24.283	0.277	0.00788	35.165	0.282	0.00771	36.576
0	0.417	0.01555	26.830	0.402	0.00996	40.382	0.398	0.00748	53.235	0.397	0.00642	61.791
1	0.519	0.01677	30.930	0.510	0.01071	47.610	0.508	0.00788	64.454	0.507	0.00672	75.446
2	0.620	0.01824	33.980	0.618	0.01128	54.805	0.618	0.00829	74.536	0.617	0.00711	86.821
3	0.721	0.01977	36.469	0.725	0.01216	59.646	0.727	0.00873	83.322	0.728	0.00739	98.444
4	0.822	0.02113	38.902	0.832	0.01242	67.021	0.836	0.00912	91.645	0.837	0.00776	107.835
5	0.923	0.02194	42.083	0.934	0.0117	79.803	0.942	0.00944	99.820	0.944	0.0082	115.085
6	1.027	0.02169	47.335	1.030	0.01257	81.941	1.043	0.01012	103.043	1.040	0.00966	107.692
7	1.129	0.01987	56.794	1.112	0.01528	72.781	1.116	0.01384	80.621	1.111	0.01403	79.195
8	1.183	0.02109	56.093	1.144	0.02292	49.926	1.175	0.0187	62.845	1.187	0.01735	68.392
9	1.156	0.03149	36.707	1.175	0.02956	39.763	1.230	0.02259	54.467	1.248	0.02095	59.589
10	1.222	0.04002	30.540	1.251	0.04214	29.677	1.253	0.02793	44.869	1.274	0.0258	49.384
11	1.301	0.05206	24.983	1.243	0.06044	20.561	1.284	0.03527	36.408	1.301	0.03274	39.725
12	1.273	0.06631	19.202	1.147	0.0821	13.976	1.330	0.0445	29.881	1.335	0.04106	32.518

E.2 Wortmann FX 63-137 airfoil

	Re = 100 000			Re = 200 000			Re = 350 000			Re = 500 000		
Alpha	C_L	C_D	C_L/C_D	C_L	C_D	C_L/C_D	C_L	C_D	C_L/C_D	C_L	C_D	C_L/C_D
-4	0.183	0.0316	5.804	0.398	0.015610	25.477	0.431	0.0117	36.838	0.442	0.010	43.897
-3	0.345	0.02748	12.555	0.546	0.013270	41.168	0.570	0.00982	58.086	0.575	0.00863	66.663
-2	0.480	0.02801	17.122	0.660	0.013990	47.148	0.688	0.01004	68.546	0.695	0.00849	81.802
-1	0.566	0.0295	19.197	0.768	0.014710	52.230	0.800	0.01037	77.165	0.809	0.00872	92.798
0	0.680	0.02962	22.954	0.880	0.014880	59.167	0.913	0.0106	86.123	0.923	0.00898	102.762
1	0.799	0.02954	27.051	0.992	0.015080	65.802	1.025	0.01086	94.365	1.035	0.00926	111.803
2	0.919	0.02944	31.206	1.103	0.015290	72.132	1.135	0.01116	101.720	1.146	0.00959	119.479
3	1.028	0.02913	35.287	1.211	0.015510	78.072	1.243	0.01156	107.543	1.254	0.01005	124.756
4	1.125	0.02829	39.760	1.317	0.015790	83.407	1.347	0.01218	110.591	1.357	0.01074	126.359
5	1.289	0.0272	47.382	1.417	0.016090	88.055	1.447	0.01284	112.664	1.458	0.01151	126.690
6	1.425	0.02698	52.809	1.499	0.016540	90.641	1.537	0.01392	110.431	1.551	0.01271	122.006
7	1.539	0.02667	57.690	1.590	0.017780	89.426	1.617	0.0152	106.349	1.634	0.01421	115.004
8	1.625	0.02748	59.141	1.660	0.019810	83.786	1.673	0.01714	97.596	1.688	0.01601	105.453
9	1.683	0.02936	57.337	1.697	0.022930	74.008	1.716	0.02048	83.770	1.734	0.01931	89.814
10	1.703	0.03328	51.181	1.713	0.028040	61.098	1.742	0.02549	68.329	1.766	0.02393	73.790
11	1.696	0.04029	42.105	1.714	0.035860	47.783	1.757	0.03233	54.352	1.791	0.02983	60.034
12	1.697	0.04887	34.729	1.713	0.045160	37.925	1.762	0.04122	42.739	1.807	0.03749	48.186

Appendix F

Aerodynamic results

F.1 Eppler E387 airfoil for the design at Constant angle of attack

r/R	Circ/(U·R)	Va/U	Vt/U	V (m/s)	Tan (Beta)	Tan (Beta i)	Alpha (°)	Pitch (°)	Twist (°)	Chord/R	Re/1000	C_L	C_D	C_L/C_D
0.151	0.0162	0.2454	0.1529	1.428	0.9441	0.6225	6.428	25.48	64.52	0.0210	25.65	1.0788	0.02942	36.67
0.162	0.0470	0.2543	0.1483	1.482	0.8832	0.5824	6.428	23.79	66.21	0.0588	74.56	1.0788	0.02423	44.52
0.182	0.0736	0.2687	0.1390	1.593	0.7834	0.5166	6.427	20.89	69.10	0.0857	116.79	1.0787	0.02020	53.39
0.213	0.0943	0.2845	0.1262	1.766	0.6719	0.4431	6.427	17.47	72.53	0.0990	149.55	1.0787	0.01762	61.22
0.252	0.1086	0.2985	0.1118	2.002	0.5673	0.3742	6.426	14.09	75.91	0.1006	172.38	1.0786	0.01582	68.20
0.299	0.1178	0.3095	0.0976	2.297	0.4778	0.3152	6.425	11.07	78.93	0.0951	186.96	1.0785	0.01466	73.55
0.353	0.1234	0.3175	0.0848	2.645	0.4048	0.2671	6.424	8.53	81.47	0.0865	195.80	1.0783	0.01396	77.22
0.412	0.1267	0.3232	0.0739	3.037	0.3464	0.2286	6.422	6.46	83.54	0.0774	201.12	1.0782	0.01360	79.27
0.476	0.1287	0.3271	0.0648	3.461	0.3003	0.1982	6.421	4.79	85.21	0.0690	204.39	1.0780	0.01352	79.75
0.542	0.1300	0.3299	0.0574	3.907	0.2637	0.1741	6.419	3.46	86.54	0.0617	206.44	1.0778	0.01346	80.05
0.608	0.1308	0.3319	0.0514	4.361	0.2348	0.1550	6.418	2.39	87.61	0.0556	207.68	1.0777	0.01343	80.24
0.674	0.1310	0.3333	0.0466	4.813	0.2119	0.1399	6.417	1.55	88.45	0.0505	208.14	1.0776	0.01342	80.31
0.738	0.1306	0.3343	0.0427	5.249	0.1937	0.1279	6.416	0.87	89.13	0.0462	207.44	1.0775	0.01343	80.21
0.797	0.1288	0.3351	0.0396	5.658	0.1792	0.1183	6.415	0.33	89.67	0.0422	204.54	1.0774	0.01350	79.78
0.851	0.1243	0.3357	0.0372	6.031	0.1679	0.1108	6.414	-0.09	90.09	0.0383	197.42	1.0773	0.01382	77.95
0.898	0.1153	0.3361	0.0353	6.357	0.1591	0.1050	6.413	-0.42	90.42	0.0337	183.19	1.0771	0.01494	72.10
0.937	0.1001	0.3365	0.0338	6.629	0.1524	0.1006	6.412	-0.67	90.67	0.0280	159.03	1.0770	0.01684	63.96
0.968	0.0779	0.3367	0.0328	6.839	0.1476	0.0974	6.411	-0.85	90.85	0.0211	123.77	1.0770	0.01961	54.91
0.988	0.0495	0.3369	0.0321	6.982	0.1446	0.0954	6.410	-0.96	90.96	0.0132	78.68	1.0769	0.02373	45.37
0.999	0.0170	0.3369	0.0318	7.054	0.1430	0.0944	6.410	-1.02	91.02	0.0045	26.99	1.0769	0.02919	36.89

F.2 Eppler E387 airfoil for the design at Optimum C_L/C_D

r/R	Circ/(U*R)	Va/U	Vt/U	V (m/s)	Tan (Beta)	Tan (Beta i)	Alpha (°)	Pitch (°)	Twist (°)	Chord/R	Re/1000	C_L	C_D	C_L/C_D
0.151	0.0162	0.2460	0.1529	1.427	0.9441	0.6221	7.668	24.22	65.78	0.0195	23.79	1.16491	0.02666	43.69
0.162	0.0471	0.2547	0.1483	1.482	0.8832	0.5820	7.532	22.67	67.33	0.0549	69.62	1.15750	0.02299	50.35
0.182	0.0738	0.2700	0.1394	1.593	0.7834	0.5156	7.213	20.06	69.94	0.0815	111.15	1.13642	0.02016	56.37
0.213	0.0945	0.2860	0.1266	1.766	0.6719	0.4421	6.535	17.32	72.68	0.0994	150.16	1.07716	0.01745	61.74
0.252	0.1089	0.3000	0.1121	2.001	0.5673	0.3734	6.005	14.47	75.53	0.1057	180.96	1.02993	0.01429	72.05
0.299	0.1180	0.3106	0.0977	2.297	0.4778	0.3147	5.691	11.78	78.22	0.1027	201.91	1.00043	0.01227	81.52
0.353	0.1236	0.3187	0.0850	2.645	0.4048	0.2666	5.685	9.24	80.76	0.0934	211.39	1.00050	0.01212	82.58
0.412	0.1269	0.3245	0.0740	3.037	0.3464	0.2282	5.682	7.17	82.83	0.0835	217.09	1.00062	0.01202	83.22
0.476	0.1290	0.3285	0.0650	3.461	0.3003	0.1978	5.680	5.51	84.49	0.0745	220.60	1.00072	0.01197	83.63
0.542	0.1303	0.3314	0.0576	3.907	0.2637	0.1737	5.679	4.18	85.82	0.0666	222.80	1.00079	0.01193	83.88
0.608	0.1311	0.3334	0.0516	4.361	0.2348	0.1547	5.679	3.11	86.89	0.0601	224.12	1.00084	0.01191	84.04
0.674	0.1313	0.3348	0.0467	4.812	0.2119	0.1396	5.679	2.27	87.73	0.0545	224.61	1.00086	0.01190	84.10
0.738	0.1309	0.3359	0.0428	5.249	0.1937	0.1276	5.679	1.59	88.41	0.0498	223.87	1.00084	0.01191	84.01
0.797	0.1291	0.3366	0.0397	5.658	0.1792	0.1181	5.680	1.05	88.95	0.0456	220.77	1.00075	0.01196	83.65
0.851	0.1246	0.3371	0.0373	6.031	0.1679	0.1106	5.684	0.63	89.37	0.0413	213.14	1.00056	0.01209	82.78
0.898	0.1157	0.3375	0.0354	6.357	0.1591	0.1048	5.743	0.24	89.76	0.0362	196.95	1.00509	0.01263	79.57
0.937	0.1005	0.3385	0.0340	6.629	0.1524	0.1003	6.335	-0.61	90.61	0.0287	162.55	1.05855	0.01636	64.70
0.968	0.0784	0.3409	0.0332	6.839	0.1476	0.0968	7.075	-1.54	91.54	0.0203	119.07	1.12690	0.01969	57.24
0.988	0.0497	0.3369	0.0322	6.982	0.1446	0.0954	7.521	-2.07	92.07	0.0123	73.50	1.15691	0.02267	51.04
0.999	0.0170	0.3376	0.0318	7.054	0.1430	0.0943	7.661	-2.27	92.27	0.0041	25.05	1.16451	0.02657	43.83

F.3 Wortmann FX 63-137 airfoil for the design at Optimum C_L/C_D

r/R	Circ/(UR)	Va/U	Vt/U	V (m/s)	Tan (Beta)	Tan (Beta i)	Alpha (°)	Pitch (°)	Twist (°)	Chord/R	Re/1000	C_L	C_D	C_L/C_D
0.151	0.0162	0.2459	0.1530	1.428	0.9441	0.6222	8.694	23.19	66.81	0.0136	16.63	1.6656	0.03538	47.07
0.162	0.0470	0.2549	0.1484	1.482	0.8832	0.5819	8.399	21.79	68.21	0.0385	48.85	1.6484	0.03264	50.50
0.182	0.0737	0.2696	0.1392	1.593	0.7834	0.5160	8.140	19.15	70.85	0.0566	77.22	1.6333	0.02985	54.72
0.213	0.0943	0.2852	0.1262	1.766	0.6719	0.4427	7.950	15.93	74.07	0.0659	99.62	1.6209	0.02748	58.99
0.252	0.1088	0.2993	0.1119	2.001	0.5673	0.3738	7.663	12.83	77.17	0.0678	116.06	1.6038	0.02582	62.12
0.299	0.1180	0.3105	0.0977	2.297	0.4778	0.3148	7.470	10.00	80.00	0.0645	126.76	1.5929	0.02468	64.53
0.353	0.1236	0.3187	0.0850	2.645	0.4048	0.2666	7.353	7.58	82.42	0.0589	133.34	1.5862	0.02399	66.13
0.412	0.1269	0.3244	0.0740	3.037	0.3464	0.2282	7.283	5.57	84.43	0.0528	137.33	1.5821	0.02357	67.13
0.476	0.1290	0.3285	0.0650	3.461	0.3003	0.1978	7.239	3.95	86.05	0.0472	139.79	1.5796	0.02331	67.77
0.542	0.1303	0.3313	0.0576	3.907	0.2637	0.1737	7.212	2.64	87.36	0.0423	141.35	1.5780	0.02314	68.19
0.608	0.1311	0.3334	0.0516	4.361	0.2348	0.1547	7.196	1.60	88.40	0.0381	142.28	1.5771	0.02304	68.44
0.674	0.1314	0.3348	0.0467	4.812	0.2119	0.1396	7.190	0.75	89.25	0.0346	142.63	1.5767	0.02301	68.53
0.738	0.1310	0.3359	0.0429	5.249	0.1937	0.1276	7.200	0.07	89.93	0.0316	142.10	1.5773	0.02306	68.39
0.797	0.1291	0.3367	0.0398	5.658	0.1792	0.1180	7.238	-0.51	90.51	0.0289	139.91	1.5796	0.02330	67.81
0.851	0.1246	0.3373	0.0373	6.031	0.1679	0.1106	7.333	-1.02	91.02	0.0261	134.56	1.5851	0.02386	66.44
0.898	0.1156	0.3375	0.0354	6.357	0.1591	0.1048	7.522	-1.54	91.54	0.0228	123.99	1.5958	0.02498	63.87
0.937	0.1003	0.3375	0.0339	6.629	0.1524	0.1004	7.835	-2.10	92.10	0.0188	106.40	1.6138	0.02680	60.21
0.968	0.0781	0.3384	0.0329	6.839	0.1476	0.0972	8.103	-2.55	92.55	0.0140	81.98	1.6312	0.02936	55.56
0.988	0.0497	0.3382	0.0322	6.981	0.1446	0.0952	8.378	-2.94	92.94	0.0086	51.60	1.6472	0.03239	50.85
0.999	0.0170	0.3379	0.0319	7.054	0.1430	0.0943	8.686	-3.30	93.30	0.0029	17.51	1.6651	0.03532	47.15

Appendix G

Power and power coefficient for selected TSRs

	Eppler 387				Wortmann FX 63-137			
	TSR = 6.75		TSR = 7		TSR = 7		TSR = 7.25	
U (m/s)	C_P	Power (W)	C_P	Power (W)	C_P	Power (W)	C_P	Power (W)
4	0.4376	84.20	0.4308	82.90	0.4375	84.18	0.4325	83.22
5	0.4424	166.26	0.4365	164.03	0.4408	165.65	0.4365	164.05
6	0.4476	290.71	0.4435	288.00	0.4441	288.39	0.4405	286.09
7	0.4528	466.96	0.4505	464.56	0.4474	461.36	0.4446	458.49
8	0.4579	704.93	0.4575	704.22	0.4508	694.01	0.4490	691.16
9	0.4630	1014.83	0.4642	1017.44	0.4544	995.87	0.4533	993.45
10	0.4661	1401.35	0.4671	1404.24	0.4579	1376.68	0.4574	1375.27
11	0.4678	1871.94	0.4689	1876.57	0.4614	1846.35	0.4615	1846.74
12	0.4693	2437.95	0.4707	2445.59	0.4648	2414.89	0.4655	2418.22
13	0.4707	3109.10	0.4723	3120.04	0.4681	3091.81	0.4694	3100.39
14	0.4720	3894.01	0.4739	3909.80	0.4712	3887.65	0.4727	3899.85
15	0.4733	4803.00	0.4755	4825.10	0.4731	4800.41	0.4745	4814.80
16	0.4746	5845.13	0.4769	5872.98	0.4744	5841.90	0.4759	5861.12
17	0.4754	7022.02	0.4777	7055.77	0.4755	7023.41	0.4772	7048.56
18	0.4757	8341.64	0.4782	8385.56	0.4765	8355.91	0.4784	8388.05
19	0.4760	9815.86	0.4787	9872.09	0.4776	9848.65	0.4794	9886.94
20	0.4762	11453.70	0.4792	11525.70	0.4785	11509.10	0.4804	11555.30

Appendix H

Comparison between selected TSRs for E387

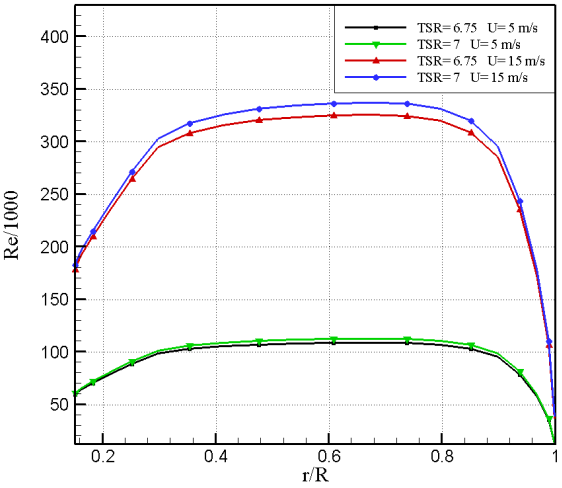

a) Reynolds number

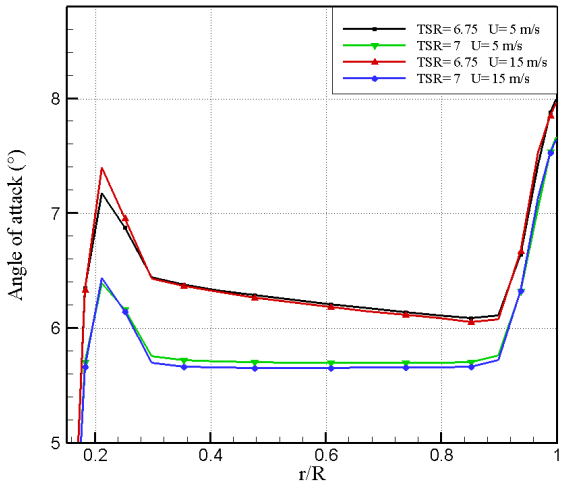

b) Angle of attack

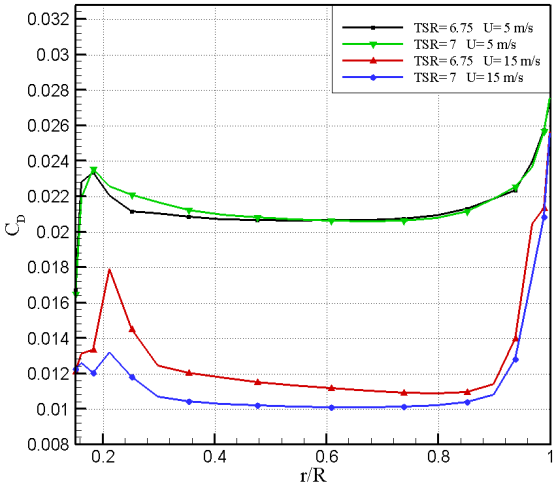

c) C_D

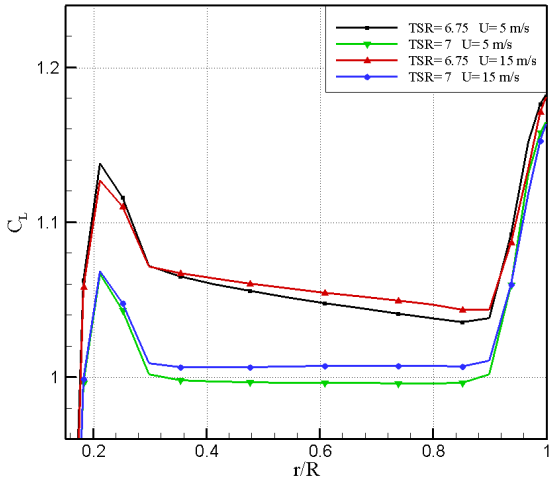

d) C_L

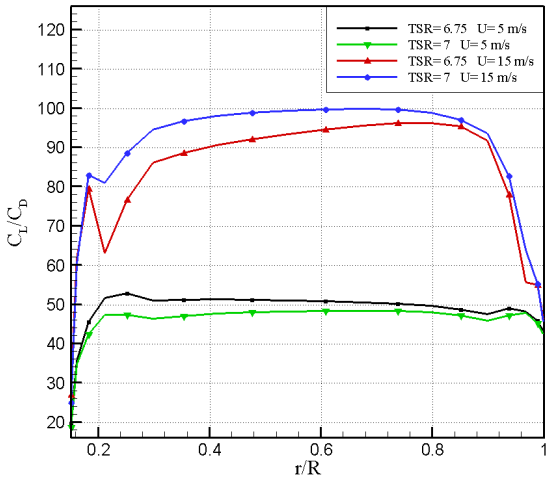

e) C_L/C_D

Appendix I

Comparison between selected TSRs for FX 63-137

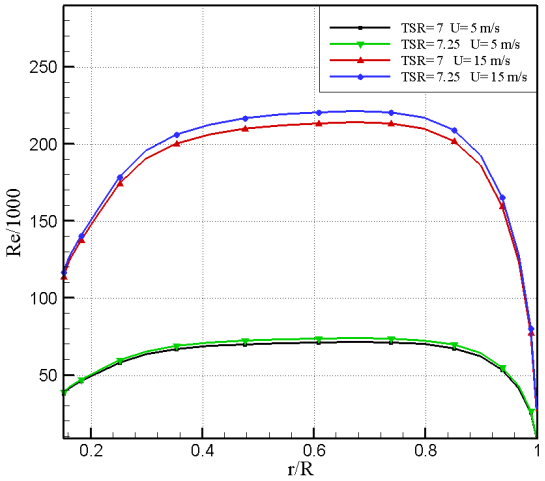

a) Reynolds number

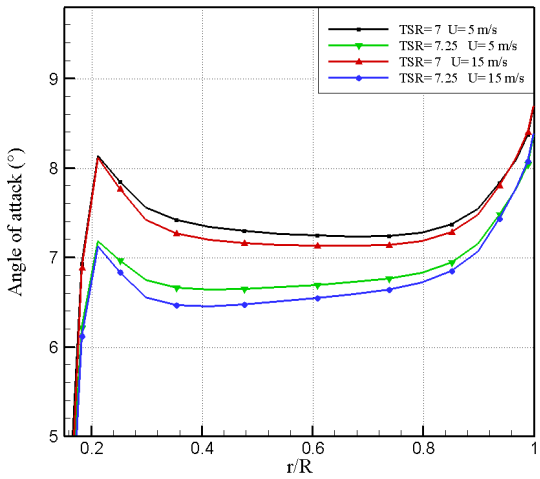

b) Angle of attack

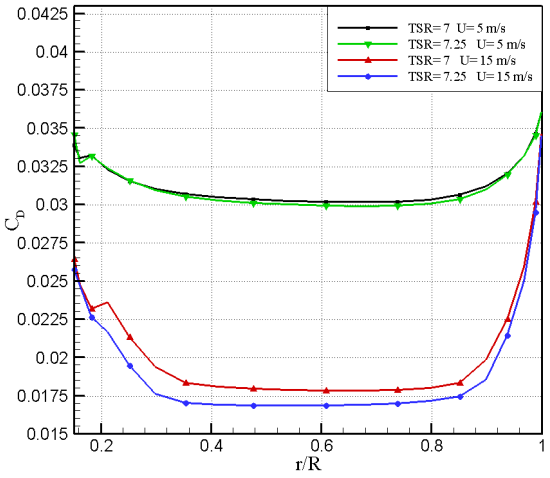

c) C_D

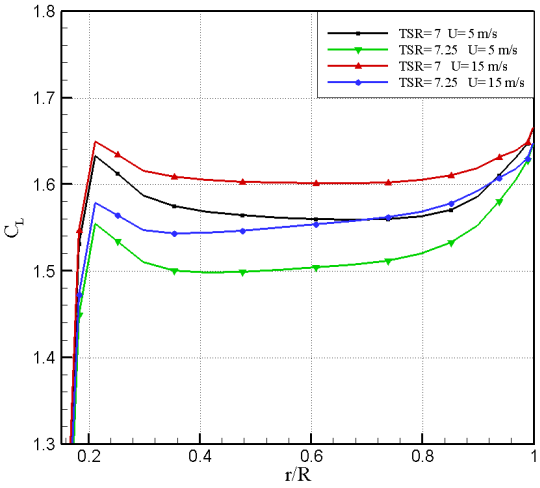

d) C_L

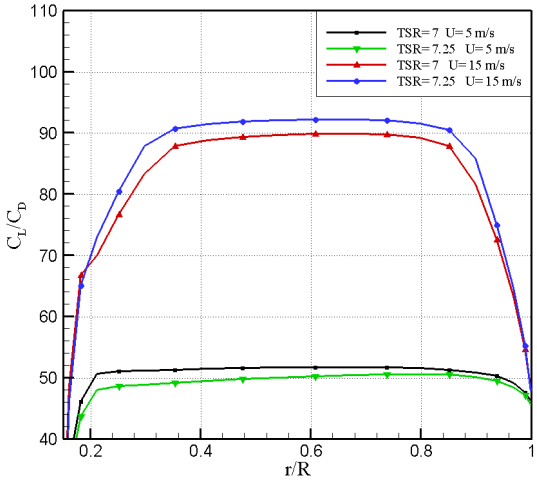

e) C_L/C_D

Appendix J: Annual Energy Production

J.1 In Montijo for Eppler E387 with selected TSRs

	Montijo							
	Eppler 387 with TSR=6.75				Eppler 387 with TSR=7			
U (m/s)	C_P	Power (W)	Frequency (%)	Energy (kWh)	C_P	Power (W)	Frequency (%)	Energy (kWh)
1	0.00	0.00	8.57	0.00	0.00	0.00	8.57	0.00
2	0.00	0.00	15.08	0.00	0.00	0.00	15.08	0.00
3	0.00	0.00	18.11	0.00	0.00	0.00	18.11	0.00
4	0.4376	84.20	17.63	130.05	0.4308	82.90	17.63	128.04
5	0.4424	166.26	14.67	213.66	0.4365	164.03	14.67	210.79
6	0.4476	290.71	10.68	272.06	0.4435	288.00	10.68	269.53
7	0.4528	466.96	6.90	282.11	0.4505	464.56	6.90	280.66
8	0.4579	704.93	3.98	245.52	0.4575	704.22	3.98	245.27
9	0.4630	1014.83	2.06	182.85	0.4642	1017.44	2.06	183.32
10	0.4661	1401.35	0.96	117.60	0.4671	1404.24	0.96	117.84
11	0.4678	1871.94	0.40	66.02	0.4689	1876.57	0.40	66.18
12	0.4693	2437.95	0.15	32.66	0.4707	2445.59	0.15	32.76
13	0.4707	3109.10	0.05	14.32	0.4723	3120.04	0.05	14.37
14	0.3768	3109.10	0.02	4.46	0.3782	3120.04	0.02	4.48
15	0.3064	3109.10	0.00	1.26	0.3075	3120.04	0.00	1.26
16	0.2525	3109.10	0.00	0.32	0.2533	3120.04	0.00	0.32
17	0.2105	3109.10	0.00	0.07	0.2112	3120.04	0.00	0.08
18	0.1773	3109.10	0.00	0.02	0.1779	3120.04	0.00	0.02
19	0.1508	3109.10	0.00	0.00	0.1513	3120.04	0.00	0.00
20	0.1293	3109.10	0.00	0.00	0.1297	3120.04	0.00	0.00
21	0.1117	3109.10	0.00	0.00	0.1120	3120.04	0.00	0.00
22	0.0971	3109.10	0.00	0.00	0.0974	3120.04	0.00	0.00
23	0.0850	3109.10	0.00	0.00	0.0853	3120.04	0.00	0.00
24	0.0748	3109.10	0.00	0.00	0.7507	3120.04	0.00	0.00
25	0.0662	3109.10	0.00	0.00	0.0664	3120.04	0.00	0.00

J.2 In Montijo for Wortmann FX 63-137 with selected TSRs

	Montijo							
	Wortmann FX 63-137 with TSR=7				Wortmann FX 63-137 with TSR=7.25			
U (m/s)	C_P	Power (W)	Frequency (%)	Energy (kWh)	C_P	Power (W)	Frequency (%)	Energy (kWh)
1	0.00	0.00	8.57	0.00	0.00	0.00	8.57	0.00
2	0.00	0.00	15.08	0.00	0.00	0.00	15.08	0.00
3	0.00	0.00	18.11	0.00	0.00	0.00	18.11	0.00
4	0.4375	84.18	17.63	130.02	0.4325	83.22	17.63	128.54
5	0.4408	165.65	14.67	212.88	0.4365	164.05	14.67	210.82
6	0.4441	288.39	10.68	269.90	0.4405	286.09	10.68	267.74
7	0.4474	461.36	6.90	278.72	0.4446	458.49	6.90	276.99
8	0.4508	694.01	3.98	241.72	0.4490	691.16	3.98	240.72
9	0.4544	995.87	2.06	179.44	0.4533	993.45	2.06	179.00
10	0.4579	1376.68	0.96	115.53	0.4574	1375.27	0.96	115.41
11	0.4614	1846.35	0.40	65.12	0.4615	1846.74	0.40	65.13
12	0.4648	2414.89	0.15	32.35	0.4655	2418.22	0.15	32.40
13	0.4681	3091.81	0.05	14.24	0.4694	3100.39	0.05	14.28
14	0.3748	3091.81	0.02	4.43	0.3758	3100.39	0.02	4.45
15	0.3047	3091.81	0.00	1.25	0.3055	3100.39	0.00	1.26
16	0.2510	3091.81	0.00	0.32	0.2517	3100.39	0.00	0.32
17	0.2093	3091.81	0.00	0.07	0.2099	3100.39	0.00	0.07
18	0.1763	3091.81	0.00	0.02	0.1768	3100.39	0.00	0.02
19	0.1499	3091.81	0.00	0.00	0.1503	3100.39	0.00	0.00
20	0.1285	3091.81	0.00	0.00	0.1289	3100.39	0.00	0.00
21	0.1110	3091.81	0.00	0.00	0.1113	3100.39	0.00	0.00
22	0.0966	3091.81	0.00	0.00	0.0968	3100.39	0.00	0.00
23	0.0845	3091.81	0.00	0.00	0.0847	3100.39	0.00	0.00
24	0.0744	3091.81	0.00	0.00	0.0746	3100.39	0.00	0.00
25	0.0658	3091.81	0.00	0.00	0.0660	3100.39	0.00	0.00

J.3 In Picarreira for Eppler E387 with selected TSRs

	Picarreira							
	Eppler 387 with TSR=6.75				Eppler 387 with TSR=7			
U (m/s)	C_P	Power (W)	Frequency (%)	Energy (kWh)	C_P	Power (W)	Frequency (%)	Energy (kWh)
1	0.00	0.00	5.23	0.00	0.00	0.00	5.23	0.00
2	0.00	0.00	8.18	0.00	0.00	0.00	8.18	0.00
3	0.00	0.00	9.96	0.00	0.00	0.00	9.96	0.00
4	0.4376	84.20	10.77	79.44	0.4308	82.90	10.77	78.21
5	0.4424	166.26	10.78	156.96	0.4365	164.03	10.78	154.85
6	0.4476	290.71	10.18	259.22	0.4435	288.00	10.18	256.80
7	0.4528	466.96	9.17	375.22	0.4505	464.56	9.17	373.29
8	0.4579	704.93	7.94	490.25	0.4575	704.22	7.94	489.75
9	0.4630	1014.83	6.63	589.31	0.4642	1017.44	6.63	590.82
10	0.4661	1401.35	5.36	657.61	0.4671	1404.24	5.36	658.97
11	0.4678	1871.94	4.20	688.70	0.4689	1876.57	4.20	690.40
12	0.4693	2437.95	3.20	683.47	0.4707	2445.59	3.20	685.61
13	0.4707	3109.10	2.37	646.49	0.4723	3120.04	2.37	648.76
14	0.3768	3109.10	1.72	467.31	0.3782	3120.04	1.72	468.95
15	0.3064	3109.10	1.21	329.52	0.3075	3120.04	1.21	330.68
16	0.2525	3109.10	0.83	226.88	0.2533	3120.04	0.83	227.67
17	0.2105	3109.10	0.56	152.62	0.2112	3120.04	0.56	153.16
18	0.1773	3109.10	0.37	100.38	0.1779	3120.04	0.37	100.74
19	0.1508	3109.10	0.24	64.59	0.1513	3120.04	0.24	64.82
20	0.1293	3109.10	0.15	40.68	0.1297	3120.04	0.15	40.82
21	0.1117	3109.10	0.09	25.08	0.1120	3120.04	0.09	25.17
22	0.0971	3109.10	0.06	15.15	0.0974	3120.04	0.06	15.21
23	0.0850	3109.10	0.03	8.97	0.0853	3120.04	0.03	9.00
24	0.0748	3109.10	0.02	5.21	0.7507	3120.04	0.02	5.22
25	0.0662	3109.10	0.01	2.96	0.0664	3120.04	0.01	2.97

J.4 In Picarreira for Wortmann FX 63-137 with selected TSRs

	Picarreira							
	Wortmann FX 63-137 with TSR=7				Wortmann FX 63-137 with TSR=7.25			
U (m/s)	C_P	Power (W)	Frequency (%)	Energy (kWh)	C_P	Power (W)	Frequency (%)	Energy (kWh)
1	0.00	0.00	5.23	0.00	0.00	0.00	5.23	0.00
2	0.00	0.00	8.18	0.00	0.00	0.00	8.18	0.00
3	0.00	0.00	9.96	0.00	0.00	0.00	9.96	0.00
4	0.4375	84.18	10.77	79.42	0.4325	83.22	10.77	78.51
5	0.4408	165.65	10.78	156.39	0.4365	164.05	10.78	154.87
6	0.4441	288.39	10.18	257.15	0.4405	286.09	10.18	255.10
7	0.4474	461.36	9.17	370.72	0.4446	458.49	9.17	368.42
8	0.4508	694.01	7.94	482.65	0.4490	691.16	7.94	480.67
9	0.4544	995.87	6.63	578.30	0.4533	993.45	6.63	576.89
10	0.4579	1376.68	5.36	646.04	0.4574	1375.27	5.36	645.38
11	0.4614	1846.35	4.20	679.28	0.4615	1846.74	4.20	679.43
12	0.4648	2414.89	3.20	677.00	0.4655	2418.22	3.20	677.93
13	0.4681	3091.81	2.37	642.89	0.4694	3100.39	2.37	644.68
14	0.3748	3091.81	1.72	464.71	0.3758	3100.39	1.72	466.00
15	0.3047	3091.81	1.21	327.69	0.3055	3100.39	1.21	328.60
16	0.2510	3091.81	0.83	225.61	0.2517	3100.39	0.83	226.24
17	0.2093	3091.81	0.56	151.77	0.2099	3100.39	0.56	152.20
18	0.1763	3091.81	0.37	99.83	0.1768	3100.39	0.37	100.10
19	0.1499	3091.81	0.24	64.23	0.1503	3100.39	0.24	64.41
20	0.1285	3091.81	0.15	40.45	0.1289	3100.39	0.15	40.56
21	0.1110	3091.81	0.09	24.94	0.1113	3100.39	0.09	25.01
22	0.0966	3091.81	0.06	15.07	0.0968	3100.39	0.06	15.11
23	0.0845	3091.81	0.03	8.92	0.0847	3100.39	0.03	8.94
24	0.0744	3091.81	0.02	5.18	0.0746	3100.39	0.02	5.19
25	0.0658	3091.81	0.01	2.95	0.0660	3100.39	0.01	2.95